La borsa di dottorato è stata cofinanziata con risorse del
Programma Operativo Nazionale Ricerca e Innovazione 2014-2020 (CCI 2014IT16M2OP005),
Fondo Sociale Europeo, Azione I.1 "Dottorati Innovativi con caratterizzazione Industriale"

UNIONE EUROPEA
Fondo Sociale Europeo

Doctoral thesis in: New green nano-materials for the reduction of friction and wear in lubricants for power transmissions

Waleed Ahmed Abdaglil Mustafa

UNIVERSITY OF SALERNO

DEPARTMENT OF INDUSTRIAL ENGINEERING

Ph.D. Course in Industrial Engineering
Curriculum in Chemical Engineering - XXXIII Cycle

Doctoral thesis in:

New green nano-materials for the reduction of friction and wear in lubricants for power transmissions

Supervisors
Prof. Maria Sarno
Prof. Adolfo Senatore
Prof. Fabrice Dassenoy

Ph.D. student
Waleed Ahmed Abdalglil Mustafa

Scientific Referees
Prof. Josefa Fernandez Perez
Dr. Valentina Zin

Ph.D. Course Coordinator
Prof. Francesco Donsì

Academic year
2020/2021

Acknowledgements

Firstly, I would like to thank God, and my advisors, Prof. Sarno, Prof. Senatore, and Prof. Dassenoy, for their, patience, research advice, and confidence in my abilities. Without their encouragement and help, I would never have been introduced to the world of nanotechnology, and tribology. I would also like to thank Ing. Di Franco for his technical guidance in RILUB S.P.A. factory's production lines. Many thanks are dedicated to my beloved lab family including Dottoressa Cirillo, Ing. Spina, Ing. Iuliano, Ing. Scarpa, Dottoressa Scudieri, and Ing. Ponticorvo, for their instructions, help to finish my experiments, and overwhelming me with love and care. I would like to thank my parents for supporting me with all of their kindness, and guidance throughout my entire life even if from far away. A special gratitude is for my lovely wife Eman for her encouragement, and this beautiful journey. Lastly, I would like to thank my second country Italy, the Italian Ministry of Education, and the University of Salerno for granting me this chance without any discrimination, but with all openness and equality.

List of publications

- A review on potentials and challenges of nanolubricants as promising lubricants for electric vehicles. Lubrication Science.
  Mustafa, W. A. A., Dassenoy, F., Sarno, M., & Senatore, A. (**2021**).
  (Submitted)
- Anti-friction and anti-wear surfactant-assisted nano-carbons stable formulations for easy industrialization. Tribology Online.
  Sarno, M., Cirillo, C., Scarpa, D., Senatore, A., & Mustafa, W. A. A (**2021**).
  Doi.org/10.2474/trol.16.1
- One-step "green" synthesis of dispersable carbon quantum dots/poly (methyl methacrylate) nanocomposites for tribological applications. Tribology international, 148, 106311.
  Sarno, M., Mustafa, W. A. A., Senatore, A., & Scarpa, D. (**2020**).
  Doi:10.1016/j.triboint.2020.106311
- rGO/GO Nanosheets in Tribology: From the State of the Art to the Future Prospective. Lubricants, 8(3), 31.
  Sarno, M., Scarpa, D., Senatore, A., & Mustafa, W. A. A. (**2020**).
  Doi:10.3390/lubricants8030031
- A Tribochemical Boost for Cu Based Lubricant Nano-Additive. In Key Engineering Materials (Vol. 813, pp. 292-297). Trans Tech Publications Ltd.
  Sarno, M., Senatore, A., Spina, D., & Mustafa, W. A. A. (**2019**).
  Doi:10.4028/www.scientific.net/KEM.813.29

Table of Contents

Index of Figures

Index of tables

Abstract

Nanomaterials have emerged as future environmentally sustainable lubricant additives to improve conventional lubricants such as car oils, industrial oils, grease and metalworking fluids. In particular, as far as this thesis is concerned, nanoparticle additives' applications in transmissions oils are based on the concepts of solid lubrication and are often used as anti-wear, anti-friction, and high-pressure additives. Their multiple advantages include small enough scale, thermal stability, unique particle chemistries, mechanical properties, and a high surface reaction rate. These benefits translate into the prolonged running of the equipment, improved fuel efficiency and extended maintenance cycles. The main drawback of solid lubricant additives is the inherent low stability of liquid base lubricant systems, which has greatly limited them from industrial applications. Thus, the current PhD thesis is aimed to design novel techniques to improve the dispersibility of nanoadditives in base oils, while encompassing both the theoretical and the industrial point of view. The concluded results from this industrial research have shown promising results in simultaneous stability and tribological improvement. Also, future use of nanoadditives in electric vehicle applications is critically discussed, and key findings are achieved.

Introduction

Lubrication is crucial for both automotive and industrial processes. Over the last decades, great attempts have been made to create environmentally sustainable lubricants to increase working performance, extend the equipment's service life, and reduce long-term costs. A lubricant performs various essential functions, including lubrication, cooling, cleaning, and preservation of metal surfaces against corrosive harm. Lubricant consists of a base fluid and additives combinations. The primary purpose of the base fluid is to lubricate and act as an additive carrier. Additives are chemicals applied to lubricating oils to provide unique properties to fully-formulated oils.

The lubricant's efficiency is improved in a variety of ways by applying a mixture of additives such as anti-friction, anti-wear, extreme pressure, anti-oxidant, anti-corrosion, and detergent. Those additives include compounds of organo-molybdenum and compounds of organo-zinc phosphate. Although these additives are mainly advantageous for friction and wear reduction, they have hazardous high amounts of sulphur and/or phosphorus in the finished lubricant. For this reason, lubricant additives and formulations that have effective lubrication performance while at the same time environmentally sustainable, are desired. Furthermore, the ever-growing severity of operational conditions and advancements in equipment technologies combined with lubrication and increasingly strict regulatory requirements across a broad range of markets are primary factors for exploring different forms of additives and enhancing their performance.

Technological developments and research breakthroughs indicate that substantial progress has been made in applying carbon nanomaterials, metals, metal oxides, metal sulphides, metal borates and metal carbonates to enhance the properties and efficiency of lubricants. Nanoparticle as additive is based on solid lubrication concepts and are mainly used as anti-wear, anti-friction and extreme-pressure additives. The advantages of nano-based lubricants additive can be summarised in operational, economic, and environmental benefits. Besides reducing friction, it can increase the efficiency of equipment and machinery and minimise fatigue, i.e. the repair frequency can be

decreased. However, the utilisation of nanoadditives involves technical challenge to achieve the stability of nanoparticles in the base oil.

Therefore, this PhD central theme is the synthesis of novel nanoadditives, and the attempt to devise new strategies to maintain their stability, resulting in their delayed sedimentation during the useful operational service life of the lubricant. In particular, the main lubricants under investigation are industrial gear lubricants as they work under extreme pressure conditions and many challenges exist for gears' operation and life span. Additionally, the thesis sheds light on the potentials and challenges of nanolubricant use for electric motors being the prime mover for the future in many applications such as electric vehicles.

This research project was conducted in collaboration with the lube industry RILUB S.P.A., a company specialising in lubricant formulation, manufacturing, and spare parts distribution. The research work conducted during the thesis aimed to improve our industrial partner products' tribological performance, in endeavour to bridge the gap between academia and the industry. Furthermore, external research period was conducted at the Laboratory of Tribology and Dynamic systems, (LTDS) France. The LTDS is a multi-site, multidisciplinary, pluricultural joint research unit which conducts and supports research, pilots, experiments, models, simulates in: Tribology, Physio-Chemistry and Dynamics of Interfaces.

Summarising, this research is aimed at studying:

- Firstly, a detailed literature scan is conducted on nanoparticles' role as additives while highlighting lubrication challenges in transmissions in the first two chapters. The literature review included general tribological definitions, nanolubricants mechanism of work, literature behaviour of selected nanolubricants, and thermal management benefits of nanoparticles in nanofluids.
- Secondly, a thematical review is presented in the third chapter on the different studies performed with nanolubricants, and how they match electric vehicles' operational requirements. The gaps of nanolubricants utilisation in electric vehicles are also highlighted, as there is no specific investigation conducted on nanolubricants application on them. Conclusions from this study can be considered as guidelines for the potential application of nanolubricants in electric vehicles and possible future research that can be accomplished on the topic.
- Thirdly, a specific focus is given to study carbon-based nanosheets' tribological action as promising and non-cost-intensive additives. Moreover, carbon-based nanoparticles are subjected to surfactant modification and experimentally evaluate anti-wear and anti-friction performance. These studies are analysed utilising different tribometers setups and surface characterisation techniques.

- Fourthly, the development of composite poly(methyl methacrylate)/carbon quantum dots (PMMA/CQDs) has been proposed for the first time via one-step, mild temperature, easily scalable oleic acid and citric acid-based green synthesis. Composite consists of an oil-compatible polymer matrix that releases anti-friction and anti-wear CQDs locally under lubrication conditions.
- Finally, conclusions are summarised as key points resulted from this PhD thesis, and some recommendations are presented on potential studies in this area.

Chapter I. Lubrication and Nanoadditives

I.1 Tribology

The word tribology is derived from the Greek word "tribos," meaning rubbing, so tribology is the science of rubbing in essence. "The science and technology of interacting surfaces in relative motion and related practices" is a more preferred definition of tribology. Tribology is primarily concerned with friction, wear and lubrication related phenomena and dates to the days of the Pharaohs in Egypt, as shown in Figure 1.1.

Figure1.1 *Egyptian illustration (1880 BC): Liquid lubricants are poured under sledge for the transportation of a massive statue (Persson, 2014).*

In today's world, tribological systems efficiencies are of a great significance as it is projected that the tribological deficiency costs are likely to surpass 1% of the developed nations' gross national product (GNP). The energy dissipation caused by friction and wear has always been one of the major concerns for humanity. Friction and wear are nearly everywhere, from manufacturing equipment to household products. It has been calculated that almost 30% of global energy is wasted due to friction and wear (Jost, 1966). Thus, the importance of understanding tribological phenomena in terms of friction reduction and wear management cannot be overemphasized. This is particularly true as oil reserves continue to decrease, and energy prices are increasingly rising. One of the great challenges for the efficient and durable operation of advanced engineered mechanical systems is addressing such vital lubrication demand.

1.1.1 Friction

In physics/mechanical engineering, friction is one of the oldest problems with significant consequences for our daily lives. The friction force (F_f) is defined as the interfacial force opposing the two contact bodies' relative movement. Differentiating between two equally significant frictional phenomena is necessary: the kinetic friction force (F_k), and the static friction force (F_s). F_k is the force necessary to sustain the sliding process, while the minimal force needed to initiate sliding is defined as F_s. Friction may be beneficial or undesirable, depending on the application. For instance, cars' ability to move along the rod is impossible without the presence of friction between the wheels and the pavement. However, friction is not desired in moving parts such as the engine, bearing, turbine, and human joints as being considered the main souse of energy loss and in extreme cases can lead to the destruction of these systems.

The two fundamental laws of friction, expressing that friction resistance is proportional to normal load and independent on the area of contact between solids, appear to be first mentioned by Leonardo da Vinci (1452-1519) and rediscovered in 1699 by Guillaume Amontons (Zhuravlev, 2013). Charles Augustin Coulomb, in 1785, confirmed these observations (Hertz, 1882). He was the one to distinguish between F_s and F_k. The Coulomb expression used today for the friction coefficient (μ) is the ratio between F_F and the normal load F_N applied to the firm touching bodies (Figure 2). For dry sliding, he experimentally found that friction is almost independent of the sliding velocity and considered that friction can be due to surface molecular adhesion and asperity interaction. The elastic contact theory described by Hertz in 1882 (Hertz, 1882; Stribeck, 1902) established the pressure distribution measurements in the contact and showed the high values of this parameter even in a low loaded contact (Figure 1.2).

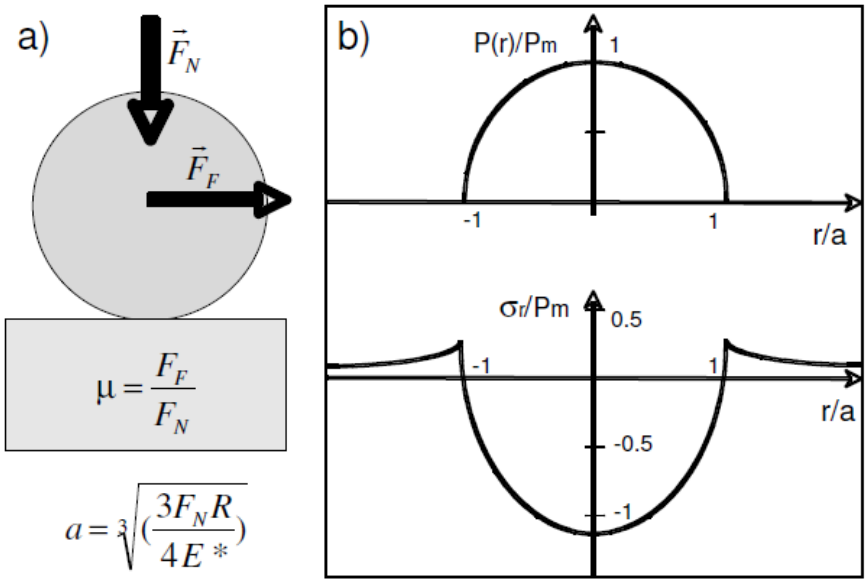

Figure 1.2 *a) Illustration of the elastic sphere on the contact plane demonstrating the F_F friction and standard F_N forces applied with coefficient of friction μ. b) Pressure distribution (P_r) and radial stress (σ_r), the radius of the contact area a, function of: Normal load F_N, reduced module E* and ball for Young radius r (Mansot et al., 2009).*

Besides Hertz models are useful in understanding the elastic behaviour and asperity of non-adhesive and adhesive surfaces such as Johnson-Kendall-Roberts (JKR) model (Johnson, 1997). However, these theories are typically highly model-dependent, for example, assuming on a single-length scale only elastic deformations and roughness (Gao et al., 2004). The continuum models have been refined by some investigators to provide more realistic surfaces that can have arbitrary roughness and plastic deformation (Persson et al., 2005; Persson, 2006). As expected, computer aid molecular dynamic (MD) simulations have shown they break down on the nano and atomic scales (Luan and Robbins, 2009). However, the simplified MD simulations have indicated that on the nanoscale, Amontons' law remains valid (Landman, Luedtke and Gao, 1996).

1.1.2 Wear

Wear is characterized as the material removal from solid surfaces induced by the mechanical motion of one moving surface relative to another. Current research indicates four wear mechanisms exist (Holmberg and Matthews, 2009) as listed in Figure 1.3.

Figure 1.3 *Wear classification in mechanical systems.*

The most common mechanism is adhesive wear, which occurs when one surface's asperities are firmly adhered to the asperities of another surface, resulting in the formation of a junction. The weaker asperities are isolated, and material is removed when these surfaces are sheared against each other (Burwell, 1957). While abrasive wear occurs when a hard surface is sheared against a significantly softer one, hence the hard asperities can penetrate the softer ones. When the same number of asperities are constantly sheared against each other, fatigue wear occurs. With time, this repeated sliding will eventually lead to surface cracks in the formation of voids that continue to propagate under the shearing action (P. Suh, 1973). Chemical wear occurs in destructive and corrosive conditions where a chemical reaction takes place and can lead to material removal when the shearing action takes place (Celis, Ponthiaux and Wenger, 2006).

In general, wear is a complex phenomenon that is why there is no unified mathematical estimation measures. However, Archard noted that the wear rate is directly proportional to the volume of wear and indirectly proportional to

the material's normal load and hardness (Archard, 1980), as indicated in the equation below:

$$K = \frac{VH}{F_N s} \quad (1.1)$$

Where the wear rate is K (wear coefficient normalized by the material's hardness), V is the volume worn, s is the movement distance, and H is the material's hardness.

1.2 Lubrication regimes

Viscous fluid lubricant is applied between two sliding surfaces, so that friction and wear between the two motion surfaces are minimized. The lubricants operation can be split into three regimes, which are shown in the well-known Stribeck curve (Figure 1.4), according to the separation distance. It defines the variation of μ, as a quantity function of Hersey's number (μν/P), where μ is the lubricant's dynamic viscosity, ν is the sliding velocity, and P is the normal load applied.

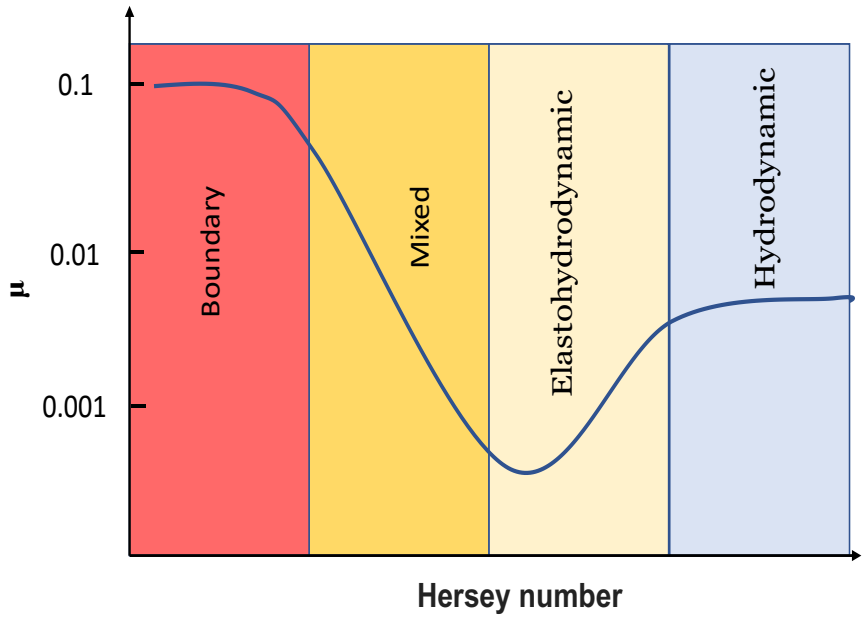

Figure 1.4 *Stribeck curve depicting the various regimes of lubrication.*

There are three main lubrication regimes: Hydrodynamic Lubrication (HL), Elastohydrodynamic Lubrication (EHL) and Boundary Lubrication (BL), in addition the mixed lubrication regime which is a status combination between BL and EHL. The following parts will address each of three main regimes.

1.2.1 Hydrodynamic Lubrication

In hydrodynamic lubrication, often referred to as "full-film" lubrication, a viscous and dense lubricant film separates the moving surfaces. In general, the film thickness is typically 10 to 100 times thicker than the moving surfaces' height of asperity. Because of these μ is on the order of 0.001-0.01 (Holmberg and Matthews, 2009). In addition, hydrodynamic lubrication demands that one of the surfaces in the direction of motion be tilted forward. This converging configuration would lead to the fluid being dragged to the shrinking gap while generating a positive pressure at the same time that will sustain the load in the gap and hold the surfaces apart (Hamrock, Schmid and Jacobson, 2004).

It is evident from the Hersey's number that this form of lubrication is governed by the fluid's viscosity and the velocity of the moving surfaces. A relatively viscous fluid and high-speed environments would avoid interaction with asperity-asperity and result in low coefficients of friction.

1.2.2 Elastohydrodynamic Lubrication (EHL)

This type of lubrication occurs when a lubricant fills the wedge between two rotating, non-conformal contact surfaces, such as those used in gears and rolling bearings (Höglund, 1999). The lubricating film thickness is usually much smaller than that used in hydrodynamic lubrication. Although pressure is still produced to pull the surfaces apart, when this pressure is high, elastic deformation of the surfaces will occur. Owing to the similarities of the pressure distribution to that of a Hertzian pressure distribution, this typically happens in the deformed region that is sometimes referred to as the Hertzian region. However, should their elastic limit be exceeded, the contact pressure can lead to plastic deformation of the surfaces (Blau, 2008).

The contact pressure influences the viscosity of the lubricant (η), in addition to the deformation of the surfaces. In fact, for non-conformal contacts, the lubricant's viscosity increases exponentially according to Equation (1.2), with increasing pressure (Stachowiak and Batchelor, 2013).

$$\eta = \eta_0 e^{\alpha P} \tag{1.2}$$

Where η_0 the lubricant's viscosity is at ambient pressure and constant temperature, the contact pressure is P, and α is the coefficient of viscosity-pressure is defined as:

$$\alpha = \frac{1}{\eta}\frac{\partial \eta}{\partial P}\Big|_{P=0} \tag{1.3}$$

When dealing with EHL, the most critical parameter is the minimum film thickness h_{min}. The film thickness is 0.1 to 1 μm, but the surfaces can still be isolated, resulting in friction and wear reduction (Rabinowicz, 1995). Lubrication regime can also be defined in mathematical terms by the lambda ratio (λ). The lambda ratio is the minimum film thickness (h_{min}) in relation to the contacting roughness (R_{a1} and R_{a2}) as shown in Equation (1.4) (Yan, 2010).

For BL λ is <0.7 and >2 for hydrodynamic lubrication (Zhu and Wang, 2013), while mixed lubrication and EHL are any value in between.

$$\lambda = \frac{h_{min}}{\sqrt{R_{a1}+R_{a2}}} \quad (1.4)$$

1.2.3 Boundary Lubrication (BL)

Typically, BL occurs under high loads where maintaining a thin film between the contacting surfaces becomes difficult, i.e., the film is squeezed out of the contact region. This squeeze occurs when the frictional forces are normally much higher than in the hydrodynamic regime (typically by a factor of 100) (Persson, 1993), and approximately independent of the sliding velocity. To avoid this, some lubrication oil "additives" are generally provided, e.g., fatty acids, which are long-chain hydrocarbons with a polar end group. These molecules, even if the load on the contact zone is very high, can react with the solid surfaces and form a tightly held monolayer that is not removed. It is this monolayer that provides the sliding surfaces with main protection (reduced wear) and lubrication.

1.3 Oil lubricants

Lubricants can be as liquids, semi-solids (fats) or as solids (including particles and coatings). The main aim of lubricants is the reduction of friction and wear with additional roles of cleaning and colling. Since cleaning and cooling functions require fluidity, greases and solid lubricants could be applied to machine elements where heat and contamination are not serious factors. Due these benefits and the advantage of handling, liquid lubricants are most common in many practical applications. Therefore, the following section will mainly focus on liquid base lubricants.

1.3.1 Classification and standards

Lubricating oil is a class of oils that are used to minimize the friction, heat, and wear between mechanical components that are in contact with each other, often simply called lubricant/lube. The formulation of lubricants is a method in which substances are combined to prepare a lubricant. In order to fulfil the requirements of machine operation, the substances should be properly chosen. In liquid lubricants, the components are divided into two groups: base fluids and additives. The primary components of lubricating fluids are base oils. Viscous fluids have been known empirically since ancient times to provide lubrication efficiency. It was discovered around a hundred years ago that if

dissolved in base fluids, certain substances would improve lubrication efficiency (Carnes, 2005).

The quality of lubricants is defined using qualifications or specifications for lubricants. In establishing these norms, several professional societies and organizations are involved: ASTM International, CEC (Coordinating European Council), DIN (Deutsches Institut für Normung), SAE (Society of Automotive Engineers), API (American Petroleum Institute), ACEA (Association des Constructeurs Europeens D 'Automobiles), AGMA (American Association of Gear Manufacturers), ISO (International Organization of Standards), NLGI (National Lubricating Grease Institute), and OEMs (Original Equipment Manufacturers).

Today, lubricating fluids are made from base oils and, depending on the practical requirement, 5 to 20 % mass of various additives. Viscous liquids with sufficient viscosity for the application are base fluids. As outlined in Table 1.1, the API describes base oil groups.

Table 1.1 *API base oil classification.*

Groups	**Saturates, Mass%**	**Aromatics, Mass%**	**Sulphur, ppm**	**Viscosity Index**
I (Solvent-refined mineral oil)	65–85	15–35	300–3000	80–119
II (Hydro-processed mineral oil)	≥93	<7	5–300	80–119
II (Hydro-cracked mineral oil)	≥95	<5	0–30	≥120
IV (Oligomers of Alkene), Synthetic hydrocarbons such as Polyalphaolefins (PAO)	-	-	-	-
V (Others not included in previous groups), such as plant oils	-	-	-	-

API Groups I-III are produced by distillation and refinery processes from crude oil (Papke, 2013). Because of their availability at a fair rate, mineral oils comprise the majority of base fluids today. The chemical contents in mineral oils are difficult to demonstrate because they differ with the processing area and the processes of the refinery. Viscosity, therefore, reflects the properties

of base oil. Conventionally, kinematic viscosity is considered for lubricants at 40ºC and at 100º.

In this context the most important property of base fluids is the viscosity index which is a temperature dependent property. If the temperature increases, the viscosity of liquids decreases. The viscosity index (VI) reflects the rate of temperature change (Michael, 2013). The "high" VI is defined as fewer viscosity variations due to changes in temperature, as shown in Figure 1.5. It is worth mentioning that there are two forms of viscosity commonly identified, kinematic and dynamic. Dynamic viscosity is the relationship between the shear stress and the shear rate of the fluid. Kinematic viscosity is the interaction between the viscous and the inertial forces of the fluid.

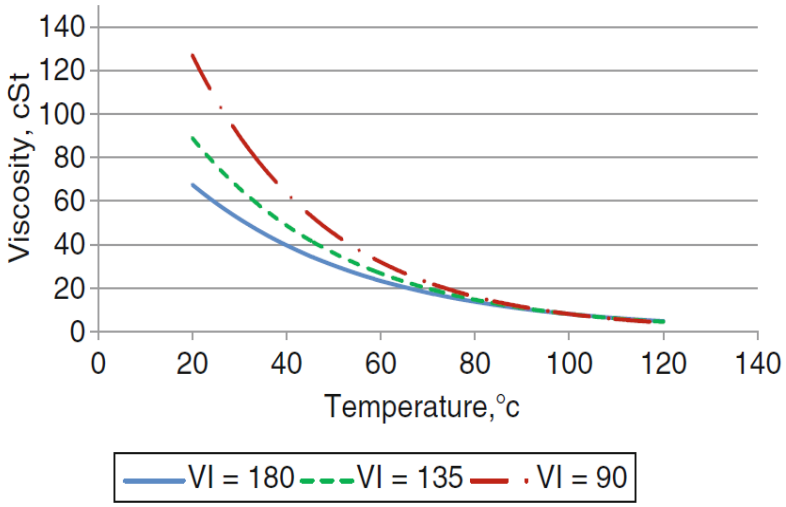

Figure 1.5 *Effect of VI on viscosity versus the behaviour of oils in temperature (Wang and Zhu, 2013).*

VI can be computed in accordance with ASTM D2270 as shown in Table 1.2 alongside other properties that describe key physical characteristics of lubricant oils.

Table 1.2 *Base oil physical properties and standard tests.*

Property	Importance	Measurement technique	ASTM NO.
Kinematic Viscosity	Define the viscosity grade of base oil	Capillary Viscometer for Gravity Flow	D445
VI	Describes viscosity-temperature relationship	Variability of viscosity between 40ºC and 100ºC, indexed	D2270
Specific Gravity	Defines oil density compared to water	Hydrometer	D1298
Flash Point	Defines the properties of high-temp volatility and flammability	Tester of the flash point, temp. The flash surface flame is achieved	D92/D93
Pour Point	Defines behaviour of low-temp oil fluidity	Gravity flow in test jar	D97/IP15

Almost all lubricants must comply with the viscosity requirements laid down by SAE, ISO and ASTM and with the performance requirements laid down by the various organizations for each type of lubricant listed below (Rizvi, 2009):

1. Transmission Fluids
   a) Automatic—OEMs
   b) Power—OEMs
2. Engine Oils
   a) Passenger vehicles—API, ACEA, JASO (Japan Automobile Standards Organization)
   b) Heavy-duty Diesel—API, OEMs
3. Automotive Gear Oils—API
4. Industrial Lubricants
   c) Anti-wear Hydraulic Fluids—OEMs, Government Agencies, Standards Organizations
   d) Industrial Gear Oils—AGMA
   e) R&O Turbine Oils—OEMs, U.S. Military, Technical Societies
5. Greases—NLGI

1.3.2 Conventional oil additives and modifiers

In practice base oil lubricants are never applied alone as it requires additional substance to improve and maintain its performance during operation. There are several types of lubricant additives available on the market. In most cases, they are marketed according to their key roles in lubrication systems. In the following sections, the main categories of additives are highlighted.

- Friction Modifiers (FM)

Generally, carboxylic acids with straight hydrocarbon chin (higher fatty acids) were the first known "lubricity-enhancing substances" to be dissolved in mineral oils (Bowden, Gregory and Tabor, 1945). Metal surfaces are typically coated with chemicals or oxide layers that can be extracted through rubbing. This exposes the active surfaces that communicate with the molecule of FM. Further rubbing provides the molecule with energy for surface reactions. It produces organic salt (carboxylic acid salt) and results in chemisorption (adsorption with chemical bond between adsorbent and adsorbent). Chemisorption has a good surface interaction compared to physisorption (Rowe, 1968)and is thus advantageous for the protection of the film against rubbing (Loehlé et al., 2015).

A few other lubricant additives take advantage of tribochemical reactions. The first step is to interact with the rubbing surface of additive molecules in a manner close to that of organic acids. In the next step, the difference emerges. As the tribo-process delivers enough energy to the molecule, the molecule decomposes into inorganic salts. As the reaction is associated with the dissociation of several chemical bonds, it requires comparatively higher energy than the chemisorption process. Inorganic salts (molybdenum disulphide for instance) are typically more robust than organic salts for heating and mechanical shearing. In comparison to the chemisorption mechanism, the organic moieties in the additive molecule were decomposed during the tribo-film formation (Minami, 2017).

- Anti-Wear Agents (AW)

It occurs under relatively harsh mixed lubrication conditions where the adsorption type FMs cannot support lubrication efficiency (Minami, 2017). Typically, hard materials are more resistant to wear than soft materials. Inorganic phosphates on steel surfaces are known as protective film (Guan, Pochopien and Wright, 2016). Zinc bis(dialkyldithiophosphates) (ZnDTPs) are the most used AWs in functional lubricants to date. Surface analysis of the working mechanism of the ZnDPTs showed the formation of inorganic compounds composed of phosphorus, sulphur, and zinc (Nicholls et al., 2005).

The mechanism relies on protective boundary film formation as it is experimentally confirmed (Parsaeian et al., 2016; Parsaeian et al., 2017).

- Extreme Pressure Additives (EP)

If tribological conditions are extreme, at higher loads and/or at higher temperatures, welding of the material can occur. EPs can stop such material failure when it comes to rubbing contact. EPs respond first to the surface, which is similar to Aws action. However, the substance does not protect the surface but gently eliminates the atoms on the upper surface (Minami, 2017). The role is known as "controlled wear." This is closely linked to the mechanism of "corrosive wear" where certain chemical compounds facilitate material wear. An example of such materials is dialkyl disulfide.

- Viscosity Modifiers (VM)

The properties of bulk lubricants depend on the structure of the base fluids. Thus, the rheological properties of lubricant can be tuned by the addition of thermal responsive materials such as VMs. VM is usually polymer in structure (Covitch, Weiss and Kreutzer, 1999). VM molecule can be packed compactly at lower temperatures, while it expands at higher temperatures. It is predicted that large-volume molecules would have resistance to flow, thus exhibiting high viscosity (Rizvi, 1999). The relevant temperature range of lubricants was expanded by the improvement of VMs. The stability under shearing is a technological challenge for advanced VMs (Snyder Jr et al., 1986).

- Pour Point Depressant

Lubricants can gum-up when the machine stops at low temperatures. This causes a lubricating failure and causes significant damage to system. Pour point depressant are useful for machines in cold climates. These substances are usually concentrated hydrocarbons (Minami, 2017). Each branched alkyl group can interact with oil molecules, preventing the crystallization of oil molecules together.

- Dispersants

These additives have the same role as the detergent soap component. That is, the polar pollutants are suspended from low oil solubility in the bulk lubricant. They do this by associating with these species through their polar ester or by imitating their functionality and keeping them dissolved in oil by associating with them through their non-polar hydrocarbon chains.

- Oxidation Inhibitors (Antioxidants)

These additives regulate the oxygen-induced degradation of the lubricant. They belong to three general classes: hydroperoxide decomposers, free radical decomposers, and metal deactivators. Hydroperoxide decomposers facilitate the decomposition of hydroperoxides to free radicals.

- Rust and Corrosion Inhibitors

These additives guard against the attack of oxygen, water, acids, bases, and salts on metal surfaces. They do this by physically adsorbing the metal surfaces through their polar functional group and by maintaining a resilient protective film on the surfaces by associating it with the lubricant.

- Detergents

They neutralize the acidic by-products of combustion and lubricant degradation and retain the precursors and pollutants that have low oil solubility in oil.

1.4 Nanolubricants

There has been a great interest in NPs for tribological applications over the last two decades. Studies have demonstrated remarkable lubricating properties, i.e., friction-reducing, and anti-wear, of certain NPs. Nanolubricant is a class of Nanofluids, which are defined as suspensions of NPs in base fluids (Sanukrishna et al., 2019). In the perspective of fully formulated nanolubricants, there are three main constituents that participate in its formation as illustrated below in Figure 1.6.

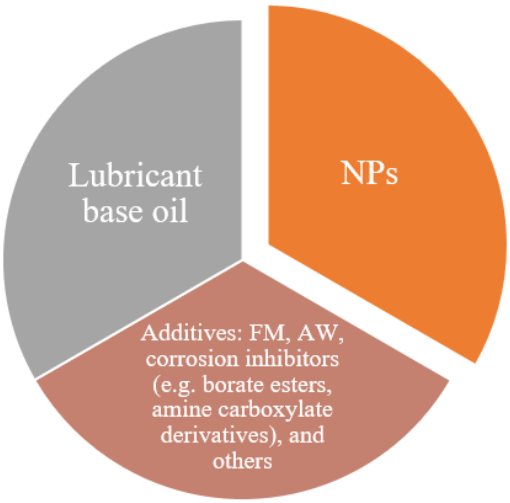

Figure 1.6 *Main constituents of fully formulated nanolubricants.*

The nanolubricants' manufacturers select these combination ratios and the nature of these fractions to achieve the desired tribological properties. Lubricant base oil nature in terms of polarity and intended application must be considered when selecting the suitable type of NPs, to achieve an acceptable compatibility level.

1.4.1 NPs for lubricants synthesis roots

Various forms of NPs have been developed and utilized as nanoadditives for lubricants: metals (e.g., Cu, Fe, Ag, Au, Zn), metal oxides (Al_2O_3, ZnO, TiO_2, SiO_2, CuO, Fe_3O_4, ZrO_2), Sulphides (MoS_2, WS_2, CuS), carbon-based nanoparticles (diamond, pristine graphene, graphene oxide, reduced graphene oxide, carbon nanotubes, fullerenes), nanocomposites (SiO_2/Cu, grapheme oxide /Cu, Al_2O_3/SiO_2, Al_2O_3/TiO_2, and rare earth compounds. Investigators have divided the methods of NPs synthesis into two main groups: physical methods and chemical methods.

The physical process of NPs synthesis requires the application of mechanical, pressure, thermal, electrical, or high-energy radiation. Various physical techniques include ball milling, inert gas condensation, electro-spraying, pulse vapor deposition, freezing, laser pyrolysis, flash spray pyrolysis. Chemical approaches include the synthesis of NPs by chemical reactions between separate precursors and solvents, decomposing them into atoms, accompanied by agglomeration into clusters (Schmidt, 2001). NPs size, morphology, stability is regulated by parameters such as precursor concentration, pH, calcification temperature (Tran and Nguyen, 2014).

1.4.2 Nanolubricants formulation methods

- Two-Step Method

The two-step method is the most used technique for formulating nanofluids. NPs are first produced as dry powders by chemical or physical methods. Then, the nano-sized powder, modified or not (Figure 1.7), is dispersed into the base fluid by several agitation techniques. These methods include intense magnetic force agitation, ultrasonic agitation, high-sharp mixing, high-pressure homogenisation, and ball milling. The two-step process is the most inexpensive method for manufacturing nanofluids on a wide scale since nano-powder synthesis methods have already been scaled to the level of industrial development. Due to the elevated surface area and surface activity, NPs tend to aggregate. However, a two-step approach may delay this phenomenon by employing intensive energy mixing techniques such as ultrasound. Additionally, stability is enhanced by adding suitable surface-active agents (dispersants) or modifying the NPs' surface (electrostatic or steric). Therefore, one of the main drawbacks of this method is the need to stabilise NPs.

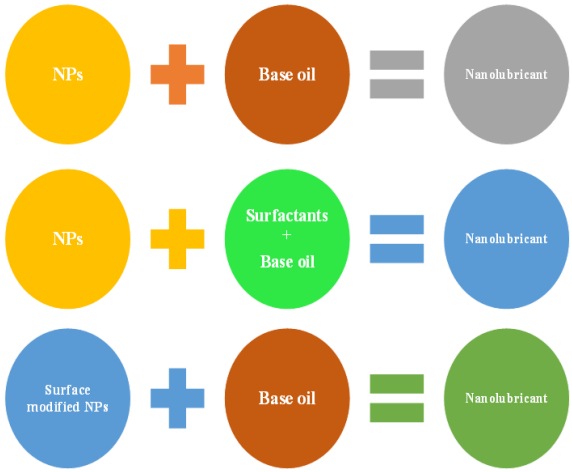

Figure 1.7 *Two-step Nanolubricants formulation options.*

Various research has been conducted on the nanolubricants with two-step synthesis. Battez et al. mixed ZnO NPs and dispersing agents in PAO6 with ultrasonic probe help(Hernandez Battez et al., 2006). Koshy et al. mixed modified CuO NPs with vegetable oils with ultrasonic shaker help(Koshy, Rajendrakumar, and Thottackkad, 2015).

- One-Step Method

The one-step method consists of the simultaneous production and dispersion of the particles in the fluid to minimise nanoparticles' agglomeration. This approach eliminates the process of cleaning, handling, transferring and dispersing nanoparticles, which minimises the agglomeration of NPs and improves the stabilisation of the fluids (Yu and Xie, 2012). The one-step processes can prepare uniformly dispersed NPs, and the particles can be stably suspended in the base fluid. Different studies have synthesised nanofluids by one step method, but the synthesis of nanolubricants have not been reported as much. However, few investigations have shown the synthesis of nanolubricants by one-step method. Ag NPs were dispersed in mineral oils, and the nanolubricant was stable for a month (Bönnemann et al., 2005). In this experiment, the particles were stabilised by Korantin, which co-ordinated the silver particle surfaces with two oxygen atoms forming a thin film around the particles. There are, however, several limitations to the one-step approach. The most significant drawback is that the residual reagents are left in the nanolubricant due to failed reactions or stabilisation. These residues could negatively affect the primary tribological functionalities and chemical stability of the different components of the fully formulated lubricating oil. Additionally, there is a significant difficulty in finding suitable precursors to synthesize desired NPs within lubricants, and hence it is not always chemically feasible.

1.4.3 Role of dispersion stability

When nanoparticles are added to a fluid media, their size is minimal enough that they remain distributed in liquids via Brownian motion. This is due to the random motion of particles, which was discovered by Robert Brown in 1905 and proved by Albert Einstein. Particles in suspension may adhere to one another and create larger agglomerates, which may settle due to gravity. Nanoparticle agglomeration causes not just sedimentation but also a loss of wear protection and friction reduction ability. As a result, dispersion stability is extremely important for consistent lubricating performance (Gulzar et al., 2016).

The strong Van der Waals interactions between NPs always favour the formation of aggregates and ultimately result in their sedimentation from the bulk phase (Azman and Samion, 2019). In order to increase the stability of nanomaterial dispersion, a number of repulsive approaches have also been envisaged to enhance the dispersion stability of nano additives in lubricating oils. This involves surface alteration by organic molecules, the use of surfactants or detergents. Coating nanoparticles with organic molecules is a simple way to stabilise them sterically and offers a tool for producing organic-inorganic – shell composites with adjustable surface properties. Organic molecules used as a capping agent typically have a polar group that can be chemisorbed on the surface of the inorganic nano-core; and a long alkyl chain helps inorganic nanoparticles dissolve in organic media (Lin, Wang and Chen,

2011). The stability and dispersion of NPs can also be improved by electrostatic control of the surface potential, the hydrophilic layer, and the increase of the steric obstruction of the particles obtained by the use of an effective surfactant. Various strategies are used to stabilise nano-dispersion of lubricants; the following section discusses their benefits and drawbacks.

- Surface modification methods

Components used are oleic acid, stearic acid, polyethene glycol, alkanethiols, octadecyl amine oleyl amine, lauric acid, alkenyl succinimide, amines, silane coupling agents.

- Advantages: do not considerably affect the physicochemical properties of NPs nor the lubricants.
- Disadvantages:

a) increase in the oil's viscosity at dispersion with surface-modified nanoparticles and the viscosity index at the upper threshold.
b) Mass production is a challenge and not cost-effective.
c) The tribo-performance of the particles are sometimes reduced/lost

- Surfactant aided dispersion

Typically uses surfactants such as sorbital monooleate (SPAN 80), Tween20, cuprammonium bromide (CTAB), sodium dodecyl sulphonate (SDS).

- Advantages:

d) Economical and straightforward system.
e) Well-developed approach.
f) Availability of a wide variety of surfactants.

- Disadvantages:

g) It can generate foams when it is heated
h) Competition between the molecules and the particles for the tribo-zone
i) At higher temperatures, the bonding between the surfactant and the nanoparticle may be weakened, resulting in nanoparticles' sedimentation.

While surface-modified nanomaterials have better dispersion stability, the process is chemical-intensive and, therefore, not very cost-effective. On the other hand, nanomaterials dispersed using traditional surfactants are well-standardised, cost-effective, and straightforward. This may be the reason why current surfactants have been used to maintain dispersion stability.

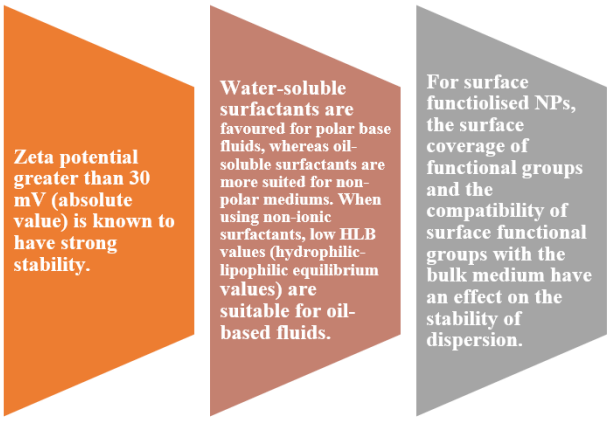

Figure 1.8 *Main consideration for improved dispersion stability. Zeta potential value is acquired from ref. (Gumustas et al., 2017).*

1.4.4 Nanoadditives tribological mechanism

In nanoadditives-containing oils, nanoparticles work through different tribological mechanisms. Although the specific nanoadditives role is still not fully clarified, since an analysis of the rubbed surfaces or in situ microscopy during tests are required for a complete understanding, experimental studies concluded that the mechanism depends on the nature of the particles, i.e. their structure, morphology, size, etc., and test conditions (Dassenoy, 2016).

NPs exhibit several tribological actions in lubricants, such as rolling, protective film formation, mending, sliding, sintering onto surfaces, and polishing, as depicted in Figure 1.9.

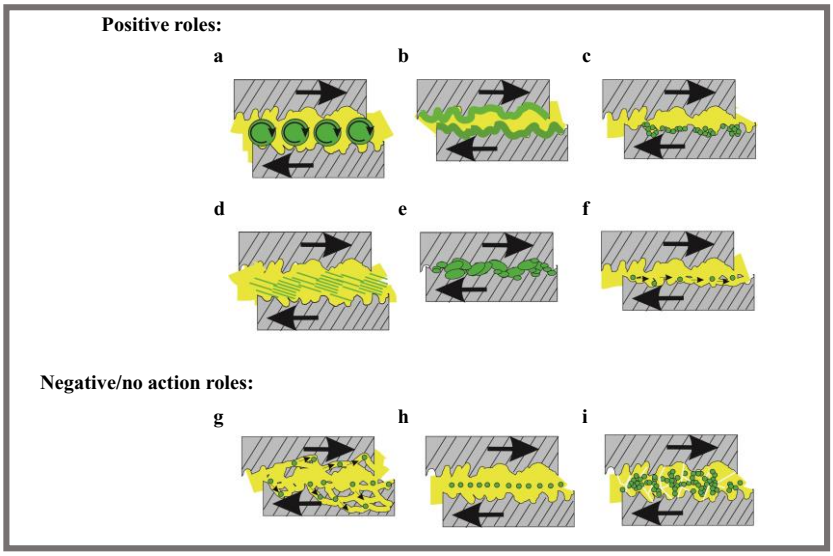

Figure 1.9 *Schematic depiction of tribological roles for NPs in lubricants, conceptualised from literature results: a) rolling, b) protective film formation, c) mending, d) sliding and shearing, e) sintering onto surfaces, f) polishing and smoothing, g) heavy abrasion on the surface, h) no tribo-interaction, i) NPs agglomeration at high concentrations resulting in negative effects.*

- Ball bearings effect

This role is played by the spherical or semi-spherical nanoparticles. Due to their intrinsic morphological properties, these nanoparticles can convert sliding friction between the mating surfaces into rolling friction, which results in a reduction of the friction coefficient (Laad and Jatti, 2018). The research about nano-lubricants with such a shape is still ongoing. Recently, it has been suggested that these nanoparticles could either roll or be embedded in the surface (Khadem et al., 2016). In particular, this study elucidated that nanoparticles behaviour depends on the differences between the hardness of the particles and the surfaces; revealing, for instance, that nano-diamonds are prone to be embedded into softer surfaces and roll on harder.

- Protective/tribofilm formation

The main hypothesis of this technique is based on the idea of the formation of a thin layer of nanoparticles on the tribo-contact zone. This layer will act as a barrier for the asperities and valleys of the contacting surfaces reducing the wear rate. An additional feature of this deposited film is the ease of shear, which can be attributed to lower friction between surfaces. The theory of tribo-film formation is considered the most dominant mechanism among the nanolubricants methods of operation: it was reported and proved in different

researches with various nanoparticles and characterization techniques (Demas et al., 2012; Padgurskas et al., 2013; Nallasamy et al., 2015). There are main parameters that affect the process of film formation, including the sufficiently small size of the dispersed nanoparticles, which must guarantee easy access to the sliding surfaces (Chen et al., 2013; Wu et al., 2016). Moreover, in the case of high loads conditions, additional tribo-chemical reactions can occur between sliding surfaces and nanoparticles (Wu, Zhai and Jie, 2009; Jifen, Wensheng and Guifen, 2010).

- Mending/repairing effect

This mechanism is important for the mechanical parts which fall under repetitive stress and may fail due to cracks. Cracks can exceed the tribo contact zone and propagate throughout the metal body. The mechanism works by filling and/or by sintering and melting small nanoparticles into the initiated macrocracks, thus reinforcing the metal surface. This effect was mentioned by several studies as a result of tribo-sintering of nanoparticle additives (Kato and Komai, 2007; Zhao et al., 2012; Flores-Castañeda et al., 2015).

- The polishing/smoothing effect

The accumulation of nanoparticles on the surface's valleys helps smooth the metal surfaces. This effect ultimately reduces friction and allows the lubricant oil to form more continuous and efficient films. This polishing effect was noticed by measuring the surface profile of test specimens before and after tests for pure lubricant oil and oil with nanoadditive, indicating a significant reduction of the surface roughness due to nanoparticles deposition (Lee et al., 2009; Chua Abdullah et al., 2014).

- Negative/ no action roles

In the case, NPs are not compatible with surface characteristics (hardness and roughness) abrasive effects may arise (Ge, Xia and Cao, 2015). Another key aspect influencing the lubricating properties of nanolubricants is the appropriate concentration (Luo et al., 2014; Koshy, Rajendrakumar and Thottackkad, 2015).In some situations, the inclusion of nanoparticles, either too little or too much, may have negative consequences by increasing friction or wear (Azman et al., 2016), or no role action.

1.4.5 NPs performance in selected lubricants

The selected lubricants refer to low-viscosity lubricants as reduced viscous flow is desired for futuristic applications such as electric vehicles and other advanced domains that require energy efficiency.

There is a significant challenge in reducing the lubricant viscosity, which results in thin oil films, contributing to increased sliding surface wear rate and contact of asperities (Turkson et al., 2016). Furthermore, this decreased film

thickness raises the operating temperature due to frequent surface contact and decreases the bearings' estimated fatigue life (Andrew, 2019). Additionally, reducing oil viscosity contributes to decreased oil's load caring capacity (Hamid et al., 2018). The increased frequency and intensity of mixed and boundary contact conditions with low-viscosity lubricants, mandate the utilisation of AF, AW, and EP additives as a practical solution. Some of the conventional additives commonly found in fully formulated oils working in such conditions are typically based on key organic compounds, including sulphurised olefins such as sulphurised isobutylene or dialkyl pentasulfide and phosphorus-containing compounds such as tricresyl phosphate (Rudnick, 2009; Johnson and Hils, 2013). However, these additives are poisonous and contain non-environmentally friendly chemical precursors with cost-intensive synthesis. In general, this transition from full film to boundary lubrication can give rise to the importance of NPs as additives, as an alternative solution for the industry while moving towards low-viscosity lubricants.

Usually, base oils have a viscosity range of 20-500 cSt at 40°C. However, as this literature scan is focused on the utilisation of NPs in the lower range from this viscosity spectrum, 70 cSt at 40°C is selected as the threshold for high temperature and high shear (HTHS), (Table 1.3). This pre-condition is satisfied by synthetic high-performance gear oils based on PAO as considered to be tried-and-tested lubricants. Additionally, a thorough discussion is performed on the utilisation of NPs in hydro lubricant as considered to be one of the future promising lubricants. Ionic liquids (ILs)are not considered here as most of their combination has a viscosity higher than 70 cSt at 40°C (Pensado, Comuñas and Fernández, 2008). Although ILs based on bis(trifluoromethylsulfonyl)amide have viscosity range of 12-60 cSt at 40°C (Pensado, Comuñas and Fernández, 2008), There is no available literature on NPs performance in them.

Table 1.3 *Literature scan on the ability of NPs in reducing wear scar diameter (WSD) and friction coefficient (COF) in different low viscosity lubricants. Besides, an indication of the different tribological mechanisms played by NPs. The blue highlighted rows signify the utilisation of NPs as mixtures to form composites. Abbreviations: NR, not relevant; WR, wear rate; CDs, carbon quantum dots; C coated, carbon-coated; GO, graphene oxide; OLC, onion-like carbon; MWCNTs-g PAM, multi-wall carbon nanotubes grafted with polyacrylamide.*

Type of NPs	Size	Type of base oil	Viscosity @ 40°C (cSt)	Reduction		Mechanism	References
				CoF	WSD		
Al_2O_3 **TiO_2**	8-12nm 10nm	PAO	54	50%	30%	Protective film	(Ashour et al., 2017)
MoS_2 (NTs)	D (100-500nm), L (NA)	PAO	30	50%	80%	Exfoliation of nano-sheets from nanotubes under shear stress and protective film.	(Kalin, Kogovšek and Remškar, 2012)
Ni	20nm	PAO	31	30%	45%	NA	(Chou et al., 2010)
CDs	2.2-3.5nm	PAO	46	30%	60%	Protective film	(Chimeno-Trinchet et al., 2020)
Cu (C coated)	25nm	PAO	31	29%	No effect	Rolling	(Viesca et al., 2011)
ZnO	20nm	PAO	31	NA	36%	Protective film	(Hernandez Battez et al., 2006)
CuS	4nm	Water	NR	78.3%	93.7%	Protective film	(Zhao et al., 2019)
Cu	3± 1nm	Water	NR	42%	17%	Protective film	(C. Zhang et al., 2014)
TiO_2	20nm	Water	NR	70.5%	84.3%	Protective film and rolling	(Pei et al., 2008a)
GO **OLC**	30-60nm 30-60nm	Water Water	NR NR	60% 50%	62% (WR) 25% (WR)	Protective film Rolling	(Wu et al., 2020)
CNC	50nm	Water	NR	75%	50%	Protective film and rolling	(Shariatzadeh and Grecov, 2019)
Al_2O_3	83-1061nm	Water	NR	50%	12%	NA	(Radice and Mischler, 2006)
MWCNTs-g PAM	D (60-80nm), L (NA)	Water	NR	45%	30%	Rolling	(Pei et al., 2008b)

1.4.5.1 NPs in Synthetic oil lubricants (PAO)

PAOs are commonly used in many industrial fields, such as automotive engine oil, vehicle gear oil, automotive automatic transmission fluid, industrial gear oil, and compressor oil. They have a robust operating temperature range due to its high viscosity index, good oxidation stability, shear stability and low corrosion efficiency (Chou et al., 2010). Additionally, PAO lubricants with a viscosity of 32 cSt at 40°C have shown superior performance in process pumps and their electric motor drivers (Morrison, Zielinsky and James, 1980). However, due to the downsides of low viscosity lubricants, researchers are trying to improve their performance by dispersing NPs into them.

The addition of the MoS_2 nanotubes to the base PAO oil was examined by Kalin, et al., resulting in a substantial improvement in friction and wear behaviour under boundary lubrication conditions (Kalin, Kogovšek and Remškar, 2012). The CoF was reduced by more than two times, while the wear was reduced by 5-9 times as much. In the observed period, nanotubes' use nearly completely removed any abrasion or deformation of the surfaces. The author's interesting mechanism is related to thin MoS_2 nano-sheets' surface adhesion, described in several steps, as shown in Figure 1.10.

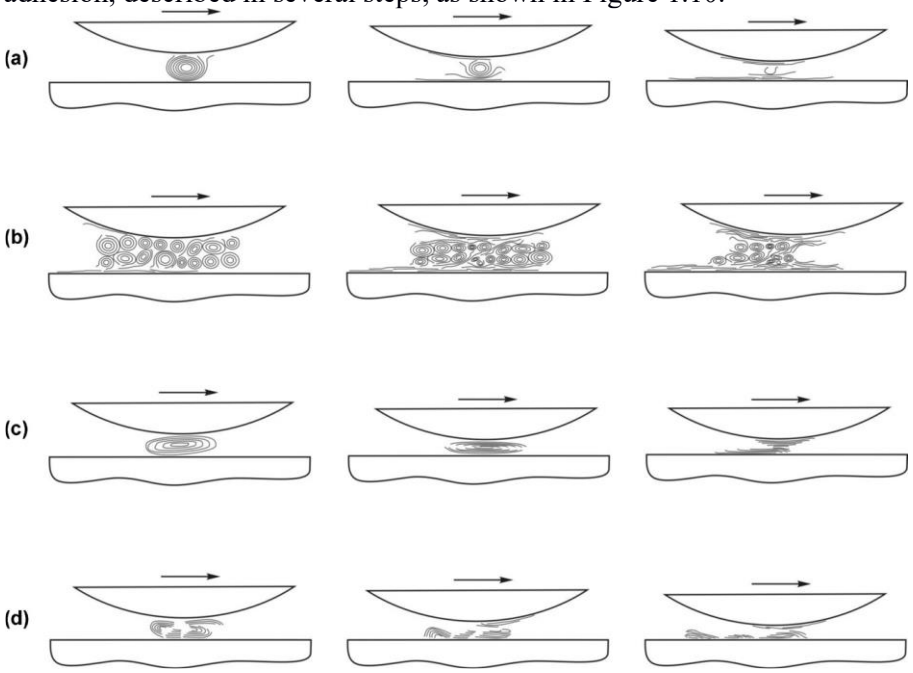

Figure 1.10 *Schematic presentation of the various mechanical routes for the exfoliation process: a) individual exfoliation of nanotubes; b) exfoliation of aggregate nano-sheets; c) exfoliation of nanotubes; d) breaking of nanotubes and exfoliation of smaller, broken multi-wall pieces. The sliding direction is shown by the arrows (Kalin, Kogovšek and Remškar, 2012).*

The impact of introducing Ni NPs of 20 nm in diameter on the tribological activity of synthetic oil (PAO6) was studied by Chou, et al. (Chou et al., 2010). Concerning PAO6, NPs suspensions reduced the average CoF and WSD. The reduction in friction was between 7 and 30 % and wear fell between 5 and 45 %. Regarding PAO6, the PAO6 + 0.5 % wt Ni suspension displayed the highest friction and wear reduction. Additionally, for all examined suspensions, the load-wear index is greater than that of the base oil, with increases between 3.4 % and 30.8 %. In another study, Ali, et al. examined the suspension of Al_2O_3, TiO_2 and Al_2O_3 / TiO_2 hybrid NPs in commercially available engine oil (5W-30) based on PAO for formulating nanolubricants at

a concentration of 0.25 wt.% (Ahmed Ali et al., 2016). Low kinematic viscosity and a 2% increase in the viscosity index were observed when adding NPs to the base oil. Tribological tests showed a 40-50% and 20-30% reduction in the ring's CoF and wear rate, respectively. The decrease in viscosity may be due to nanoparticles' presence between the layers of lube oil, facilitating the relative movement between the layers of nanolubricants.

Carbon quantum dots (CDs) were obtained directly from methyltrioctylammonium chloride by Chimeno-Trinchet, et al., which proved to be a good candidate as an additive in synthetic base oils (Chimeno-Trinchet et al., 2020). Adding 0.1% w/v of CDs in harsh lubrication regimes, decreased CoF by approximately 30% and WSD by more than 60% even under the most extreme conditions tested (120 N). Alternatively, Viesca, et al. analysed the effect on the tribological activity of PAO6 of the addition of 25 nm carbon-coated copper (Cu C_{coated}) NPs and contrasted this behaviour with the case of non-coated copper NPs, evaluating the impact of the coating (Viesca et al., 2011). The results showed that all suspensions decreased wear under mixed lubrication between 10 and 50% for PAO6. Moreover, under extreme pressure conditions, the load-wear index for all suspensions examined is higher than that of the base oil, with increases between 7 and 29%. This tribological enhancement is due to the deposition on the rubbing surfaces of nanoparticles and possibly through their function as small bearings. The copper nanoparticles coated with carbon did not behave better than the non-coated ones. Battez, et al. studied the tribological activity of ZnO NPs as an additive in PAO6 and the effect of commercial stabilising agent dispersing agents (OL100 and OL300) (Hernandez Battez et al., 2006). The findings showed that the best EP activity with 36% wear reduction was shown by PAO6 + 3% OL300 + 0.3% ZnO.

Regarding tribological behaviours of NPs as a function of viscosity in different lubrication conditions, it was found that, when the viscosity of raw oil was low under high normal load conditions, the addition of NPs additives to lubricant was more effective (Ku et al., 2010), as shown in Figure 1.11. Contradictory the addition of NPs to lubricants increases their viscosity, as Guimarey, et al. has investigated the viscosity behavoiur of synthetic oils and ZrO_2 NPs-based nanolubricants (Guimarey et al., 2018). The study was performed on dimethoxy end-capped poly(propylene glycol) and synthetic esters (isotridecyl trimellitate, TTM, and biodegradable polymer ester, BIOE). The results show that the density increases (around 2%) as the mass concentration of ZrO_2 nanoparticles increases. The same happens with the viscosity of nanolubricants; however, lubricants based on isotridecyl trimellitate ester have higher increments of up to 8 %. Furthermore, the decrease in particle size increases the viscosity of the fluid (Pastoriza-Gallego et al., 2011). This behaviour was also confirmed by Sui, et al. as the viscosity activity of silica NPs as lubricant additives have been affected by both functional groups and particle size (Sui et al., 2018).

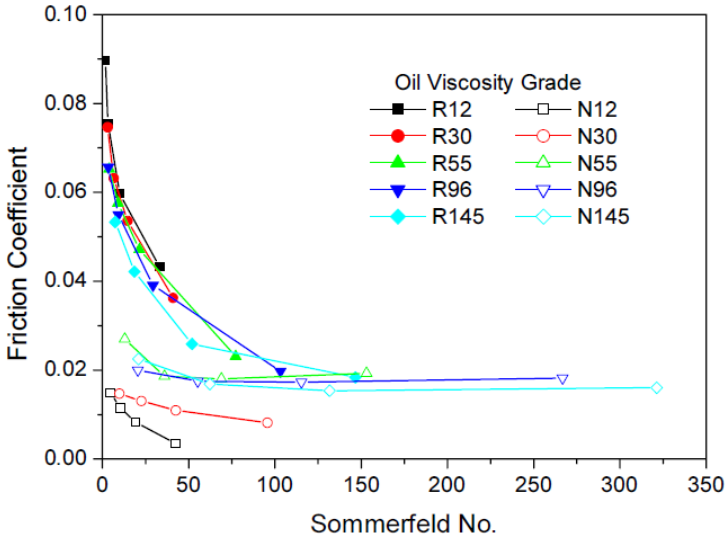

Figure 1.11 *The relationship between the coefficients of friction as a function of the grade of oil viscosity and the amount of Sommerfeld with raw oil (R) and nano-oil (N), (Ku et al., 2010).*

Another aspect that must be considered is NPs interactions with the relatively high polarity of ester base oils in contrast to mineral oils (Xiong et al., 2019). These base stocks' polar natures correlated with NPs detrimental effects on lubrication process (Alves et al., 2013). This negative attributed to the unfavourable polar compound findings are connected to the fact that the polar molecules will also attract metallic nanoparticles (Alves et al., 2013; Guzman Borda et al., 2018) , covering them with an oil film that prevents their ball-bearing role and their deposition. This hurdle can be overcome by surface functionalisation of NPs with non-polar compounds to minimise these interactions.

Most NPs are metal-based and therefore eco-unfriendly and are predominantly hydrophilic and hence unstable in organic media, which eventually contributes to aggregation/ sedimentation and the loss of good properties. Therefore, the efficient use of NPs must resolve problems such as the stability of dispersion and abrasiveness (Gulzar et al., 2016). It is not only a matter of using a lower-viscosity oil for the future developed oil groups, but also one that will preserve its viscosity under conditions of HTHS, in which NPs excel.

1.4.5.2 NPs in Hydro lubricants

Water is the obvious choice of essential raw material when looking for a product that can keep up with both general and industry-specific challenges: globally abundant, non-toxic, and non-flammable. The advantages are

apparent, but the tribological limitations are also prominent. These include not only extremely low viscosity, but also evaporation and freezing points, microbiological growth, oxidation, and corrosion. Water-based lubricants consisting of less than 5% additives may give many advantages compared to traditional oil and grease lubricants, such as high thermal conductivity, and oil cost savings (Pei et al., 2008b). Recent research has been dedicated to using different NPs as nanoadditives dispersed in water in order to enhance the lubrication capacity of water (A. He et al., 2017; A. He, Huang, Yun, et al., 2018a; Su, Chen and Huang, 2020).

Via modifying CuS NPs with Bis (2-hydroxyethyl) dithiocarbamic acid (HDA), Zhao, et al. prepared water-soluble CuS NPs as water-based lubricant additives (Zhao et al., 2019). The results show that HDA-CuS nanoparticles, as prepared, can effectively increase the tribological behaviour and thermal conductivity coefficient of distilled water. The CoF and wear rate are decreased by 78.3% and 93.7%, respectively, with a concentration of only 0.8 wt.%. It was found that, during the friction process, a complex lubricating film was created on the surface of the friction pairs. In a different study on Cu NPs capped by methoxylpolyethyleneglycol xanthate, formulated by Zhang, et al., used as an additive in distilled water (C. Zhang et al., 2014). The load-caring capacity value can be increased from 88 N of distilled water to 696 N by adding 5% wt. of these modified NPs. This increment is due to the formation of boundary lubrication film composed of Cu, FeS and FeSO4 on the rubbed steel surface.

In the presence of sodium-dodecyl-benzene-sulfonate (SDBS) and glycerol, Wu, et al. investigated the tribological efficiency of water-based NPs using TiO2 NPs, which exhibited outstanding dispersion stability and wettability (Wu et al., 2020). In contrast to pure water, the water-based nanolubricant containing 4 wt.% TiO_2 and 0.4 wt.% of SDBS showed superior tribological efficiency by minimising friction and ball wear coefficients by up to 70.5% and 84.3%, respectively. The lubrication mechanisms were primarily attributed to the TiO2 NPs' lubricating film formation and ball-bearing effect.

Su, et al. have investigated the lubricating performance of graphene oxide (GO) nano-sheets and onion-like (OLC) as lubricant additives in water (Su, Chen and Huang, 2020). Also, the effects of sandblasting of a steel disc were evaluated on the tribological behaviour. The results show that, when used as lubricant additives in the water, the two nanomaterials, GO and OLC, effectively reduce the friction and wear of sliding discs, which is independent of the treatment of the disc surface. It is noted that GO exhibits superior friction-reducing and antiwear capabilities when applying heavy loads compared to OLC. A trace amount of GO can achieve a lubricating capacity equivalent to an abundant OLC amount. OLC 's friction-reduction and antiwear capabilities in water can be due to its onion-like structure that induces rolling action and tribofilm formation during the process of sliding. The GO's excellent lubricating ability was due to the forming on the contact surfaces of

thin protective films and its 2D structure providing better shear and slipping between the two surfaces of mating wear.

The use of cellulose nanocrystals (CNC) as additives in water-based lubricants was investigated by Shariatzadeh, Mohammad Javad, and Dana Grecov (Shariatzadeh and Grecov, 2019). It was found that the addition of 2 wt.% of CNC in water improved lubrication and provided a very low Cof of approximately 0.09. The wear depth and width can reduce by more than 50%. The enhancement of the friction and wear coefficient was primarily due to the high strength and alignment of CNC rods, as indicated in Figure 1.12.

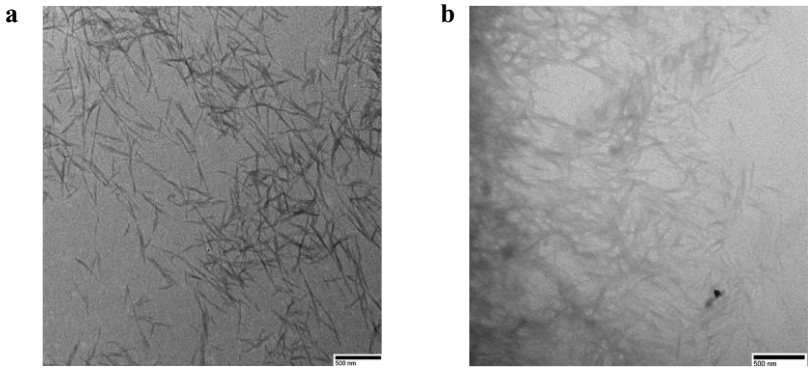

Figure 1.12 *Transmission electron microscope (TEM) images of 0.005 wt.% concentration CNC suspensions sonicated at 1000 J/g, a) prior to friction test, b) following friction test, (Shariatzadeh and Grecov, 2019).*

The effect of alumina NPs (Al_2O_3) suspended in an aqueous acetate buffer solution was studied by Radice, et al. By adding 10% volume of Al_2O_3 NPs to an acetate buffer solution, it was possible to minimise CoF by a factor of 2 and the wear of stainless steel by a factor of 10 (Radice and Mischler, 2006). Solutions containing either sedimented NPs or larger sized Al_2O_3 particles were less effective than stable suspensions in reducing wear and friction. Multi-walled carbon nanotubes (MWCNTs-g PAM) grafted with polyacrylamide (PAM), soluble in polar solvents such as water, tetrahydrofuran and acetone, were formed by Pei, et al. The results indicated that the composites exhibit strong antiwear and friction reduction properties as well as load-carrying capacity. This merit was due to the likelihood that the composites would behave during lubrication as nano-meter-sized small bearings (Pei et al., 2008b).

In the case of hydro lubrication, pH can also play a role in the tribological behaviour as He, et al. illustrated that the flexible and large GO sheets were broken down and reduced chemically when the pH increased from 3.1 to 9.7 (A. He et al., 2017). Besides, by using the 0.06 wt% GO suspension, noise and vibration were removed in tribological studies, while COF and WSD were decreased by 44.4% and 17.1% relative to baseline water, respectively. While the pH increases in the GO suspensions substantially increased COF and wear.

This different results under elevating pH were due to variation in the GO sheets' morphological and physicochemical properties.

The main challenge of utilising NPs as nanoadditive in hydro lubricants its poor dispersibility which is similar to that of oil-based lubricants (A. He, Huang, Yun, et al., 2018b) . Although efforts were made to decrease NPs high activity on the surface and avoid aggregation. Some problems, such as avoiding water evaporation, which changes the lubricant's concentration, are still to be solved (Chen et al., 2020).

1.4.6 Heat transfer attributes of NPs in nanofluids

Almost before one hundred- and fifty-years Maxwell's mixture states theory suggested that the suspension of solid particles in a liquid would significantly increase this liquid's effective thermal conductivity (Maxwell, 1881). Following these researchers used millimetre or micrometre particles dispersed in traditional heat transfer fluids in early studies (He et al., 2007). Even though these dispersions' thermal conductivity had increased, the practical application was impeded by stability and particles sedimentation. However, nano-sized particles have shown a superior stability and heat transfer performance compared to that of larger dimensions this is evident in many experimental studies that have been carried out on heat transfer of nanofluids (Hemmat Esfe, Yan, et al., 2016; Aberoumand et al., 2016; Nabil et al., 2018). Additionally, the studies have indicated that nanofluids' heat transfer is more than that calculated by the theoretical predictions (Hemmat Esfe, Hassani Ahangar, et al., 2016; Hemmat Esfe, Afrand, et al., 2016; Zadeh and Toghraie, 2018). This abnormality can be explained by the unfathomable large specific surface areas some of these NPs have, such as graphene that can have a specific surface area up to 2600 m^2/g (Chae et al., 2004), coupled with its outstanding thermal conductivity of roughly 5200 W/mK (Balandin et al., 2008).

The thermal improvement imposed by NPs dispersed into a base fluid can be classified into three main mechanisms as illustrated by Figure 1.13, that can be summarized by:

I. Enhanced liquid molecules organisation at NPs/liquid interface: Choi first observed this phenomenon, Choi, et al. when he produced suspensions of nanotubes-in-oil and measured their efficient thermal (Choi et al., 2001). With nanotube loadings, the measured thermal conductivity is anomalously more superb than theoretical predictions and is non-linear. For solid/liquid suspensions, the anomalous phenomena demonstrate the fundamental limits of conventional heat conduction models. The nature of heat conduction in nanotube suspensions and an organised structure at the

solid/liquid interface interprets this enhanced thermal conductivity as two consequences of nanotubes' presence in the liquid. Thus, it was hypothesised that such ordered liquid molecules could link through the interface to generate more efficient thermal transport (Yu et al., 1999; E. et al., 2015).

II. Brownian motion: Because of the surrounding liquid molecules' random collisions. It is expected that Brownian motion-induced particle collisions will increase heat transport between particle diffusion modes and thus increase the nanofluids' thermal conductivity (Keblinski et al., 2002; Wei, Zou and Li, 2017). The particles' Brownian motion can lead to convection of the surrounding base fluid and increase thermal conductivity (Prasher, Bhattacharya and Phelan, 2005).

III. Agglomeration of NPs: Suspended NPs, driven by their high surface energy, is forced to attract each other (Sarno et al., 2020). Since cluster structures allow more heat to be transported along the heat flux path, the heat conduction could be increased (Prasher et al., 2006). The conventional effective medium theory predicts the nanofluid has a more excellent thermal conductivity in these aggregates (Nan, 1993; Nan et al., 1997).

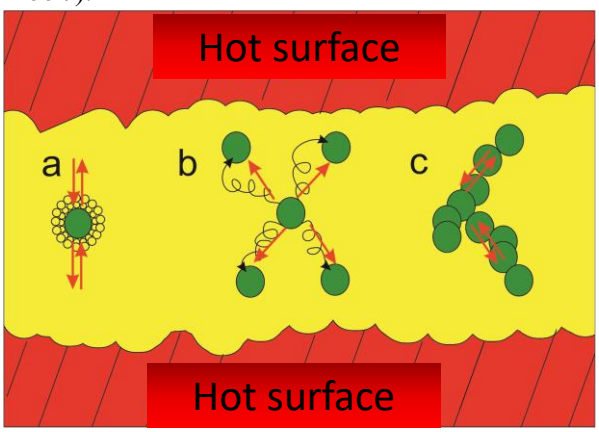

Figure 1.13 *Illustration graph about the suggested mechanisms of heat transfer induced by NPs in nanofluid, a) enhanced liquid molecules organisation at NPs/liquid interface, b) NPs Brownian motion, and c) agglomeration of NPs.*

1.4.6.1 Factors affecting thermal conductivity in nanofluids

Various studies have shown that the enhancement in different nanofluids' thermal conductivity relies on NP's concentration (Walvekar, Faris and

Khalid, 2012; Li et al., 2015; Karimi et al., 2015; Karamallah and Hussein., 2016), size (Prasher et al., 2006; Anoop, Sundararajan and Das, 2009), morphology (Jeong et al., 2013), base fluid nature (Tsai et al., 2008; Buongiorno et al., 2009), and temperature (Das et al., 2003; sen Gupta et al., 2011). Regarding NPs concentration in the base fluid, it seems that k increases with the addition of NPs in a linear manner (Li et al., 2015; Karimi et al., 2015; Mohamed, Tirth and Kamel, 2020). However, non-linear increases in thermal conductivity with nanoparticle volume fraction have also been reported (Xie, Yu and Chen, 2010). While the NPs size seems inversely proportional to k as decreasing the grain size, the heat transfer coefficient increases (Karamallah and Hussein., 2016). This inverse proportionality was confirmed by Liu, Kan. when investigating the impact of Cu NPs having a grain size of 25, 40-60 and 60-80 nm dispersed into PAO on heat transfer rate. The results showed that with the smallest particle size (25 nm), the coefficient of heat transfer was increased (Liu, 2011). Nevertheless, this behaviour is not always true, as smaller particles are expected to be more efficient. This phenomenon was confirmed as clusters formed in a uniform distribution due to aggregation of particles have also been found to enhance k of nanofluids better than individual NPs (Prasher et al., 2006).

Moreover, the morphology of NPs can be a factor in nanofluid performance as Jeong, et al. studied the ZnO nanofluids' thermal conductivity, which increased for the spherical and almost rectangular form NPs by up to 12% and 18% at 5.0 vol. %, compared to that of the water, respectively (Jeong et al., 2013). In differnt study conducted by Cui, et al. comparing spherical and cylindrical Cu NPs it was found that cylindrical NPs outperformed spherical NPs in the air with k enhancement of 20% and 14% respectively, in the air (Cui et al., 2011), attributed to the enhanced cylindrical shape micro-convection from rotational motion, increasing thermal conductivity.

Concerning base fluid nature, experimental results indicate that the Brownian motion and the convection-like action are very active in the low viscous base fluid and cause the measurable enhancement of thermal conductivity (Tsai et al., 2008). Additionally, NPs thermal conductivity improvement in PAO base fluids is higher than that of water-based fluids (Buongiorno et al., 2009).

The temperature rise, in nanofluid results in an upward trend in thermal conductivity (Nguyen et al., 2007; Aberoumand et al., 2016). This pattern is due to the rising bulk temperature, which is associated with an increase in the distribution of NPs in the base fluid, which promote the increasing Brownian motion of the NPS, therefore elevating the heat transfer of the base fluid.

In general, carbon-based nanofluids, particularly carbon nanotubes (CNT), have been known to outperform all metallic and metal oxide nanofluids in thermal conductivity (k), as shown in Figure 1.14, even in small concentrations (Patel et al., 2003; Li and Peterson, 2007; Lotfi and Shafii, 2009; Walvekar, Faris and Khalid, 2012), while graphene oxide outperforms pristine graphene in water base fluid due to the latter's poor stability in the

polar medium (Park and Kim, 2014). Gupta et al. measured the temperature-dependence thermal conductivity of graphene nanofluid. They stated that the thermal conductivity depended on the temperature, unlike the case of carbon nanotubes nanofluid (sen Gupta et al., 2011), which was attributed to Hybrid Brownian Motion-percolation.

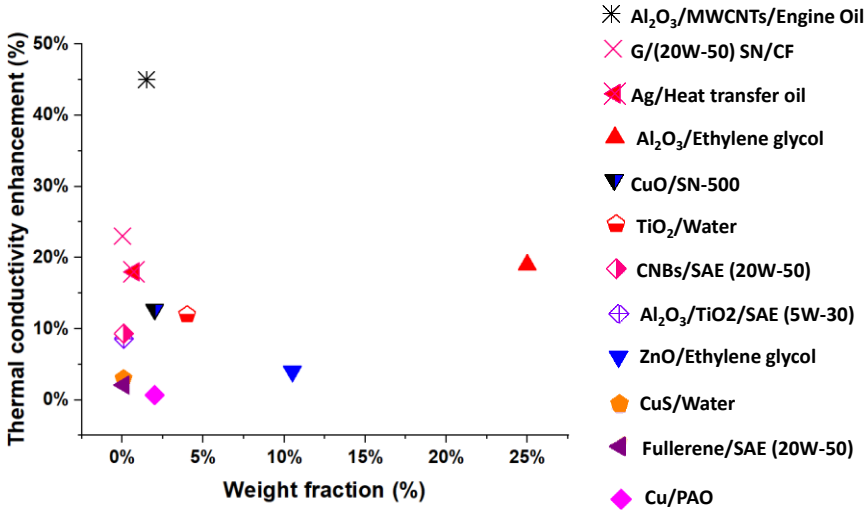

Figure 1.14 *Thermal conductivity enhancement of different NPs and different base fluids versus NPs wight fraction (Pastoriza-Gallego et al., 2011; Liu, 2011; Saeedinia, Akhavan-Behabadi and Razi, 2012; Ettefaghi, Rashidi, et al., 2013; Li et al., 2015; Aberoumand et al., 2016; Rasheed et al., 2016; Asadi et al., 2018; Zhao et al., 2019; Ali and Xianjun, 2020).*

1.4.6.2 Thermal conductivity enhancement of different NPs in different base fluids

Many scientific reports revealed the positive effects of adding different NPs, with different sizes, shapes and concentrations in a fluid in thermal conductivity improvement. Some of these studies are summarised in Table 1.4, for instance, the thermal conductivity of Al_2O_3 in ethylene glycol nanofluids was experimentally determined by Pastoriza-Gallego, et al., as a function of volume concentration and temperature (Pastoriza-Gallego et al., 2011).

Thermal conductivity is found to increase with the concentration of NPs, while increasing the temperature, viscosity decreases, and the thermal conductivity increases with improvements of up to 19 %. In different investigation Wei, Baojie, Changjun Zou, and Xiaoke Li. Studied TiO_2 NPs dispersed in diathermic oil(Wei, Zou and Li, 2017) (Wei, Zou and Li, 2017).

The thermal conductivity of nanofluids was tested, and the results showed that the thermal conductivity of TiO_2 nanofluids was greater than that of the base fluid. Also, there was a linear association between the change in thermal conductivity and the rise in NPs concentration. Two of the significant variables affecting the thermal conductivity of TiO_2 nanofluids are the nature of heat transfer in NPs and Brownian motion. Thermogravimetric analysis conducted by Ali, Mohamed Kamal Ahmed, and Hou Xianjun., revealed that when utilising Al_2O_3/TiO2 hybrid in reference oil (SAE 5W-30), the oxidation initiation temperature and burnout temperature can be delayed by 54°C and 38°C respectively (Ali and Xianjun, 2020). Additionally, compared to the reference oil, the Al_2O_3/TiO_2 nano lubricants showed an improvement in heat transfer characteristics and by 9-14 % (Ali and Xianjun, 2020).

Table 1.4 *Literature scan on the ability of NPs in thermal conductivity enhancement in different base fluids. Also, the concentrations in which these NPs are used is reported. The blue highlighted rows signify the utilisation of NPs as mixtures to form composites. Abbreviations: G, graphene; CNBs, carbon nanoballs; MWCNT, multi-wall carbon nanotubes.*

Type of NPs	Size	Type of base oil	Concentration	Thermal conductivity enhancement	References
Al_2O_3 **TiO_2**	10nm 8-12nm	SAE (5W-30)	0.1 wt.%	3.9-8.6%	(Ali and Xianjun, 2020)
Al_2O_3 **MWCNTs**	20 nm D (10-20nm), L (10-30nm)	Engine Oil	1.5 wt.%	45%	(Asadi et al., 2018)
Al_2O_3 **SiO_2**	13nm 30nm	Polyalkylene glycol	0.1 vol.%	2.4%	(Zawawi et al., 2019)
Al_2O_3	40-50nm	Ethylene glycol	25 wt.%	19%	(Pastoriza-Gallego et al., 2011)
TiO_2	10nm	Water	4 vol.%	12%	(Hojjat et al., 2011)
TiO_2	10nm	Diathermaic oil	1.0 vol.%	8%	(Wei, Zou and Li, 2017)
SiO_2	20-30nm	Water- Ethylene glycol	5 vol.%	45.5	(Esfahani and Toghraie, 2017)
Cu	25nm	PAO	2 wt.%	0.7%	(Liu, 2011)
CuO	50nm	SN-500	2 wt.%	12.7%	(Saeedinia, Akhavan-Behabadi and Razi, 2012)
CuS	4nm	Water	0.08 wt.%	3%	(Zhao et al., 2019)
ZnO	30nm	Ethylene glycol	10.5 wt.%	4%	(Li et al., 2015)
G	12nm	(20W-50) SN/CF	0.01wt.%	23%	(Rasheed et al., 2016)
MWCNTs	D (20-50nm), L (NA)	Ethylene glycol Synthetic oil	1.0 vol.% 2.0 vol.%	12.4% 30%	(Liu et al., 2005)
CNBs	70 nm	SAE (20W-50)	0.1 wt.%	9.3%	(Ettefaghi, Rashidi, et al., 2013)
Dimond	30-50nm	Ethylene glycol	1.3 Vol.%	75%	(Kang, Kim and Oh, 2006)
Fullerene	10nm	SAE (20W-50)	0.1 wt.%	2.1%	(Ettefaghi, Rashidi, et al., 2013)
Ag	20nm	Heat transfer oil	0.72wt.%	18%	(Aberoumand et al., 2016)

Liu, et al. examined thermal conductivity enhancements in ethylene glycol and synthetic oil in the presence of multiwalled carbon nanotubes (MWCNTs) (Liu et al., 2005). The study used the volume concentration of suspensions of MWCNTs-ethylene glycol of 1.0 vol. % and that of suspensions of MWCNTs -synthetic engine oil of 2.0 vol. %. Thermal conductivity is increased by 12.4 % for MWCNTs -ethylene glycol. On the other hand, thermal conductivity is increased by 30 % for MWCNTs -synthetic engine oil suspension. In another study that utilised MWCNTs done by Ahmadi, et al., it was functionalised by dodecylamine to avoid their agglomeration and precipitation in the base oil (SAE 20W-50). It dispersed using the planetary

ball mill (Ettefaghi, Ahmadi, et al., 2013). Thermal conductivity improved by 22.7 % at a concentration of 0.5 wt.% of MWCNTs. This shift can be attributed to the improved stability in the base oil bulk phase induced by fictionalisation. However, the rise in nanoadditive concentrations due to agglomeration and nanotubes precipitation has decreased the oil's lubricating properties. Asadi assessed the Al2O3/MWCNT combination in engine oil nanolubricant heat transfer efficiency over various temperatures (25-50°C) and NPs ratios (0.125%-1.5%), (Asadi et al., 2018). The thermal conductivity with the temperature and solid concentration increased up to 10% compared to the pure oil.

Rasheed, et al. experimented on nano lubricants formulated using graphene nanoflakes (G) and engine oil compliant with API 20W-50 SN/CF and API 20W-50 SJ/CF requirements (Rasheed et al., 2016). The addition of 0.01 % graphene to API 20W-50 SN/CF results in a thermal conductivity (k) increase of 23% at 80 C. Besides, in the presence of graphene, a 70% improvement in the engine's heat transfer rate is also achieved. In an experimental scan Rashidi, et al. studied the thermal activity of various carbon nanostructures when applied to SAE 20W-50 oil, including MWCNTs, G, carbon nanoballs (CNBs) and fullerene nanoparticles (C60) (Ettefaghi, Rashidi, et al., 2013). CNBs exhibited superior performance in enhancing the coefficient of thermal conductivity and the base fluid's flashpoint by 9.3% and 18%, respectively at 0.1 wt. % in concentration. Hwang studied NPs with different natures, Hwang, et al. to boost thermal conductivity and lubrication, including MWCNTs, fullerene, CuO, SiO_2, and Ag (Hwang et al., 2006). DI water, ethylene glycol, gasoline, silicon oil and PAO were used as base fluids. This study's findings concluded that with growing particle volume fraction, nanofluid thermal conductivity increases except for water-based fullerene nanofluid as it was lower than that of pure DI water.

Saeedinia, et al. prepared stable CuO-Base oil nanofluids with various fractions of particle weight of 0.25 to 2% for thermal properties investigation in different flow conditions (Saeedinia, Akhavan-Behabadi and Razi, 2012). For 2 wt. % nanofluid at the highest Reynolds number tested, a maximum increase of 12.7 % in the heat transfer coefficient was observed. Alternatively, in a recent study performed by Zhao, et al., showed that when applying water-soluble CuS modified NPs to water, its thermal conductivity can be increased by 3%, coupled with friction heat reduction which resulted in tribological performance enhancement (Zhao et al., 2019). The modification was done by Bis (2-hydroxyethyl) dithiocarbamic acid (HDA) to ensure the water solubility of NPs. Esfahani, M. A., and Toghraie, D. analysed SiO_2 and Water-Ethylene glycol thermal conductivity as the base nanofluid, measured in the temperature range of 25-50°C with volume fractions of 0.1, 0.5, 1, 1.5, 2, 3, and 5 % (Esfahani and Toghraie, 2017). According to the measurements, thermal conductivity improved as temperature and volume fraction increased. Also, a higher cumulative effect on thermal conductivity was shown by

volume fraction. The results also showed that at 50°C, the maximum thermal conductivity (45.5 %) took place in the 5 % volume fraction. Zawawi, et al. investigated the thermo-physical properties of Al_2O_3/SiO_2 (50:50, hybrid) in polyalkylene glycol (PAG) nanolubricant for various NPs ratios at 30-80°C temperatures (Zawawi et al., 2019). At the 80°C temperature, a maximum thermal conductivity gain of 2.41 % occurred.

Li, et al. prepared ethylene glycol (EG)-based nanofluids containing ZnO NPs, with different mass fractions of between 1.75% and 10.5% (Li et al., 2015). The experimental results show that as the temperature rises from 15 to 55°C, the thermal conductivity increases slightly. It relies heavily on the concentration of particles and increases non-linearly with the concentration within the range studied. Sharma, et al. demonstrated that, relative to pure ethylene glycol, the thermal conductivity of Ag NPs nanofluid with concentrations of 1000 ppm, 5000 ppm, and 10,000 ppm increased to 10%, 16%, and 18% respectively (Sharma et al., 2011). In conclusion, the increase in thermal conductivity of nanofluids relies mainly on the volume fraction of the suspended NPs and the temperature range adopted in the experiments. Simultaneously, carbon-based NPs have excellent properties in boosting thermal conductivity compared to other types of NPs. This dominance is evident from the literature overview as other NPs need to be employed in an elevated concentration to achieve the same effect of carbon-based NPs.

1.5 References

ABEROUMAND, S. et al. (2016) Experimental study on the rheological behavior of silver-heat transfer oil nanofluid and suggesting two empirical based correlations for thermal conductivity and viscosity of oil based nanofluids. *Applied Thermal Engineering*, 101, pp. 362–372.

AHMED ALI, M.K. et al. (2016) Enhancing the thermophysical properties and tribological behaviour of engine oils using nano-lubricant additives. *RSC Advances*, 6(81), pp. 77913–77924.

ALI, M.K.A. and XIANJUN, H. (2020) Improving the heat transfer capability and thermal stability of vehicle engine oils using Al2O3/TiO2 nanomaterials. *Powder Technology*, 363, pp. 48–58.

ALVES, S.M. et al. (2013) Tribological behavior of vegetable oil-based lubricants with nanoparticles of oxides in boundary lubrication conditions. *Tribology International*, 65, pp. 28–36.

ANDREW, J.M. (2019) The future of lubricating greases in the electric vehicle era. *Tribology & Lubrication Technology*, pp. 38–44.

ANOOP, K.B., SUNDARARAJAN, T. and DAS, S.K. (2009) Effect of particle size on the convective heat transfer in nanofluid in the developing region. *International Journal of Heat and Mass Transfer*, 52(9–10), pp. 2189–2195.

ARCHARD, J.F. (1980) "Wear theory and mechanisms." In: *Wear control handbook*. p. 58.
ASADI, A. et al. (2018) Heat transfer efficiency of Al2O3-MWCNT/thermal oil hybrid nanofluid as a cooling fluid in thermal and energy management applications: An experimental and theoretical investigation. *International Journal of Heat and Mass Transfer*, 117, pp. 474–486.
ASHOUR, M.E. et al. (2017) Novel Tribological Behavior of Hybrid MWCNTs/MLNGPs as an Additive on Lithium Grease. *Journal of Tribology*, 139(4), [Online] Available from: doi.org/10.1115/1.4035345.
AZMAN, N.F. and SAMION, S. (2019) Dispersion Stability and Lubrication Mechanism of Nanolubricants: A Review. *International Journal of Precision Engineering and Manufacturing-Green Technology*, 6(2), pp. 393–414.
AZMAN, S.S.N. et al. (2016) Study of tribological properties of lubricating oil blend added with graphene nanoplatelets. *Journal of Materials Research*, 31(13), pp. 1932–1938.
BALANDIN, A.A. et al. (2008) Superior Thermal Conductivity of Single-Layer Graphene. *Nano Letters*, 8(3), pp. 902–907.
BLAU, P.J. (2008) *Friction science and technology: from concepts to applications*. CRC press.
BÖNNEMANN, H. et al. (2005) Monodisperse copper- and silver-nanocolloids suitable for heat-conductive fluids. *Applied Organometallic Chemistry*, 19(6), pp. 768–773.
BOWDEN, F.P., GREGORY, J.N. and TABOR, D. (1945) Lubrication of Metal Surfaces by Fatty Acids. *Nature*, 156(3952), pp. 97–101.
BUONGIORNO, J. et al. (2009) A benchmark study on the thermal conductivity of nanofluids. *Journal of Applied Physics*, 106(9), p. 094312.
BURWELL, J.T. (1957) Survey of possible wear mechanisms. *Wear*, 1(2), pp. 119–141.
CARNES, K. (2005) The ten greatest events in tribology history. *Tribology & Lubrication Technolog*, 61(6), p. 38.
CELIS, J.-P., PONTHIAUX, P. and WENGER, F. (2006) Tribo-corrosion of materials: Interplay between chemical, electrochemical, and mechanical reactivity of surfaces. *Wear*, 261(9), pp. 939–946.
CHAE, H.K. et al. (2004) A route to high surface area, porosity and inclusion of large molecules in crystals. *Nature*, 427(6974), pp. 523–527.
CHEN, W. et al. (2020) Macroscopic Friction Studies of Alkylglucopyranosides as Additives for Water-Based Lubricants. *Lubricants*, 8(1), p. 11.
CHEN, Y. et al. (2013) Preparation of Nickel-Based Nanolubricants via a Facile In Situ One-Step Route and Investigation of Their Tribological Properties. *Tribology Letters*, 51(1), pp. 73–83.
CHIMENO-TRINCHET, C. et al. (2020) New metal-free nanolubricants based on carbon-dots with outstanding antiwear performance. *Journal of Industrial and Engineering Chemistry*, 87, pp. 152–161.

CHOI, S.U.S. et al. (2001) Anomalous thermal conductivity enhancement in nanotube suspensions. *Applied Physics Letters*, 79(14), pp. 2252–2254.
CHOU, R. et al. (2010) Tribological behavior of polyalphaolefin with the addition of nickel nanoparticles. *Tribology International*, 43(12), pp. 2327–2332.
CHUA ABDULLAH, M.I.H. et al. (2014) Effect of hBN/Al2O3 Nanoparticle Additives on the Tribological Performance of Engine Oil. *Jurnal Teknologi*, 66(3), [Online] Available from: doi.org/10.11113/jt.v66.2685.
CORPORATION, N. (2014) Lubricant Additives - A Practical Guide. *Machinery Lubrication*.
COVITCH, M.J., WEISS, J. and KREUTZER, I.M. (1999) Low-temperature rheology of engine lubricants subjected to mechanical shear: Viscosity modifier effects. *Lubrication Science*, 11(4), pp. 337–364.
CUI, W. et al. (2011) On the Influencing Factors and Strengthening Mechanism for Thermal Conductivity of Nanofluids by Molecular Dynamics Simulation. *Industrial & Engineering Chemistry Research*, 50(23), pp. 13568–13575.
DARMINESH, S.P. et al. (2017) Recent development on biodegradable nanolubricant: A review. *International Communications in Heat and Mass Transfer*, 86, pp. 159–165.
DAS, S.K. et al. (2003) Temperature Dependence of Thermal Conductivity Enhancement for Nanofluids. *Journal of Heat Transfer*, 125(4), pp. 567–574.
DASSENOY, F. (2016) Applications I: Nanolubricants. In: *Nanosciences and Nanotechnology*. Cham: Springer International Publishing, pp. 175–181.
DEMAS, N.G. et al. (2012) Tribological Effects of BN and MoS2 Nanoparticles Added to Polyalphaolefin Oil in Piston Skirt/Cylinder Liner Tests. *Tribology Letters*, 47(1), pp. 91–102.
E., E.J.M. et al. (2015) Cerium oxide–ethylene glycol nanofluids with improved transport properties: Preparation and elucidation of mechanism. *Journal of the Taiwan Institute of Chemical Engineers*, 49, pp. 183–191.
ESFAHANI, M.A. and TOGHRAIE, D. (2017) Experimental investigation for developing a new model for the thermal conductivity of Silica/Water-Ethylene glycol (40%–60%) nanofluid at different temperatures and solid volume fractions. *Journal of Molecular Liquids*, 232, pp. 105–112.
ETTEFAGHI, E., AHMADI, H., et al. (2013) Preparation and thermal properties of oil-based nanofluid from multi-walled carbon nanotubes and engine oil as nano-lubricant. *International Communications in Heat and Mass Transfer*, 46, pp. 142–147.
ETTEFAGHI, E., RASHIDI, A., et al. (2013) Thermal and rheological properties of oil-based nanofluids from different carbon nanostructures. *International Communications in Heat and Mass Transfer*, 48, pp. 178–182.
FLORES-CASTAÑEDA, M. et al. (2015) Bismuth nanoparticles synthesized by laser ablation in lubricant oils for tribological tests. *Journal of Alloys and Compounds*, 643, pp. S67–S70.

GAO, J. et al. (2004) Frictional Forces and Amontons' Law: From the Molecular to the Macroscopic Scale. *The Journal of Physical Chemistry B*, 108(11), pp. 3410–3425.

GUAN, B., POCHOPIEN, B.A. and WRIGHT, D.S. (2016) The chemistry, mechanism and function of tricresyl phosphate (TCP) as an anti-wear lubricant additive. *Lubrication Science*, 28(5), pp. 257–265.

GUIMAREY, M.J.G. et al. (2018) Effect of ZrO2 nanoparticles on thermophysical and rheological properties of three synthetic oils. *Journal of Molecular Liquids*, 262, pp. 126–138.

GULZAR, M. et al. (2016) Tribological performance of nanoparticles as lubricating oil additives. *Journal of Nanoparticle Research*, 18(8), p. 223.

GUMUSTAS, M. et al. (2017) Effect of Polymer-Based Nanoparticles on the Assay of Antimicrobial Drug Delivery Systems. In: *Multifunctional Systems for Combined Delivery, Biosensing and Diagnostics*. Elsevier, pp. 67–108.

SEN GUPTA, S. et al. (2011) Thermal conductivity enhancement of nanofluids containing graphene nanosheets. *Journal of Applied Physics*, 110(8), p. 084302.

GUZMAN BORDA, F.L. et al. (2018) Experimental investigation of the tribological behavior of lubricants with additive containing copper nanoparticles. *Tribology International*, 117, pp. 52–58.

HAMID, Y. et al. (2018) Numeric based low viscosity adiabatic thermo-tribological performance analysis of piston-skirt liner system lubrication at high engine speed. *Tribology International*, 126, pp. 166–176.

HAMROCK, B.J., SCHMID, S.R. and JACOBSON, B.O. (2004) *Fundamentals of Fluid Film Lubrication*. CRC Press.

HE, A. et al. (2017) The pH-dependent structural and tribological behaviour of aqueous graphene oxide suspensions. *Tribology International*, 116, pp. 460–469.

HE, A. et al. (2018a) Tribological Characteristics of Aqueous Graphene Oxide, Graphitic Carbon Nitride, and Their Mixed Suspensions. *Tribology Letters*, 66(1), p. 42.

HE, A. et al. (2018b) Tribological Characteristics of Aqueous Graphene Oxide, Graphitic Carbon Nitride, and Their Mixed Suspensions. *Tribology Letters*, 66(1), p. 42.

HE, Y. et al. (2007) Heat transfer and flow behaviour of aqueous suspensions of TiO2 nanoparticles (nanofluids) flowing upward through a vertical pipe. *International Journal of Heat and Mass Transfer*, 50(11–12), pp. 2272–2281.

HEMMAT ESFE, M., AFRAND, M., et al. (2016) An experimental study on viscosity of alumina-engine oil: Effects of temperature and nanoparticles concentration. *International Communications in Heat and Mass Transfer*, 76, pp. 202–208.

HEMMAT ESFE, M., HASSANI AHANGAR, M.R., et al. (2016) Designing an artificial neural network to predict dynamic viscosity of aqueous nanofluid

of TiO2 using experimental data. *International Communications in Heat and Mass Transfer*, 75, pp. 192–196.

HEMMAT ESFE, M., YAN, W.-M., et al. (2016) Estimation of thermal conductivity of Al2O3/water (40%)–ethylene glycol (60%) by artificial neural network and correlation using experimental data. *International Communications in Heat and Mass Transfer*, 74, pp. 125–128.

HERNANDEZ BATTEZ, A. et al. (2006) The tribological behaviour of ZnO nanoparticles as an additive to PAO6. *Wear*, 261(3–4), pp. 256–263.

HERTZ, H.R. (1882) "About the contact of solid elastic bodies and about hardness." In: *Negotiation of the Association for the Promotion of the GewerbefleiBes*. Berlin, p. 449.

HÖGLUND, E. (1999) Influence of lubricant properties on elastohydrodynamic lubrication. *Wear*, 232(2), pp. 176–184.

HOJJAT, M. et al. (2011) Thermal conductivity of non-Newtonian nanofluids: Experimental data and modeling using neural network. *International Journal of Heat and Mass Transfer*, 54(5–6), pp. 1017–1023.

HOLMBERG, K. and MATTHEWS, A. (2009) *Coatings tribology: properties, mechanisms, techniques and applications in surface engineering*. Elsevier.

HUNTER, M. (2014) *Fifth Annual Corporate Member Profiles Issue*.

HWANG, Y. et al. (2006) Thermal conductivity and lubrication characteristics of nanofluids. *Current Applied Physics*, 6, pp. e67–e71.

JEONG, J. et al. (2013) Particle shape effect on the viscosity and thermal conductivity of ZnO nanofluids. *International Journal of Refrigeration*, 36(8), pp. 2233–2241.

JIFEN, W., WENSHENG, Z. and GUIFEN, J. (2010) Preparation and tribological properties of tungsten disulfide hollow spheres assisted by methyltrioctylammonium chloride. *Tribology International*, 43(9), pp. 1650–1658.

JOHNSON, D. and HILS, J. (2013) Phosphate Esters, Thiophosphate Esters and Metal Thiophosphates as Lubricant Additives. *Lubricants*, 1(4), pp. 132–148.

JOHNSON, K.L. (1997) Adhesion and friction between a smooth elastic spherical asperity and a plane surface. In: *Proceedings of the Royal Society of London. Series A: Mathematical, Physical and Engineering Sciences*. pp. 163–179.

JOST, H.P. (1966) *Tribology; Education and Research; Report on the Present Position and Industry's Needs (submitted to the Department of Education and Science by the Lubrication Engineering and Research)*.

KALIN, M., KOGOVŠEK, J. and REMŠKAR, M. (2012) Mechanisms and improvements in the friction and wear behavior using MoS2 nanotubes as potential oil additives. *Wear*, 280–281, pp. 36–45.

KANG, H.U., KIM, S.H. and OH, J.M. (2006) Estimation of Thermal Conductivity of Nanofluid Using Experimental Effective Particle Volume. *Experimental Heat Transfer*, 19(3), pp. 181–191.

KARAMALLAH, A.A. and HUSSEIN., A.A. (2016) Convective heat transfer and stability of oil–based nanofluid. *ndian Journal of Science and Technology*, 48(9).

KARIMI, A. et al. (2015) Experimental investigation on thermal conductivity of water based nickel ferrite nanofluids. *Advanced Powder Technology*, 26(6), pp. 1529–1536.

KATO, H. and KOMAI, K. (2007) Tribofilm formation and mild wear by tribo-sintering of nanometer-sized oxide particles on rubbing steel surfaces. *Wear*, 262(1–2), pp. 36–41.

KEBLINSKI, P. et al. (2002) Mechanisms of heat flow in suspensions of nano-sized particles (nanofluids). *International Journal of Heat and Mass Transfer*, 45(4), pp. 855–863.

KHADEM, M. et al. (2016) Ultra-thin carbon-based nanocomposite coatings for superior wear resistance under lubrication with nano-diamond additives. RSC Advances, 6(62), pp. 56918–56929.

KITA, T. and YAMAMOTO, Y. (1997) Fretting Wear Performance of Lithium 12-Hydroxystearate Greases for Thrust Ball Bearing in Reciprocation Motion. *apanese Journal of Tribology*, 42(6), p. 773.

KOSHY, C.P., RAJENDRAKUMAR, P.K. and THOTTACKKAD, M.V. (2015a) Analysis of Tribological and Thermo-Physical Properties of Surfactant-Modified Vegetable Oil-Based CuO Nano-Lubricants at Elevated Temperatures - An Experimental Study. *Tribology Online*, 10(5), pp. 344–353.

KOSHY, C.P., RAJENDRAKUMAR, P.K. and THOTTACKKAD, M.V. (2015b) Evaluation of the tribological and thermo-physical properties of coconut oil added with MoS 2 nanoparticles at elevated temperatures. *Wear*, 330–331, pp. 288–308.

KU, B.-C. et al. (2010) Tribological effects of fullerene (C60) nanoparticles added in mineral lubricants according to its viscosity. *International Journal of Precision Engineering and Manufacturing*, 11(4), pp. 607–611.

KVEREL, E. and DILOYAN, G. (2019) Inorganic fullerene-like particles and inorganic tubular-like particles in fluids and lubricants and applications to subterranean drilling.

LANDMAN, U., LUEDTKE, W.D. and GAO, J. (1996) "Atomic-scale issues in tribology: interfacial junctions and nano-elastohydrodynamics." *Langmuir*, 12(19), pp. 4514–4528.

LAAD, M. and JATTI, V.K.S. (2018) Titanium oxide nanoparticles as additives in engine oil. Journal of King Saud University - Engineering Sciences, 30(2), pp. 116–122.

LEE, C.-G. et al. (2009) A study on the tribological characteristics of graphite nano lubricants. *International Journal of Precision Engineering and Manufacturing*, 10(1), pp. 85–90.

LI, C.H. and PETERSON, G.P. (2007) The effect of particle size on the effective thermal conductivity of Al2O3-water nanofluids. *Journal of Applied Physics*, 101(4), p. 044312.

LI, H. et al. (2015) Experimental investigation of thermal conductivity and viscosity of ethylene glycol based ZnO nanofluids. *Applied Thermal Engineering*, 88, pp. 363–368.

LIN, J., WANG, L. and CHEN, G. (2011) Modification of Graphene Platelets and their Tribological Properties as a Lubricant Additive. *Tribology Letters*, 41(1), pp. 209–215.

LIU, K. (2011) *Heat transfer measurement in oil-based nanofluids.*

LIU, M.-S. et al. (2005) Enhancement of thermal conductivity with carbon nanotube for nanofluids. *International Communications in Heat and Mass Transfer*, 32(9), pp. 1202–1210.

LOEHLÉ, S. et al. (2015) Mixed lubrication of steel by C18 fatty acids revisited. Part I: Toward the formation of carboxylate. *Tribology International*, 82, pp. 218–227.

LOTFI, H. and SHAFII, M.B. (2009) Boiling heat transfer on a high temperature silver sphere in nanofluid. *International Journal of Thermal Sciences*, 48(12), pp. 2215–2220.

LUAN, B. and ROBBINS, M.O. (2009) Hybrid Atomistic/Continuum Study of Contact and Friction Between Rough Solids. *Tribology Letters*, 36(1), pp. 1–16.

LUO, T. et al. (2014) Tribological properties of Al2O3 nanoparticles as lubricating oil additives. *Ceramics International*, 40(5), pp. 7143–7149.

MANSOT, J.L. et al. (2009) Nanolubrication. *Brazilian Journal of Physics*, 39(1a), [Online] Available from: doi.org/10.1590/S0103-97332009000200011.

MAXWELL, J.C. (1881) A Treatise on Electricity and Magnetism: pt. III. Magnetism. pt. IV. Electromagnetism. *Clarendon press*, 2.

MICHAEL, J. (2013) Covitch Viscosity Index Additives. In: WANG, Q. and CHUNG, Y. (eds.) *Encyclopedia of Tribology*.

MINAMI, I. (2017) Molecular Science of Lubricant Additives. *Applied Sciences*, 7(5), p. 445.

MOHAMED, A., TIRTH, V. and KAMEL, B.M. (2020) Tribological characterization and rheology of hybrid calcium grease with graphene nanosheets and multi-walled carbon nanotubes as additives. *Journal of Materials Research and Technology*, 9(3), pp. 6178–6185.

MORRISON, F.R., ZIELINSKY, J. and JAMES, R. (1980) Effects of Synthetic Fluids on Ball Bearing Performance. *ASME Publication*, 80.

NABIL, M.F. et al. (2018) Experimental investigation of heat transfer and friction factor of TiO2-SiO2 nanofluids in water:ethylene glycol mixture. *International Journal of Heat and Mass Transfer*, 124, pp. 1361–1369.

NALLASAMY, P. et al. (2015) Tribological investigations on MoS 2 -based nanolubricant for machine tool slideways. *Proceedings of the Institution of Mechanical Engineers, Part J: Journal of Engineering Tribology*, 229(5), pp. 559–567.

NAN, C.-W. et al. (1997) Effective thermal conductivity of particulate composites with interfacial thermal resistance. *Journal of Applied Physics*, 81(10), pp. 6692–6699.
NAN, C.-W. (1993) Physics of inhomogeneous inorganic materials. *Progress in Materials Science*, 37(1), pp. 1–116.
NGUYEN, C.T. et al. (2007) Temperature and particle-size dependent viscosity data for water-based nanofluids – Hysteresis phenomenon. *International Journal of Heat and Fluid Flow*, 28(6), pp. 1492–1506.
NICHOLLS, M.A. et al. (2005) Review of the lubrication of metallic surfaces by zinc dialkyl-dithiophosphates. *Tribology International*, 38(1), pp. 15–39.
P. SUH, N. (1973) The delamination theory of wear. *Wear*, 25(1), pp. 111–124.
PADGURSKAS, J. et al. (2013a) Tribological properties of lubricant additives of Fe, Cu and Co nanoparticles. *Tribology International*, 60, pp. 224–232.
PADGURSKAS, J. et al. (2013b) Tribological properties of lubricant additives of Fe, Cu and Co nanoparticles. *Tribology International*, 60, pp. 224–232.
PALIWAL, R., BABU, R.J. and PALAKURTHI, S. (2014) Nanomedicine Scale-up Technologies: Feasibilities and Challenges. *AAPS PharmSciTech*, 15(6), pp. 1527–1534.
PAPKE, B.L. (2013) "Mineral Oil Base Fluids." In: WANG, Q. and CHUNG, Y. (eds.) *Encyclopedia of Tribology*. New York: Springer.
PARK, S.S. and KIM, N.J. (2014) Influence of the oxidation treatment and the average particle diameter of graphene for thermal conductivity enhancement. *Journal of Industrial and Engineering Chemistry*, 20(4), pp. 1911–1915.
PARSAEIAN, P. et al. (2017) A new insight into the interfacial mechanisms of the tribofilm formed by zinc dialkyl dithiophosphate. *Applied Surface Science*, 403, pp. 472–486.
PARSAEIAN, P. et al. (2016) An experimental and analytical study of the effect of water and its tribochemistry on the tribocorrosive wear of boundary lubricated systems with ZDDP-containing oil. *Wear*, 358–359, pp. 23–31.
PASTORIZA-GALLEGO, M. et al. (2011) Thermal conductivity and viscosity measurements of ethylene glycol-based Al2O3 nanofluids. *Nanoscale Research Letters*, 6(1), p. 221.
PATEL, H.E. et al. (2003) Thermal conductivities of naked and monolayer protected metal nanoparticle based nanofluids: Manifestation of anomalous enhancement and chemical effects. *Applied Physics Letters*, 83(14), pp. 2931–2933.
PEI, X. et al. (2008a) Synthesis of water-soluble carbon nanotubes via surface initiated redox polymerization and their tribological properties as water-based lubricant additive. *European Polymer Journal*, 44(8), pp. 2458–2464.
PEI, X. et al. (2008b) Synthesis of water-soluble carbon nanotubes via surface initiated redox polymerization and their tribological properties as water-based lubricant additive. *European Polymer Journal*, 44(8), pp. 2458–2464.

PENSADO, A.S., COMUÑAS, M.J.P. and FERNÁNDEZ, J. (2008) The Pressure–Viscosity Coefficient of Several Ionic Liquids. *Tribology Letters*, 31(2), pp. 107–118.

PERSSON, B.N.J. (2006) Contact mechanics for randomly rough surfaces. *Surface Science Reports*, 61(4), pp. 201–227.

PERSSON, B.N.J. et al. (2005) On the nature of surface roughness with application to contact mechanics, sealing, rubber friction and adhesion. *Journal of Physics: Condensed Matter*, 17(1), pp. R1–R62.

PERSSON, B.N.J. (1993) Theory of friction and boundary lubrication. *Physical Review B*, 48(24), pp. 18140–18158.

PERSSON, B.N.T. (2014) History of Tribology. In: *Encyclopedia of Lubricants and Lubrication*. Berlin, Heidelberg: Springer Berlin Heidelberg, pp. 791–797.

PRASHER, R. et al. (2006) Effect of aggregation on thermal conduction in colloidal nanofluids. *Applied Physics Letters*, 89(14), p. 143119.

PRASHER, R., BHATTACHARYA, P. and PHELAN, P.E. (2005) Thermal Conductivity of Nanoscale Colloidal Solutions (Nanofluids). *Physical Review Letters*, 94(2), p. 025901.

RABINOWICZ, E. (1995) *"Friction and Wear of Materials, Jhon Wiley & Sons."* Inc., New York.

RADICE, S. and MISCHLER, S. (2006) Effect of electrochemical and mechanical parameters on the lubrication behaviour of Al2O3 nanoparticles in aqueous suspensions. *Wear*, 261(9), pp. 1032–1041.

RASHEED, A.K. et al. (2016) Heat transfer and tribological performance of graphene nanolubricant in an internal combustion engine. *Tribology International*, 103, pp. 504–515.

RIZVI, S.QA. (1999) Additives for automotive fuels and lubricants. *Tribology & Lubrication Technology*, 55(4), p. 33.

RIZVI, S.QA. (2009) *"Lubricant chemistry, technology, selection, and design."* ASTM International, Conshohocken.

ROWE, G.W. (1968) The chemistry of tribology, friction, lubrication and wear. *Royal Institute of Chemistry, Reviews*, 1(2), pp. 135–204.

RUDNICK, L.R. (2009) *Lubricant additives: chemistry and applications*. CRC press.

SAEEDINIA, M., AKHAVAN-BEHABADI, M.A. and RAZI, P. (2012) Thermal and rheological characteristics of CuO–Base oil nanofluid flow inside a circular tube. *International Communications in Heat and Mass Transfer*, 39(1), pp. 152–159.

SANUKRISHNA, S.S. et al. (2019) Enhancing the thermophysical properties of PAG lubricant using graphene nano-sheets. In: *Journal of Physics: Conference Series*. p. 012041.

SARNO, M. et al. (2020) rGO/GO Nanosheets in Tribology: From the State of the Art to the Future Prospective. *Lubricants*, 8(3), p. 31.

SHARIATZADEH, M. and GRECOV, D. (2019) Aqueous suspensions of cellulose nanocrystals as water-based lubricants. *Cellulose*, 26(7), pp. 4665–4677.

SHARMA, P. et al. (2011) Enhancement of thermal conductivity of ethylene glycol based silver nanofluids. *Powder Technology*, 208(1), pp. 7–19.
SNYDER JR, C.E. et al. (1986) Development of a shear stable viscosity-index improver for use in hydrogenated polyalphaolefin-based fluids. *Lubrication engineering*, 42(9), pp. 547–557.
STACHOWIAK, G. and BATCHELOR, A.W. (2013) *Engineering tribology*. Butterworth-Heinemann.
STRIBECK, R. (1902) "Die wesentlichen eigenschaften der gleit-und rollenlager." *Zeitschrift des Vereines Deutscher Ingenieure*, 46, pp. 1341–1348.
SU, F., CHEN, G. and HUANG, P. (2020) Lubricating performances of graphene oxide and onion-like carbon as water-based lubricant additives for smooth and sand-blasted steel discs. *Friction*, 8(1), pp. 47–57.
SUI, T. et al. (2018) Dispersibility and rheological behavior of functionalized silica nanoparticles as lubricant additives. *Ceramics International*, 44(15), pp. 18438–18443.
TSAI, T.-H. et al. (2008) Effect of viscosity of base fluid on thermal conductivity of nanofluids. *Applied Physics Letters*, 93(23), p. 233121.
TURKSON, R. et al. (2016) Modeling and Multi-Objective Optimization of Engine Performance and Hydrocarbon Emissions via the Use of a Computer Aided Engineering Code and the NSGA-II Genetic Algorithm. *Sustainability*, 8(1), p. 72.
UFLYAND, I.E., ZHINZHILO, V.A. and BURLAKOVA, V.E. (2019) Metal-containing nanomaterials as lubricant additives: State-of-the-art and future development. *Friction*, 7(2), pp. 93–116.
VIESCA, J.L. et al. (2011) Antiwear properties of carbon-coated copper nanoparticles used as an additive to a polyalphaolefin. *Tribology International*, 44(7–8), pp. 829–833.
WALVEKAR, R., FARIS, I.A. and KHALID, M. (2012) Thermal conductivity of carbon nanotube nanofluid-Experimental and theoretical study. *Heat Transfer-Asian Research*, 41(2), pp. 145–163.
WANG, Q.J. and ZHU, D. (2013) Surface Texture Generation with a Numerical Process. In: *Encyclopedia of Tribology*. Boston, MA: Springer US, pp. 3493–3498.
WEI, B., ZOU, C. and LI, X. (2017) Experimental investigation on stability and thermal conductivity of diathermic oil based TiO2 nanofluids. *International Journal of Heat and Mass Transfer*, 104, pp. 537–543.
WU, H. et al. (2020) Novel water-based nanolubricant with superior tribological performance in hot steel rolling. *International Journal of Extreme Manufacturing*, 2(2), p. 025002.
WU, J.F., ZHAI, W.S. and JIE, G.F. (2009) Preparation and tribological properties of WS 2 nanoparticles modified by trioctylamine. *Proceedings of the Institution of Mechanical Engineers, Part J: Journal of Engineering Tribology*, 223(4), pp. 695–703.

WU, L. et al. (2016) Tribological properties of oleic acid-modified zinc oxide nanoparticles as the lubricant additive in poly-alpha olefin and diisooctyl sebacate base oils. *RSC Advances*, 6(74), pp. 69836–69844.

XIE, H., YU, W. and CHEN, W. (2010) MgO nanofluids: higher thermal conductivity and lower viscosity among ethylene glycol-based nanofluids containing oxide nanoparticles. *Journal of Experimental Nanoscience*, 5(5), pp. 463–472.

XIONG, S. et al. (2019) Tribological behavior of mineral and synthetic ester base oil containing MoS2 nanoparticles. *Journal of Dispersion Science and Technology*, pp. 1–10.

YAN, Y. (2010) Tribology and tribo-corrosion testing and analysis of metallic biomaterials. In: *Metals for Biomedical Devices*. Elsevier, pp. 178–201.

YU, C.-J. et al. (1999) Observation of Molecular Layering in Thin Liquid Films Using X-Ray Reflectivity. *Physical Review Letters*, 82(11), pp. 2326–2329.

YU, W. and XIE, H. (2012) A Review on Nanofluids: Preparation, Stability Mechanisms, and Applications. *Journal of Nanomaterials*, 2012, pp. 1–17.

ZADEH, A.D. and TOGHRAIE, D. (2018) Experimental investigation for developing a new model for the dynamic viscosity of silver/ethylene glycol nanofluid at different temperatures and solid volume fractions. *Journal of Thermal Analysis and Calorimetry*, 131(2), pp. 1449–1461.

ZAWAWI, N.N.M. et al. (2019) Experimental investigation on stability and thermo-physical properties of Al2O3–SiO2/PAG nanolubricants with different nanoparticle ratios. *Journal of Thermal Analysis and Calorimetry*, 135(2), pp. 1243–1255.

ZHANG, C. et al. (2014) Preparation and Tribological Properties of Surface-Capped Copper Nanoparticle as a Water-Based Lubricant Additive. *Tribology Letters*, 54(1), pp. 25–33.

ZHAO, F. et al. (2012) Tribological properties of serpentine, La(OH)3 and their composite particles as lubricant additives. *Wear*, 288, pp. 72–77.

ZHAO, J. et al. (2019) A Simple Preparation of HDA-CuS Nanoparticles and Their Tribological Properties as a Water-Based Lubrication Additive. *Tribology Letters*, 67(3), p. 88.

ZHU, D. and WANG, Q. (2013) *"EHL history (elastohydrodynamic lubrication)."* Springer.

ZHURAVLEV, V.PH. (2013) On the history of the dry friction law. *Mechanics of Solids*, 48(4), pp. 364–369.

Chapter II. Industrial challenges for transmission lubrications and environmental aspects

2.1 Transmissions lubrication

Transmissions or gears are machines parts in which teeth are cut across cylindrical or cone-shaped surfaces with equal space. They are used to transfer rotations and pressures from the driving shaft to the driven shaft by meshing a pair of toothed-wheels. Throughout the industrial sector, gears play a crucial role; among the different applications in which they are used, we remember, for example, mixers, conveyors, extruders, dosers, and overhead cranes.

Gears can be categorised by form as involute, cycloidal or trochoidal gears. Often, shaft positions may be categorised as parallel shaft gears, intersecting shaft gears, and non-parallel and non-intersecting shaft gears. In the following section, the primary classification of gears is presented (Figure 2.1).

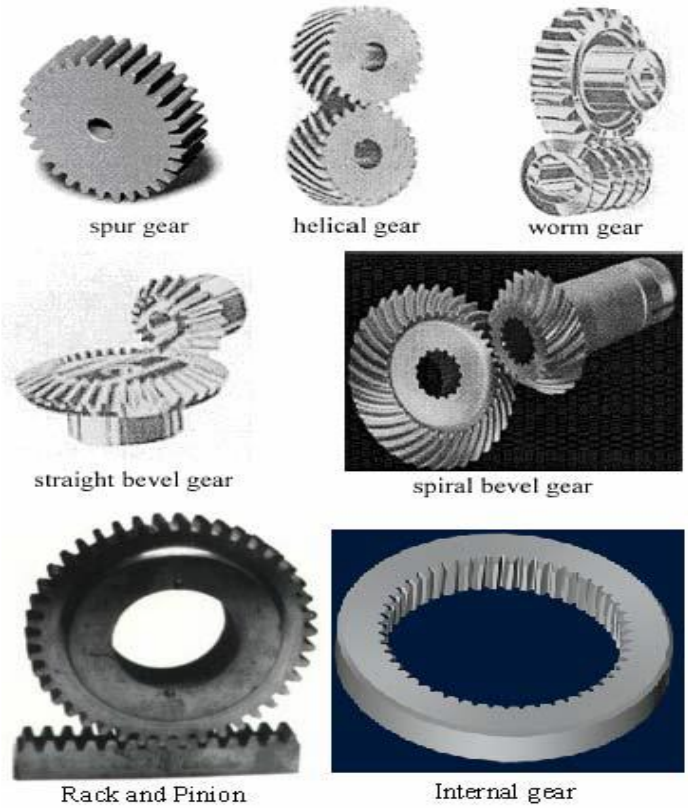

Figure 2.1 *Different industrial gears (Safavi et al., 2007).*

• Spur gear

Gears with cylindrical pitch surfaces are considered cylindrical gears. Spur gears fit into the parallel shaft gear group which are cylindrical gears with a tooth line that is flat and parallel to the shaft. Spur gears are the most commonly used gears that can reach high precision with relatively simple manufacturing processes. They have the characteristic of having no axial load (thrust load).

• Helical gear

Helical gears are used with parallel shafts like to spur gears which are cylindrical gears with winding tooth lines. They have stronger teeth than spur gears and have superior quietness and can transmit higher loads, making them ideal for high-speed applications. When helical gears are used, they produce a thrust force in the axial direction, involving thrust bearings. Helical gears come with a right hand and a left-hand twist involving opposite hand gear for a meshing pair.

• Gear rack

The same size and shaped teeth cut at similar intervals over a flat surface or straight rod are called a gear rack. The gear rack is a cylindrical gear, the radius of the pitch cylinder being infinite. It transforms rotational motion into linear motion by meshing with a cylindrical gear pinion. Gear racks can be commonly categorised into straight tooth racks and helical tooth racks, but all have straight tooth lines.

- Straight bevel gear

Bevel gears have a cone-shaped design and are used to transfer force between two shafts which intersect at one point (intersecting shafts). The bevel gear has a cone as its pitch surface, and the teeth are cut along the cone.

- Spiral bevel gear

Spiral bevel gears are bevel gears with a bent tooth. They are better than straight bevel gears in performance, strength, vibration, and noise because of the higher tooth contact ratio.

- Worm gear

The screw form of the shaft is the worm, the mating gear is the worm wheel, and together on the non-intersecting shafts, the worm gear is called the worm gear. Worms and worm wheels are not restricted to cylindrical shapes. There is a form of an hourglass that can improve the contact ratio, but manufacturing becomes more difficult, owing to the sliding touch of the gear surfaces, friction must be minimised.

- Internal gear

Internal gears have teeth cut on the interior of cylinders or cones which are connected with external gears. The primary use of the internal gears is for planetary gear drives and gear form shaft couplings.

2.1.1 Transmissions lubrication and challenges

In recent years, advanced gearbox technologies and OEMs have specified the necessary gear oils to satisfy these new designs' lubrication specifications. Modern gearboxes work under harsh conditions while retaining their durability to ensure the competitiveness of end-users. The new generation of automotive gear lubricants must improve efficiency even under extreme operational conditions for maximum durability and decreased operating costs.

Gears work with mixed slipping and rolling motion above and below the pitch line. Under low-speed and high-temperature settings, the EHL layer will be comparatively thin, and boundary conditions will prevail (McKenna et al., 2010). Knowing this high VI is one of the critical characteristics that a lubricant must provide to be appropriate for these applications (ExxonMobil, 2018). It guarantees a sufficient thickness of the lubricant layer, to isolate the contact surfaces entirely under high pressure. The use of additives is another

significant thing to consider. The requisite characteristics for the lubrication of the gear can be described as (McKenna et al., 2010):

- The optimum viscosity at operating temperatures to ensure the lubricant application to all touch surfaces and the creation of an EHL film at operating speeds and loads.
- Sufficient low-temperature fluidity to allow circulation at the lowest planned start-up temperature.
- Chemical durability to reduce oxidation under high temperatures and agitation in the presence of oxygen and to have the desired lubrication life for maintenance intervals.
- Strong de-miscibility to allow water separation to be extracted.
- Strong anti-wear efficiency in guarding against wear in boundary lubrication.
- Extreme pressure additives to reduce metal welding under excessive loads.
- Low traction in order to monitor operating temperatures under extreme operation.
- Anti-rust properties to protect gears and bearing surfaces from rust.
- Non-corrosive chemistry is such that gears and bearings are not subject to a lubricant chemical attack.
- Foam resistance to allow the air to be isolated from the lubricant.
- Compatibility for seals that are widely used.

In reality, if not correctly chosen, they can have dramatic results resulting in a pronounced phenomenon of micropitting. Through ad hoc experimental investigations, it has been shown that the use of additives for typical extreme pressures can accentuate the phenomenon of micropitting (Hochmann and Siebert, 2012). For example, in worm gears, the screw is usually made of steel while the wheel is made of bronze (Figure 2.2). Lubricants containing conventional EP additives dependent on sulphur and chlorine react with the wheel's bronze surface accelerate its wear and reduce its useful life (Cober, 2013).

Figure 2.2 *EP additives are causing damage to a bronze worm wheel (Cash, 2012).*

Use of mineral-based lubricants is common in industrial screw gears, but it is shown that the use of synthetic bases such as polyalphaolefins (PAOs) or polyalkylene glycols (PAGs) increases performance and decreases operating temperatures (Fitch, 2016). Figures 2.3 and 2.4 show that using PAG oils the period elapsed between one lubricant shift and another rises considerably relative to mineral oils. In comparison, working temperatures and overall losses are also minimised. However, the key pitfalls include incomplete compatibility with some materials, such as sealing gaskets, and high costs.

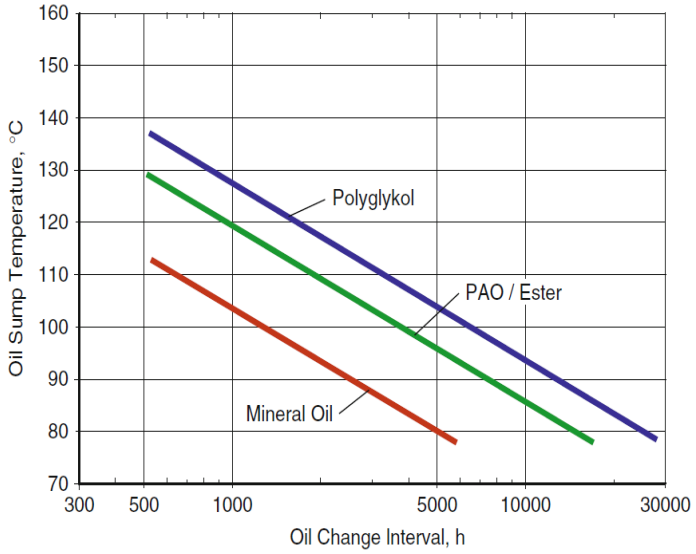

Figure 2.3 *Enlargement of the oil change time between polyalphaolefin/ester and polyglycol versus mineral oil (Laing et al., 2014).*

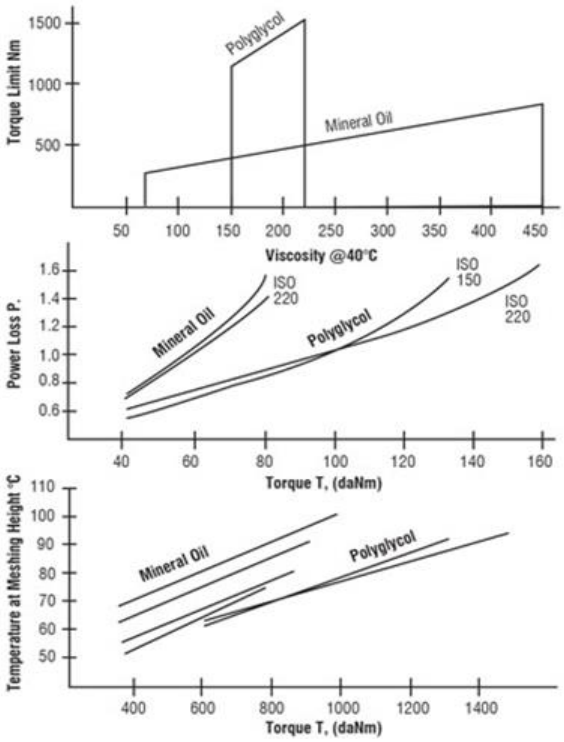

Figure 2.4 *Comparison between PAG oils and mineral oils (Fitch, 2016)*.

In applications where operating conditions are extreme, for example in highly charged slow gears, the pressures involved, as well as the temperatures, may reach exceptionally high values. This results in a reduction of the thickness of the lubricant film interposed between the kinematic components. In particular, due to a mutual increase in pressure and temperature, the lubricant coating fails and is no longer able to resist direct interaction with the surfaces' roughness in relative motion. In this way, adhesion and a rapid rise in friction and wear (Forbes, 1970) and energy costs (Canter, 2007) are highly probable. Thus, these conditions mandate the use of EP additives as described in chapter I. Recent experiments have shown that the addition of NPs, such as graphene oxide and others, to base oils enhances their friction reduction capabilities under extreme pressure conditions. (Senatore et al., 2013; Thakre and Thakur, 2015; Abdullah et al., 2016).

2.1.2 Micropitting wear in Gears

Micropitting, also known as peeling, surface spalling or grey staining is a surface-induced fatigue condition (Figure 2.5) arising during the gear meshing

process between interactive surfaces in which a cluster of micropits has a grey-coloured appearance. Compared to the classical macropitting that happens in the nominal Hertzian contact zone and can be identified with the naked eye, the size of the gear micropits can range no more than tens of μm in-depth and width along with the tooth profile (Oila and Bull, 2005), while its length along the axial direction can typically exceed 100 μm (Brandão et al., 2015).

Figure 2.5 *Gear micropitting (grey staining) exposure to contact fatigue (Sun, Giusca and Lancaster, 2017).*

BS ISO 1122-1:1998 has structured the terminology defining the gear's geometry (ISO 1122-1, 1998). Figure 2.6, a summarises the geometric terms, micropitting is more concentrated around the addendum, and Dedendum (ExxonMobil, 2018)(Figure 2.6, b). EP or anti scuffing agents are the most potent factor in restricting the volume of micropitting (O'Connor, 1970). However, NPs can be a green alternative, as discussed earlier.

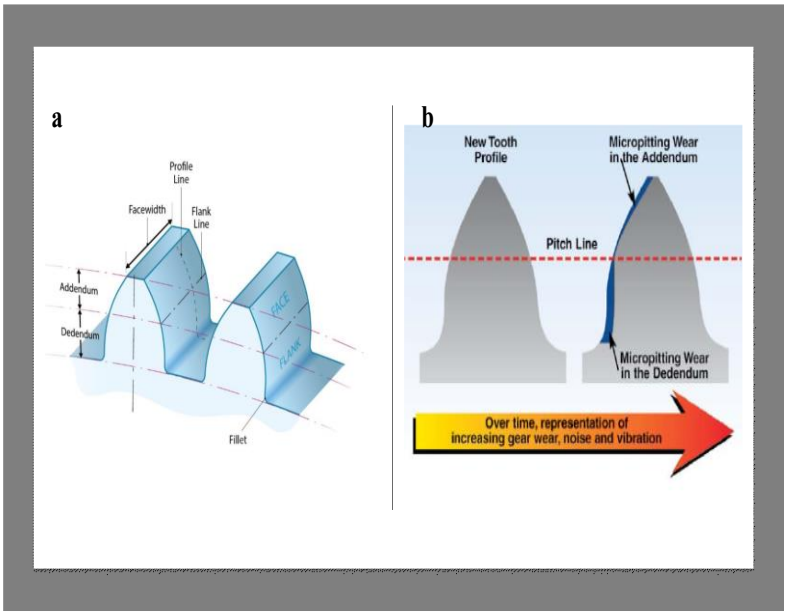

Figure 2.6 *a) Standard Gear geometry vocabulary(Sun, Giusca and Lancaster, 2017), b) tooth shape evolution due to micropitting (ExxonMobil, 2018).*

2.2 Environmental and safety aspects

2.2.1 Operational safety and toxicity

Occupational exposure to NPs is a problem, and they often stay suspended in the workplace atmosphere for a prolonged period. NPs have been described as one of the key threats and targets of OHSA in reviewing various state, EU and international regulations and guidelines (Rauscher, Rasmussen and Sokull-Klüttgen, 2017). The potential high risk is associated with emerging manufacturing applications involving nanoparticles and the lack of information on the toxicity of NPs contributing to insufficient safety procedures, ineffective risk management and an adverse atmosphere throughout the workplace. So far, the health effects of nanoparticles in general, have been overlooked. Exposure to nanoparticles is difficult to determine. There is no precise sampler to measure the concentration of particles below 100 nm in diameter. Therefore, it is essential to establish monitoring methodologies and equipment that enable measurements of representative exposure to airborne NPs. In any case, smaller particles follow air streams more readily than larger particles, meaning that nanoparticles can be easily

evacuated in ventilated enclosures. In addition, high-quality particulate air (HEPA) filters are readily collected. Respirators with HEPA filters should be adequately secured from inhalation of NPs.

In toxicity research, the dosage is known to be a key factor influencing the parameter; however, in the case of nanoparticles, certain other parameters matter more, such as particle mass, scale, quantity, surface area, or a combination of all of the above (Hou et al., 2019). Nanomaterials' health consequences include inflammation, asthma, genotoxicity, and carcinogenicity, while developmental and reproductive toxicity includes pregnancy and fatal development, the central nervous system, the reproductive system, and the immune system (Mo et al., 2016). Hou et al. described the three key pathways by which TiO_2 NPS has a toxicity effect on organisms to be: 1) production of reactive oxygen species (ROS), 2) cell wall disruption and lipid peroxidation of the cell membrane due to NP-cell attachment, and 3) NP attachment to biological macromolecules and intercellular organelles (Pickrell, 2007). Oxidative stress is one of the main cytotoxicity effects of nanoparticles; this is attributable to the peculiar redox properties that it exhibits for the capacity to generate ROS (Mo et al., 2016). The brain is believed to be the most damaged organs, but not in close interaction with NPs, as in the case of lungs, skin, gastrointestinal, eye and nasal structures; this is mostly due to ROS, which decreases the oxygen required for proper brain activity (Pickrell, 2007). Czajka et al. outlined how NPs, as exemplified by TiO_2, can affect the central nervous system by in vitro and in vivo pathways (Czajka et al., 2015).

2.2.2 Sustainability and Environmental impact

Sustainability issues are at the core of nanofluid growth in general. A significant number of critical environmental concerns are based on process-level parameters. These parameters, including limiting the use of conventional harmful additives and reducing the resources used on machining, and energy consumption, have significant environmental consequences. However, for future advances, nanofluids' sustainability studies must be conducted to determine their environmental effects from a system-level perspective using the Life Cycle Assessment.

The prevention and management of nanofluids' multiple environmental impacts would rely primarily on the nanofluid's optimised configuration for the intended particular use. The type of NP and its loading concentration, along with its synthesis path, must be considered when selecting the NP for nanofluid development. The use of natural materials such as silica, alumina, iron oxides, and many others is inherited with much lower environmental impacts, so there is no need for such particles' industrial processing. This, in essence, would reduce the energy and materials needed to generate NPs. The

use of NPs from natural resources has a further benefit in enhancing the productivity of nanofluids. The use of such natural material tends to reduce the energy and material production requirements. The use of non-toxic NPs, which are typically natural NPs, further reduces the possible toxicity of NFs during application and when disposed of to the environment. Correspondingly, the use of lower NP loadings could minimise any environmental implications involved with the final disposal of nanofluid and should be more considered when using nanofluids with possible marine life contamination and harmful environmental consequences. Interaction between NPs and the nanofluid-forming base fluid should be noted since it can result in additional dangerous or more serious environmental impacts.

2.3 References

ABDULLAH, M.I.H.C. et al. (2016) Effect of hexagonal boron nitride nanoparticles as an additive on the extreme pressure properties of engine oil. *Industrial Lubrication and Tribology*, 68(4), pp. 441–445.

BRANDÃO, J.A. et al. (2015) An approach to the simulation of concurrent gear micropitting and mild wear. *Wear*, 324–325, pp. 64–73.

CANTER, N. (2007) Special Report: Trends in extreme pressure additives. *Tribology and Lubrication Technology*, 63(9), p. 10.

CASH, W. (2012) The Effects of EP Additives on Gearboxes. *Machinery Lubrication*, Jun.

COBER, G. (2013) Avoiding Common Gearbox Lubrication Problems. *Machinery Lubrication*, Jun.

EXXONMOBIL (2018) *Micropitting can lead to macro problems in gearing*. Available from : https://www.createdigital.org.au/micropitting-lead-problems-gearing/ [Accessed 20/12/20].

FITCH, B. (2016) The Right Way to Lubricate Worm Gears. *Machinery Lubrication*, Feb.

FORBES, E.S. (1970) Antiwear and extreme pressure additives for lubricants. *Tribology*, 3(3), pp. 145–152.

HOCHMANN, M. and SIEBERT, H. (2012) Gear lubrication—stopping micropitting by using the right lubricant. *Klüber Lubrication M'unchen*.

ISO 1122-1 (1998) Vocabulary of gear terms — Part 1: Definitions related to geometry. In: *ISO 1122-1*.

LAING, D. et al. (2014) Food and Pharma Industry Lubrication. In: *Encyclopedia of Lubricants and Lubrication*. Berlin, Heidelberg: Springer Berlin Heidelberg, pp. 645–679.

MCKENNA, K.G. et al. (2010) High performance industrial gear lubricants for optimal reliability. *powertransmission*.

O'CONNOR, B. (1970) The influence of additive chemistry on Micropitting. *Gear thechnology*.

OILA, A. and BULL, S.J. (2005) Assessment of the factors influencing micropitting in rolling/sliding contacts. *Wear*, 258(10), pp. 1510–1524.

RAUSCHER, H., RASMUSSEN, K. and SOKULL-KLÜTTGEN, B. (2017) Regulatory Aspects of Nanomaterials in the EU. *Chemie Ingenieur Technik*, 89(3), pp. 224–231.

SAFAVI, S.M. et al. (2007) Use of Mechatronic System to Manufacture Spiral Bevel Gear using 3-Axis CNC Milling Machine. In: *15th Annual (International) Conference on Mechanical Engineering*. Iran: Amirkabir University of Technology, Tehran, Iran.

SENATORE, A. et al. (2013) Graphene Oxide Nanosheets as Effective Friction Modifier for Oil Lubricant: Materials, Methods, and Tribological Results. *ISRN Tribology*, 2013, pp. 1–9.

SUN, W., GIUSCA, C. and LANCASTER, A. (2017) *Surface texture measurements of gear surfaces using stylus instruments*. National Physical Laboratory.

THAKRE, A.A. and THAKUR, A. (2015) Study of behaviour of aluminium oxide nanoparticles suspended in SAE20W40 oil under extreme pressure lubrication. *Industrial Lubrication and Tribology*, 67(4), pp. 328–335.

Chapter III. Potential and challenges of nanolubricants for electric vehicles

3.1 Overview

In recent times, electric vehicles (EVs), including battery electric vehicles (BEV), hybrid electric vehicles (HEV), plug-in hybrid electric vehicles (PHEV), fuel cell electric vehicles (FCEV), have become more prevalent in the transport sector. This shift in transportation is intended to replace the internal combustion engine (ICE) vehicles in the future, as the current trend suggests (Senatore, 2020). One example of such dramatic change is seen in the UK as by 2030; the government has decided to ban new fossil fuel vehicle production. Accordingly, this would help reduce car emissions to the equivalent of 46 million tons of CO_2 in the UK alone(Ambrose, 2020). CO_2 global emissions from combustion engine vehicles are 4.5 times higher than electric cars when the electricity is supplied from renewable energy sources. Worldwide sales are on the rise due to subsidies from governments and car producers for EVs to offset the extra battery costs. These incentives and public environmental awareness have reflected on car purchasing habits, particularly in the EU countries, in contrast to ICE vehicles (Figure 3.1). Additionally, around 7.5 million BEVs/PHEVs worked worldwide at the end of 2019 (Irle, 2019).

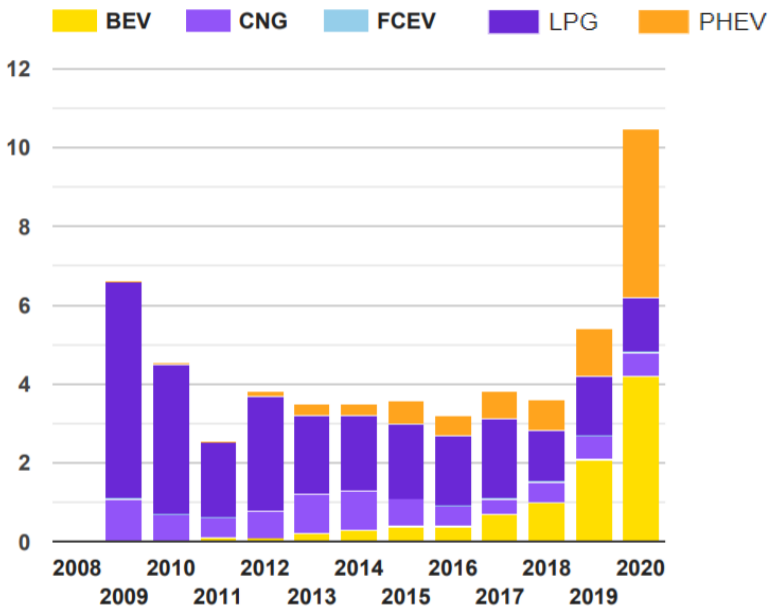

Figure 3.1 *Newly registered alternative fuel vehicles cars (in %), data collected by the European AF Observatory, contractually commissioned by the European Commission(Anon, 2020). Abbreviations: BEV, battery electric vehicles; CNG, compressed natural gas; FCEV, fuel cell electric; LPG, liquefied petroleum gas; PHEV, Plug-in hybrid electric vehicles.*

The current global industry demands improved lubricants to improve energy efficiency, sustainability, and cost reduction (Lee and Carpick, 2017; Salmeron and Benjamin, 2019). This need also holds for EVs as about 57% of the energy supplied to an EV is used to overcome friction, including 41 % to rolling resistance 19 % goes to acceleration and braking inertia (Holmberg and Erdemir, 2019). However, with this conversion pace, the automotive industry sees hitherto unknown technological changes as electric motors and electric vehicles are becoming more prominent. Over decades of joint development efforts, lubricants have been optimised for vehicles with ICE, and now they have to master these new challenges of electric mobility. Compared with the conditions in a traditional ICE vehicle, the mechanical parts of EVs have higher speeds, loads, elevated temperatures, and electrical currents. Today's available practical solution to mitigate these challenges includes applying reduced oil viscosities to counter the high electric motor speeds. Hydro-lubes, a mixture of polyalkylene glycol thickened water (PAGs), allows simultaneous battery cooling and gear lubrication. However, these solutions can not withstand the evolving industry as these harsh conditions are pushed even further by the manufacturers to improve EV's range and performance

(Karki et al., 2020).Therefore, to overcome these propagating hurdles, the development of new lubricant formulations is a must. Nanolubricants, a nanofluid class dedicated to lubrication, have shown success in reducing the wear and coefficient of friction in conventional ICE lubricants (Nallusamy and Logeshwaran., 2017; Hemmat Esfe and Esfandeh, 2018; Paul et al., 2019; Goodarzi et al., 2019; Dassenoy, 2019; Ali, Hou and Abdelkareem, 2020). However, their performance has never been discussed and reviewed in terms of EVs' tribological conditions. This chapter explores the behaviour of various nanolubricants combinations composed of single or several types of nanoparticles (NPs). The theme in which nanolubricants are evaluated is their performance in greases, electrical compatibility, thermal management, lubricants oxidation stability, and copper corrosion. These areas are selected as they are being considered the main criteria of assessment when applying a lubricant to an EV.

3.2 NPs ability to enhance grease performance

3.2.1 Greases challenges in EVs

Grease is described as a solid to semi-fluid substance or a thickening agent dispersion into a liquid lubricant (Anon, 1961). Lubrication greases are categorised according to their type of thickener (fatty acid soaps), which constitutes between 10-15% of the grease (Lugt, 2016). These thickeners are fibrous in shape, with lengths that approximately range from 1 to 100 μm while its length is one order of magnitude greater than its diameter, whereas this dimension ratio is associated with the consistency of the grease for a given thickener concentration (Scarlett, 1967). Lubricating oil that may be either mineral or synthetic makes up the most significant portion of the grease formula. It is mostly the thickener that specifies the operating temperature range. The tribo-performance of conventional greases is determined predominantly by the base oil and additives (Lugt, 2016).

About 80-90% of rolling bearings, in general, are lubricated with grease (Lugt, 2016), this is due to the significant lead of greases over oils in their durability and ability to maintain properties under shear at a broader range of temperatures. Besides, greases act against moisture and contamination as a sealing agent. The use of greases in many parts or systems within an EV includes powertrain, wheel bearings, chassis, and other parts (Barrie and Lemieux., 1993). In most of grease’s operations there is no need to replace or refill grease. However, when considering the most significant role of greases is within bearings, it directly impacts the friction, which reflects in vehicle performance, and it is crucial in determining the mileage that an EV can run. Therefore, to improve the EVs' efficiency, the improvement of greases' performance in rolling element bearings is vital to ensure their reliability.

EVs mechanical configuration establishes novel challenges for grease usage in bearings. These challenges are due to the extreme lubrication environment that greases undergo sealed in motors at high-speeds and elevated-temperatures, which poses long-term efficiency complications. This is evident as the most frequent failure inside an electric motor is the greased bearings elements (He, Xie and Luo, 2020); thus, new kinds of lubricating greases need to be created.

The historical track for enhanced commercial greases formulation started with aluminium and sodium soaps greases as they have better capabilities to cope with higher temperatures than the previously invented calcium greases. Following this, new barium, lithium, and calcium-based greases were created with even superior properties compared to the previous era (Gow and Christiernsson, 1995). Polymer grease (Meijer and Lankamp, 1995), is considered one of the latest technological advances with chemical inertness properties. However, due to their many beneficial properties such as high dropping point, corrosion protection, pleiotropic efficiency, and moisture resistance, lithium greases have ubiquitously been used as lubricants for ICE (internal combustion engine) automobiles (Radulescu and Radulescu, 2006; Krawiec, 2011). Lubricating door locks, hinges, and other components, lithium greases may typically be utilised in EVs.

However, an electric motor requires dedicated greases to meet various property requirements, such as lower noise levels. Besides, tribo-contact points are affected by electrical fields and currents produced by magnetic fields (Preisinger, 2002). Furthermore, a significant challenge for greases is EVs' torque characteristics; an EV motor produces higher torque, in contrast to ICE, and can provide the maximum power over an extensive speed range, even at slow speeds. The latter fact indicates the possibility of extreme boundary lubrication conditions. Moreover, when dealing with higher rotational speeds, which can reach up to 20,000 rpm (Farfan-Cabrera, 2019), air may penetrate the components and causes the fluids to foam, leading to extreme stress the motor. Therefore, low-viscosity greases are more fitting for reducing frictional torque, as the friction losses caused by rolling resistance can diminish considerably.

Nonetheless, it accelerates the decline in bearing life due to the thinning in lubricant film and the realisation of heavy wear (Lugt, 2016). In such cases, Nanolubricants can play a significant role due to its anti-vibration damping effect, distinct from antiwear (AW), anti-frictional (AF), and even extreme pressure (EP) additives. Most conventional friction modifiers have fatty acid chain lengths similar to the grease thickener and are thus trapped by the thickener and do not reach the surface to form low friction layers (Lugt, 2016). Knowing this merit of NPs paired with ‘classical additives' significant drawbacks, NPs will perform better in EVs conditions.

3.2.2 NPs tribological role in Greases form EVs lubrication perspective

Since the revolutionary formulation of nanolubricants composed of WS_2 NPs with closed-cage structure (fullerene-like IF) conducted by Professor Tenne's group (Rapoport, Fleischer and Tenne, 2003), nanolubricants have been considered a game-changer in the field of tribology (Yadgarov et al., 2013). However, most of the studies in nanolubrication focus on enhancing oil properties than grease since the latter composition can be created in many formulations and properties (Vengudusamy, Enekes and Spallek, 2019), magnifying its analysis complexity. However, the relatively few studies on lubricating greases indicate that nanomaterials have many advantages that manifest on the friction pair (Qiang et al., 2019).
NPs can be categorised according to their chemical nature into metallics, metal oxides, sulphides, clays, carbon-based, rare-earth, and others. In the following section, as indicated in Table 3.1, a literature scan is performed on utilising several types of NPs as additives in greases, with critical discussion on its tribological action.

Table 3.1 *Literature scan on the ability of NPs in reducing wear scar diameter (WSD) and friction coefficient (COF) in different grease bases. Besides, an indication of the different tribological mechanisms played by NPs. The blue highlighted rows signify the utilisation of NPs as mixtures to form composites. Abbreviations: CNTs, carbon nanotubes; G, graphene; MWCNTs, multi-wall carbon nanotubes; rGO, reduced graphene oxide; NGT, nano graphite; CS, carbon spheres;.*

Type of NPs	Size	Type of Grease base	Reduction		Mechanism	References
			CoF	WSD		
TiO_2 **CNTs**	21nm D (10-12nm), L (1-20µm)	Calcium	72.3%	60%	Protective film	(Mohamed et al., 2020)
ZnO **Si_3N_4**	60nm 100nm	Lithium	34.3%	8.3%	Sintering and mending	(Q. He, Li, Wang, et al., 2018)
G **MWCNTs**	10-20nm D (10-20nm), L (5-10µm)	Lithium	66%	91%	Protective film	(Ashour et al., 2017)
G **Cu**	NA 20-50nm	Lithium	15%	85%	Protective film	(Jing et al., 2017)
BN **MoS_2**	NA NA	Lithium	46%	75%	Sliding (Ability to change adhesive wear to abrasive)	(Yan et al., 2019)
MoS_2	50-150nm	Lithium	42%	61%	Protective film	(Rawat et al., 2019)
TiO_2	20nm	Water-Glycerol	49.5%	97.8%	Rolling and mending	(Wu et al., 2017)
CeO_2	500nm	Lithium	28%	13%	Polishing	(Q. He, Li, Guo, et al., 2018)
rGO	500nm	Lithium	60%	35%	Protective film	(Singh, Kumar and Tandon, 2018)
αAl_2O_3	40nm	Lithium	Negative effect		Abrasion	
$CaCo_3$	50nm	Lithium	33%	20%	Protective film	
$CaCO_3$	45nm	Lithium	7.5%	12%	Protective film	(Ji et al., 2011)
CNTs	D (5nm), L (5µm)	Lithium	81.5%	63%	Protective film	(Mohamed et al., 2015)
CaF_2	60nm	Lithium	19%	29%	Protective film	(Wang et al., 2007)
G	NA	Lithium	50%	50%	Protective film	(Cheng and Qin, 2014)
$Ca_3(BO_3)_2$	70nm	Lithium	10%	33%	Tribochemical reaction and protective film	(Zhao et al., 2014)
TiO_2	35nm	PTEF	14%	3%	Protective film	(Ge, Xia and Cao, 2015)
SiO_2	30nm	PTEF	14%	Negative effect	Protective film	
SnO_2	20nm	PTEF	Negative effect		Deterioration of grease's mechanical properties	
NGT	2-6µm	Lithium	No effect		No action	(Niu and Qu, 2018)
		Titanium	14.6-12.9%	2-2.3%	Tribochemical reaction and protective film	
TiO_2	40-60nm	Lithium	40%	50%	Protective film	(Chang et al., 2014)
CuO	90-110nm	Lithium	20%	60%	Protective film	
CuO	15-530nm	Lithium	30%	13%	Polishing and mending	(Zheng et al., 2020)
ZrO_2	12.7nm	Lithium	48.8%	46.5%	Sintering	(Xia et al., 2010)
SiO2	>100nm	Lithium	26%	7%	Protective film	(Q. He et al., 2017)
CS	>600nm	Lithium	20%	40%	Rolling	(Li et al., 2019)
Bi	10-30nm	Lithium	13.4%	19.2%	Mending	(X. Zhang et al., 2014)
BN	255-955nm	Lithium	20%	10%	Protective film and sliding	(Wang et al., 2020)

These results listed in Table 1 are ample evidence that the addition of nanoparticles to greases would significantly enhance its tribological performance. Although these findings are not performed under the same experimental conditions or on similar surface materials and roughness, it is apparent that the size, morphology, crystal structure, and compatibility with lubricating base oil influence the nanoparticle's tribo-performance.

Moreover, nanoparticles addition to greases would significantly enhance its load-carrying capacity and extreme-pressure performance. In particular, carbon-based nanoparticles have superior abilities to improve the load-carrying capacity due to its excellent mechanical properties (Cha et al., 2013; Crevillen, Escarpa and García, 2018). Mohamed, et al. revealed that lithium-based greases' load-carrying capacity could rise by about 52 % with just 1% wt. of CNTs (Mohamed et al., 2015). In another study, Ashour, et al. showed that the overall maximum seizure pressure increased by 75% when 1 wt. % of multi-layered nanographene was incorporated into lithium grease (Ashour et al., 2017).

Composites typically exhibit superior performance compared to individual nanoparticles due to the synergetic effect of more than one type of nanoparticle (Irtegov et al., 2016; Nazir et al., 2018). According to Kumara, et al. Ag, and Pd NPs modified by Dodecanethiol can interact actively, modifying their sizes, forms, and electronic structures. A mixture of these two quasi-spherical ultra-small sizes (2-6 nm) NPs could form a stable suspension and effectively increase tribological efficiency in the 0.1-1 % concentration range in a lubricating fluid. In contrast to either NP alone at the same overall NP concentration, the Ag-Pd NP combination further decreased friction and wear by > 30 % and > 80 %, respectively. The superior lubricating activity was due to the formation of two forms of ultra-thick tribofilm (up to 3 μm), caused by the Ag-Pd combination's electron donation capacity (Kumara, Meyer and Qu, 2019). Also, granular Ag Nanoparticles can be used with other nano laminar particles such as MoS_2 or graphene to boost lubrication efficiency by acting against the nanosheets' shear restacking (Zhang et al., 2012; Meng, Su and Chen, 2016). Besides, Ag NPs enhanced the MoS_2's ultra-high temperature (> 450°C) lubrication efficiency (Zhang et al., 2012). This composite feature can significantly benefit as the elevated temperatures during electric motor bearing operations. Only a few researches have been presented in investigating the use of nanocomposites in greases (Ashour et al., 2017; Yan et al., 2019; Mohamed et al., 2020). For instance, He, et al. demonstrated that composite grease based on ZnO-Si_3N_4 nanoparticles has excellent potential for vibration reduction and temperature rise in high-speed bearings (55,000 rpm), coupled with excellent properties of lubrication and antifriction (Q. He, Li, Wang, et al., 2018).

Another aspect for incorporating NPs as additives is its impact on grease's microstructure and rheological behaviour, but firstly, it is better to classify grease lubrication phases to comprehend the possible role for nanoparticles. It

is possible to classify the grease lubricating phases into two stages, based on the film thickness (Gafitanu et al., 2001). The initial phase, referred to as the "churning" phase, is a lubricant redistribution phase that relies primarily on the grease rheology and bearing's geometry and characteristics. The churning phase is a fully flooded state where the dominant phenomenon is frictional viscous heating. Churning is the shortest phase compared to the second phase of bearing operation since the quantity of grease in the bearing raceways would be decreased due to the grease shift to the sides of the raceway (Lugt, 2016). The second phase, recognised as "bleeding," is accountable for most of the lubrication during the lifetime of the bearing and is characterised by the discharge of base oil from the thickener stricture, so that the mixture of base oil and thickener perform its action in the rubbing zone (Leckner and Westbroek, 2017). NPs role in the churning phase can be considered on the downside, as NPs tends to increase the viscosity of the grease with considerable proportions that can be equal or greater than 50% (Kamel et al., 2017; Mohamed et al., 2020)., contribute to the power losses in the friction drag and magnification in the friction torque required for rotation.

In the bleeding phase, the lubrication mechanism is governed by the starvation, which indicates the balance between supply and loss processes of the lubricant in the contact zone that will govern the thickness of the Elasto-Hydrodynamic Lubrication (EHL) film. However, with the prolonged operation, the thickness of the EHL film and the lubricant's' loss becomes so extreme at some point in time that the boundary regime dominates, and metal-to-metal contact can occur, leading to bearing failure (HOSHINO, 2002). The degradation rate of EHL film could accelerate within EVs lubrication conditions and in this case, NPs positive contribution to viscosity and shear stress can extend the EHL operation. Furthermore, NPs can interact with the grease's microstructure and elevate its dropping point (Kamel et al., 2017), resulting in a significant gain during these conditions. Nevertheless, the presence of NPs in relatively high concentrations can cause the bonds between grease fibers to break due to NPs agglomeration, resulting in deterioration in the grease's performance (Ashour et al., 2017). This effect is highly probable as a combination of Van der Waals and capillary forces holds-up the base oil within the thickener structure (Bauer, Finkelstein and Wiberley, 1960), and the presence of NPs that usually contain active functional groups can interfere with these bonding forces' effectiveness. This effect is not only limited to NPs; according to Gow, some 90% of all conventional AW and EP additives disrupt the thickener structure of grease because they are mostly formalised from surface-active materials, contributing to what is widely referred to as the mayonnaise effect (softening and de-colouring) (Gow, 2007). He also indicates that some 90% of the remaining 10% do not perform well as AW and EP, due to the polar nature of additives, which will adhere to the almost always very polar (metallic soaps) soap structure rather than to the metal surface (Gow and CHRISTIERNSSON, 1995).

On the other extreme, at the prevalence of boundary conditions, NPs can demonstrate direct tribo-role as discussed earlier, since its effectiveness to act as AW, AF, and even extreme EP additives rely on the presence of boundary lubrication. Nevertheless, care must be taken as excessive concentration and or non- surface-compatible NPs can result in heavy abrasive action (Singh, Kumar and Tandon, 2018).
EVs have short-range 66, which makes them the ideal vehicle to use in urban areas. However, urban driving requires slow or medium speed operation, and these ranges require a great deal of torque that can reach up to 125 Nm (Chan, 2002). Additionally, EV's electric motor can provide constant maximum torque from zero to base (Wu et al., 2018). Therefore, it is safe to postulate that EVs lubrication conditions will always suffer from harsher conditions than ICE, and NPs can play a considerable beneficial role.

3.3 NPs electrical components compatibility

3.3.1 Lubrication challenges in the electrical environment

In addition to friction-reducing and antiwear function, lubricants play a crucial role in electro-mechanical system operation, such as preventing corona discharge and removing arc, making the lubrication's electrical properties of particular importance (Sudges, 1968; Low et al., 2013). In a series of EVs' components such as bearings, seals, pads, and gears, the induced shaft voltages and currents can cause premature failure problems and can also cause electromagnetic interference (EMI) and radio frequency interference problems that make the motor unstable (Nippes, 2004; Mukherjee, Patra and Banerjee, 2010; Ahola et al., 2011). These problems can lead to bearing instability, vibration, noise, and more extreme mechanical failures (Boškoski et al., 2010; Walther and Holub, 2014). Additionally, studies have shown that the utilization of frequency inverters to control inverter-fed electrical motors and generators of variable speed creates harm to the rolling bearings as bearing currents can cause a detrimental effect (Preisinger, 2002; Romanenko, 2017). Dependent on the composition and electrical and rheological properties of the lubricant, these currents that arise show different characteristics on the smoothness of operation (Gonda et al., 2019). These currents discharge happen through the bearing balls and raceways, causing significant energy dispersion and electrical wear within a split second. Electrical wear or electrical tribo-failure stem from dissymmetrical effect when voltage differences are created between the shaft and the bearing housing, current passes through the fragile lubricating film. The current causes sparks, arcing and the resulting melting of the bearing (Raadnui and Kleesuwan, 2012). According to these currents' intensity, frequency, and duration, frequent electrical wear is classified into the surface frosting, fluting, pitting, spark

tracks, and welding (Boyanton and Hodges, 2002; Sunahara et al., 2011; Costello, n.d.).

However, electro-lubricants interactions must be considered as an additional cause for tribo-failure. While nonpolar oil-based lubricants are generally chemically inert, the potential and energy needed for its chemical reactions is given by shaft voltage and bearing current, accelerating the oil degradation process (Romanenko, Muetze and Ahola, 2016). This process occurs when the free radicals formed in oil by electrical excitation react to form peroxide groups with oxygen, which in turn will cause the formation of new radical groups, and such a chain reaction will gradually form products containing carboxyl (Yu and Yang, 2011). The final degraded oil lubricant will be in the form of highly viscous and acidic degradation products and additive agglomeration, in which case oil lubricity is lost (Romanenko, Muetze and Ahola, 2016). Moreover, the electric field induces interfacial stress in the case of polar lubricants, such as water-based lubricants, confined between two metallic surfaces affecting its wetting properties, which may result in an alternation in its lubrication action (McHale et al., 2019). Furthermore, electrostatic forces on interfacial tension of microbubbles in polar lubricants are affected and can transform to vulnerable points for electrical breakdown (Xie et al., 2008). Besides, the evaporation of the lubricant component, which is believed to be the key reason for the grease failure of cylindrical roller bearings, may also have induced by the thermal effect of the undesired electrical discharge process (Komatsuzakl, Uematsu and Kobayashl, 2000). Additionally, an assumption can be made on the occurrence of lubricant's additives (AF, AW, and EP) chemo-physical surface absorption and reaction shifts under the influence of an external electric field, resulting in a variation of lubrication behaviour.

Naturally, nonpolar lubricants have inherited high electrical resistance that can act as superior insulating agents in the 800V EVs, with minimal 25KV breakdown voltage (Wang and Wang, 2008). This property is true for the most common lubricants as the ester-based oils' dielectric strength is comparable to mineral oil. However, ester-based oils' dielectric values have a greater coefficient of variance, suggesting its unpredictability and potentially a higher likelihood of oil breaking down at lower voltages (Wang and Wang, 2008). Nevertheless, breakdown voltage decreases dramatically for mineral oil with the rise in water content and contaminants (Wang and Wang, 2008). This electrical resistivity depends on a fully formed lubricating film between the rubbed pairs, which is not always the case in high torque conditions of EVs operation and metal-to-metal contact is almost always inevitable (HOSHINO, 2002).

Another possibility of facing harmful electrical discharges challenge is the utilisation of high conductivity lubricants that can prevent the build-up of high potential discharges bypassing the currents safely between the parts. In this technique, ionic liquids (ILs) come in as a first choice. As a lubricant additive,

ILs can effectively improve wear resistance and lower lubricant components conductivity (Flores-Torres, Holt and Carey., n.d.). In general, ILs consist of an organic cation, usually containing nitrogen or phosphorus, and an anion that is weakly coordinated. Imidazolium, phosphonium, pyridinium, and ammonium are some of the most common cations, while some common anions are BF_4, PF_6, CF_3SO_3, and $N(CF_3SO_2)$ (Bermúdez et al., 2009). ILs do not emit volatile organic compounds, rendering them "green" lubricants. However, possible drawbacks to ILs as lubricants are corrodsion of the lubricated substrate and the formation of flammable or harmful by-products when decomposed (Palacio and Bhushan, 2010).

Another radical solution can depend on utilising different construction insulating materials, such as ceramic sheeting, on the bearing to block the high-frequency current (White, 2015). However, an insulated bearing reduces the heat flow dissipation from the rotor, which can result in severe mechanical failure due to thermal shocks at high rpm (Panda et al., 2002). Therefore, another engineered solution must be devised in which NPs can participate in solving this obstacle.

3.3.2 NPs as anti-electro-discharge additives (AEDA)

It is essential to choose the functional purpose of NPs when formulating a lubricant that works under electrically charged conditions. This essentiality comes from the fact that NPs working as AEDA paly in two contradictory roles. One route for NPs functionality is to increase the insulation properties of the oil-based lubricants. In this case, elevating lubricant's electrical resistance and dielectric strength is directly proportional the threshold voltage in which electrical discharge with destructive currents can occur (Muetze and Binder, 2006), thus increasing the tribo-protection.

On the other hand, NPs can be employed to increase the lubricants' electrical conductivity to conduct the electric current so that point-to-point flashovers are eradicated, and no build-up for electrical potential occurs. This effect has been proven as fluting can be prevented by high conductive greases (Suzumura, 2016).

Tribological studies of NPs as AEDA in literature are still scarce as the importance of electro-mechanical lubrication is just on the rise alongside modern applications like EVs tribological designs. Nevertheless, Ge, et al. have shown that when applying oleophilic nano-TiO2 and nano-SiO2 as additives in oil-based grease, the alternating current (AC) breakdown strength increases by 10.4 % and 8.2 % at power frequency, respectively. Additionally, when the additives in naphthenic oil are 0.1 %, the grease volume resistivities are also enhanced by 23% and 30 % compared to base grease, (Ge, Xia and Cao, 2015). Figure 3.2, a, shows the greases' volume resistivity; as the content of additives increases, the volume resistivity escalates.

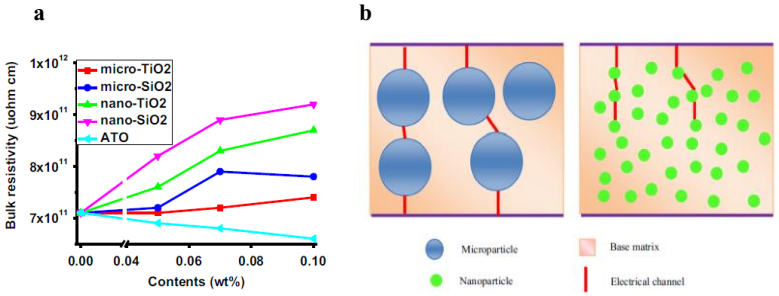

Figure 3.2 *a) Volume resistivity of greases with various concentrations, b) the insulating mechanism of the base matrix nanoparticle and microparticles, (Ge, Xia and Cao, 2015).*

The study explains this insulating behaviour of NPs with the principle of electron capture, as illustrated in Figure 3.2, b. This principle relies on incorporating electrons with oil molecules by polarising them and forming a group that will float for a short period under the local electric field's influence. Then in a traps manner, the capture and release of electrons due to the groups splitting and reforming result in slow electrons passage in the base matrix, and eventually contribute to the slow development of the electrical channel (Hwang et al., 2008; Li et al., 2010). Li, et al. have also indicated that trap and release mechanism of electrons is a function of the particles size as nanometric particles are more efficient than micrometric ones (Li et al., 2010). This drawback of microparticles is due to the defects they impart within the matrix allowing electrons to float effortlessly, which leads to a reduction in the base matrix's breakdown strength and volume resistivity (Kozako et al., n.d.).

In another dry friction study, Guo, et al. studied Al_2O_3 / Cu composites (1.0 vol. %) reinforced with different sizes of αAl_2O_3 particles on an electrical sliding wear test (Guo et al., 2016). The results show that Al_2O_3/Cu composites' wear rates have a reverse variation with the composite hardness of Al_2O_3/Cu, and the composite electrical conductivity decreases with the NPs size increment. The highest wear resistance properties are in the 50-100 nm range of αAl_2O_3 NPs, which corresponds to relatively high electrical conductivity and high hardness (Figure 3.3). The wear mechanisms are due to a combination of adhesive wear, plastic deformation accompanied by arc damage.

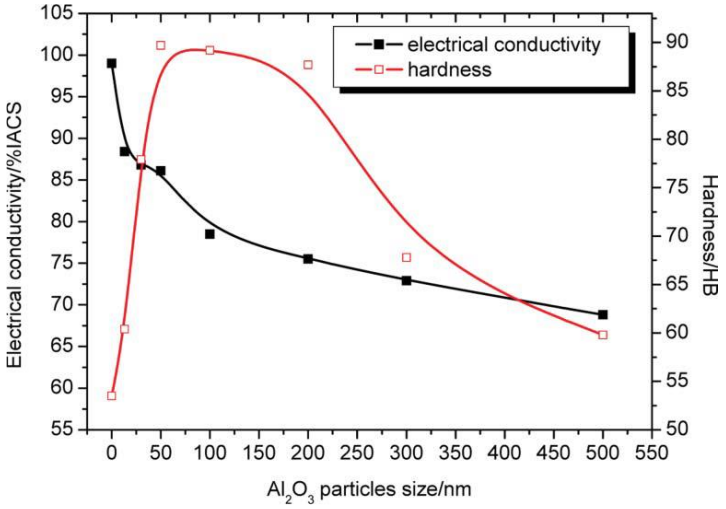

Figure 3.3 *Variation of electrical conductivity and hardness of Al_2O_3 / Cu particle size composites of Al_2O_3 (Guo et al., 2016).*

The alternative approach depends on reducing the electrical conductivity of greases, Christensen, et al. have utilised carbon nanotubes (CNTs) as lowering electrical resistivity additives (Christensen et al., 2020). The study showcased that the addition of hydroxyl functionalised multiwall carbon nanotubes (MWCNT-OH) in both oil-based and water-based lubricants can result in an extremely low electrical resistivity, as shown in Figure 3.4, a. This low resistivity is attributed to the functionalisation of MWCNT with hydroxyl groups as resistivity drops to 22.4 Ω·cm with 7.5 %wt. of the additive in oil-based grease in contrast to the resistivity of an equivalent sample made with multiwall nanotube (MWCNT) of 7880 Ω·cm. In a water-based grease sample formed from 75% Glycerol, 25% Water, and 4.5 %wt. of MWNT-OH, the resistivity measured plummeted ton10.0 Ω·cm. The study suggests this electric conductivity improvement is due to hydrogen bonding into the grease of any form, easing electrons movement.

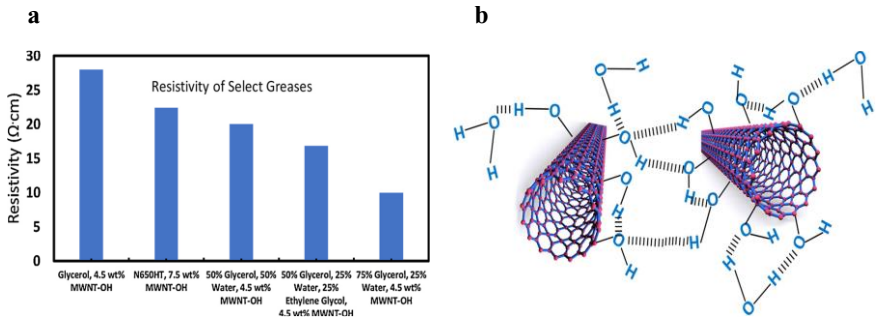

Figure 3.4 *a) Resistivity of diverse samples of grease, b) hydrogen bonding schematic between CNT-OH and a water molecule, (Christensen et al., 2020).*

The later water-based grease can be advantageous in EV's electrical motor lubrication due to its low viscosity nature compared to oil bases. However, as the study highlights, such high-load nanotube grease with low electrical conductivity will present a problem for commercial applications. A highly conductive grease with a lower carbon loading that can have the same or better efficiency would benefit several respects, including a more favourable viscosity and improved cost savings. Additionally, such densely surface functionalised NPs can have a detrimental effect on the grease's structure discussed earlier in NPs greases tribological role section.

3.4 Thermal management challenges in EVs

Electric motors are designed to be lightweight, with higher rotational speeds to save space which results in superior performance as an EV can travel equal to, or more distance than a traditional vehicle can travel with a full tank. Such agile design philosophies are referred to as in-wheel setup, in which wheels are directly mounted by the driving motor, which has the advantages of improving driving efficiency by maximising mass distribution and improving the degree of freedom in terms of vehicle layout and design (Wang et al., 2011). However, as mentioned, such structures are carried out in a limited space in which such systems need effective cooling to achieve proper miniaturisation and high-power output and durability (Kim, Lee and Um, 2009; Bonnett, n.d.). Additionally, studies on the thermal effects of electric motors in EVs have shown that motor heat generation reduces range, charging, longevity and endangers its safe operation (B. Zhang et al., 2014; Seong et al., 2014), as if a cell becomes too hot, a thermal runaway can be triggered, causing neighbouring cells to ignite after the initial event, resulting in a chain reaction that can lead to fire and possibly an explosion. Furthermore, knowing that EV's lithium batteries' operating temperature ranges from -40-84 °C (Chan, 2002), and the heat generated from the motor can reach up to 221°C while the requirements for motor control restrict the maximum temperature to 150°C (Lim and Kim, 2014), heat management gains significant importance. Depending on the operating fluid, the driving motors for electric vehicles (EV) have different cooling modes: oil (Huang et al., 2012), air (Nakahama et al., 2006; Kim, Lee and Um, 2009), and water (Fujita, Itoh and Urano, 2019). Based on the capability of the motor, the most appropriate model is selected. While air-cooled mode has the advantage of a simple cooling system design for its cooling capacity, it is relatively limited, making it challenging to apply to a miniaturised high-capacity motor. The oil-cooled mode typically has a lower cooling power than the water-cooled model; its benefit is that it can simultaneously cool and lubricate.

Today's EVs run at about 20,000 rpm, and it is expected that the next generation speed to exceed 30,000 rpm (Doppelbauer and Winzer, 2016). This increase in speed will result in excessive heat generation; therefore, the current

lubricant cooling capacities need to be improved accordingly. In that sense, nanolubricants can play a significant role in adapting to these new challenges.

3.5 Lubricant Oxidation control

In terms of thermo-oxidation stability, lubricant quality is paramount in EVs operation, as harsh conditions such as elevated temperature and high rpm accelerate this phenomenon. Additionally, EV's low-viscosity lubricants, designated to friction loss reduction, are intertwined with oxidisation, as a low thin layered lubricant is more prone to oxidise than a thicker one. Oxidation is a chemical reaction that upon exposure to an oxidising agent such as oxygen, occurs in lubricants and can be catalysed by copper and iron, which are components abundantly available in EV's structure (Soleimani et al., 2018). Besides, an electrically charged environment can also encourage lubricant oxidation as mention in the electrical compatibility section. The oxidised lubricant products may polymerise and form layers, such as sludge and varnish, as the degradation progresses (Naidu, Klaus and Duda, 1984). This deterioration results in a major colour change, viscosity, greater acidity, sludge and varnish formation, and corrosion (Duong et al., 2018). Therefore, the stability of oxidation is one of the most significant parameters responsible for lubricant ageing, in general (Singh et al., 2016). Furthermore, these negative consequences, are of particular importance in EVs, as low viscosity lubricants and anti-corrosiveness, are two main vital attributes in smooth and consistent performance as discussed in the previous sections.

One of the most appropriate additives for extending lubricants' lifespan is a group of chemicals termed as anti-oxidants. Anti-oxidants are categorised as primary anti-oxidants (radical scavengers), secondary anti-oxidants (peroxide decomposers), and metal deactivators, based on the mechanism of action (complex-forming or chelating agents) (Soleimani et al., 2018). However, the critical decision needs to be made in selecting anti-oxidants combinations in a formulation, as that relies on the base oil, application and other ingredients present in fully formulated oil. The presence of certain other antagonistic ingredients in the product may also suppress the role of anti-oxidants (Soleimani et al., 2018). This counterintuitive behaviour can shorten the lubricant's life span. As a result, novel antioxidation techniques must be presented to the evolving industry. Promising solutions can rely on adding electrically conductive NPs or advanced polymers such as rubber, polypropylene and methyl pentene, all of which have shown encouraging outcomes in high-speed applications, the problem of thermal and oxidative stability can be alleviated (Farfan-Cabrera, 2019).

Considering NPs role in this matter, NPs can act as a sacrificial material, oxidising instead of the lubricant bulk phase. Li, Dan, Wenjie Xie, and Wenjun Fang, highlighted this action in a thermal oxidation reaction, the

hydroperoxide concentration level in Cu kerosene nanofluids is low (Li, Xie and Fang, 2011). Indicating that before the kerosene was oxidised, the Cu nanoparticles reacted with oxygen. Moreover, Rasheed, et al. studied thermal degradation of mineral oil lubricants based on graphene using thermogravimetric analysis (TGA) (Rasheed et al., 2015). The study procedure included synthesising different test samples, as-synthesised graphene sheets of 8, 12, and 60 nm thick and engine oil formulations 20W-50 SN/CF and 20W-50 SJ/CF were used. TGA showed that in the presence of graphene, the starting temperature of oxidation for the SN/CF oil could be delayed by 17°C as shown in Figure 3.5. Likewise, the rate of oxidation could be delayed by more than 30°C while weight loss of oil reaches 40% in the presence of graphene.

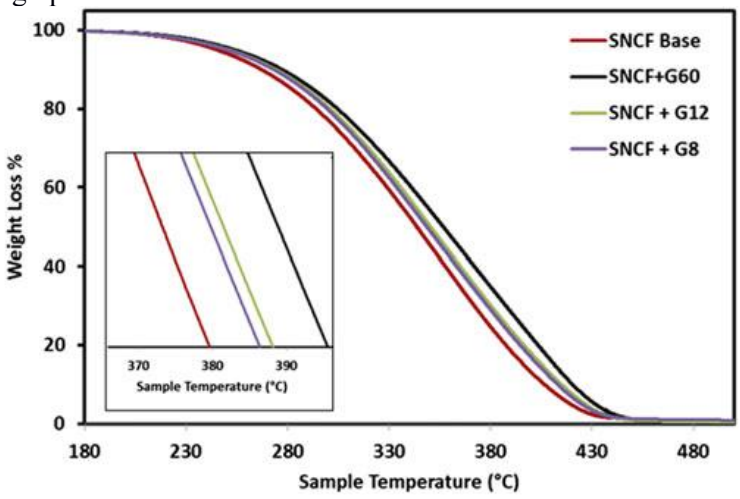

Figure 3.5 *Left: SAE 20W-50 SN/CF thermogravimetric (TG) curves with graphene (60, 12, 8 nm). Right: Derivative weight % of SAE 20W-50 SN/CF with graphene (60 nm) under a nitrogen purge of 20 mL/min at a heating rate of 5°C/min, (Rasheed et al., 2015).*

In a different study conducted by Ivanov, et al that investigated the catalytic behaviour of colloidal dispersions of various mineral and synthetic oil nanocarbon additives, Fullerenes and a conventional chemical anti-oxidant were compared with the oxidation performance of mineral oil and synthetic oil containing detonating nanodiamonds (NDs/DNDs), detonating soot and commercial analogues. The anti-oxidant properties of both fullerenes and DNDs were shown in mineral oil, with DND performance depending on the deagglomeration method (Ivanov et al., 2018). In PAO oil, DNDs and fullerenes' anti-oxidant performance is less effective than in mineral oil as indicated by total acidy number TAN shown in Figure 3.6.

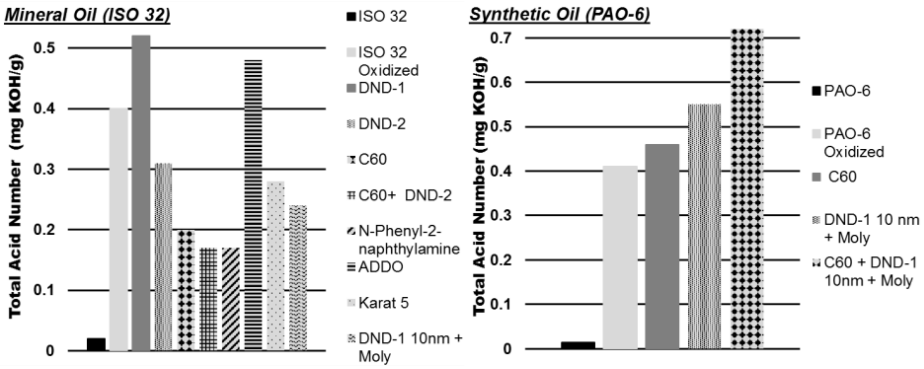

Figure 3.6 *a) TAN values for ISO 32 mineral oil before and after oxidation, with and without additives, b) TAN values for PAO-6 synthetic oil before and after oxidation, with and without additives. Note that bars are in order from left to right on each bar chart according to legend listed from top to bottom, (Ivanov et al., 2018).*

Zhongyi, et al. evaluated the synergistic tribological and anti-oxidant behaviours of Sulphonate-modified nano calcium carbonate (SMC), the average size of 35 nm, and with ashless anti-oxidant N-phenyl-a-naphthylamine (T531) in hydrogenated oil (5 cSt) (Zhongyi et al., 2013). The results show that adding this synthetic additive even at a low quantity (2.0 wt. %) can have a good synergistic anti-oxidant effect with T531 as reviled by oxidation induction period test shown in Figure 3.7, which verifies that a multi-functional and high-performance role of the nano calcium carbonate compound.

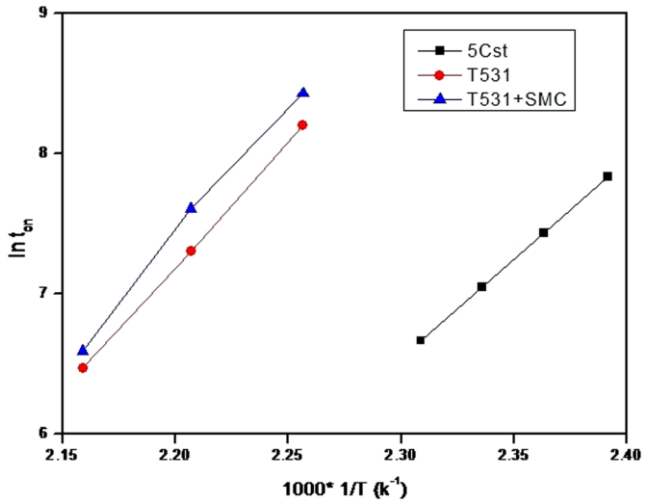

Figure 3.7 *Oxidation induction period (ln t_{on}≈1/T) curve at different temperatures, (Zhongyi et al., 2013).*

Zaarour, et al. reported another revolutionary method that utilises NPs nano-mesh for lubricant anti-oxidation objective (Zaarour et al., 2019). Zeolite nanocrystals have been used in the study as proactive agents to extend commercial lubricants' lifetime. The nanosized zeolites were introduced into four lubricants and subjected to oxidation (90°C and 150°C). NMR (nuclear magnetic resonance) and FTIR (Fourier-transform infrared spectroscopy results, indicated that nano-zeolites protect the zinc dialkyldithiophosphate (ZDDP) additive, even after heating at 150°C for 24 hours. The FTIR profiles of lubricants aged in the presence of LTL (Linde Type L zeolite, Figure 3.8) showed a lower degree of oxidation, while the oxidation products formed (aldehydes, ketones and acids) were adsorbed as scavengers on the zeolite crystals.

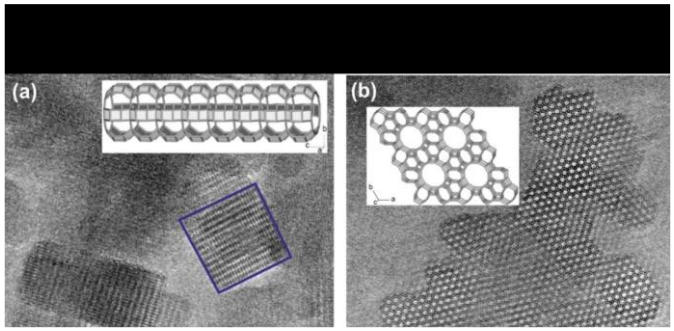

Figure 3.8 *Resolution TEM images of LTL nanocrystals projected along with the directions [100] in a) and [001] in b) (SG P6/mmm), (Zaarour et al., 2019).*

NPs seem to directly affect lubricant as oxygen scavenger resulting in antioxidation tributes coupled with synergetic action with conventional anti-oxidants chemicals. However, synergism scan must be performed on NPs and anti-oxidant to grantee the best performance. Another possibility that makes use of the porous structures of some NPs, is nano-meshing. The latter procedure can act as a carrier for a chemical anti-oxidant and free fatty acid collector, thus braking the free radicals oxidation reaction chain. However, more studies are required to be done by researchers on the topic.

3.6 Copper corrosion performance

Copper is a vital element in EVs. Its longevity, malleability, reliability, and superior electrical conductivity are used in electric motors, batteries, inverters, wiring, and in charging stations. According to the copper development association, an EV can use 85 to 183 pounds of copper (Association, 2020). Consequently, the utilisation of lubricants compatible with copper and prevents its corrosion is of great significance. This compatibility is an additional task added upon lubricants in EVs operation. Other varieties of complementary roles lubricants have to perform, include reducing friction and wear inside metallic components, providing a liquid seal on moving contacts, and removing wear and soot particles (Boyde, 2002). In general, metallic elements undergo corrosion in a reduction/oxidation reactions chains which are the primary mechanism of corrosion propagation (Williams et al., 1991; Punckt, 2004). Corrosion is even made worse in the presence of electrochemically reactive contaminants (such as water and air) which can further intensify metal dissolution by the association of metal cations with oxygen or halide ions (Frankel, 1998).

Present solutions for the use of metals in corrosive conditions rely heavily on passive metal oxide layers to restrict the spread of corrosion, significantly changing and restricting such critical metal characteristics as mechanical strength and electrical conductivity (Xue et al., 2007). Alternative solutions conducted by lubricant formulators rely on corrosion inhibition and EPs performance enhancers, which are generally achieved with various chemical components for EHD and boundary lubrication regimes. Although these performance-enhancing additives have distinct chemical compositions, they are usually 'surface active' chemistries that seek out and attach themselves to the metal surfaces being lubricated by polar bonding. Rust inhibitors and EP additives can interact with each other without proper additive selection and result in a decreased effectiveness of one or both additives (Sander, McDaniel and Piangerelli., 2007). This chemisorption competition is not as prominent in nanolubricant, giving it an extra merit characteristic.

When comparing nano-coating and nanolubricant in corrosion protection perspective, it can be argued that the former always relies on the existence of a uniform layer of NPs on the surface, which is not always the case; moreover, it can act as a pocket for corrosive reactants. Lee, J. and Berman, D. discussed this behaviour, in a study case in which graphene-coated surface had higher than regular corrosion rates (i.e. pitting corrosion) were found at the defective edges of the graphene films led to the trapping of the corrosive chlorine ions (Lee and Berman, 2018), as derived from the Energy-dispersive X-ray spectroscopy (EDS) results (Figure 3.9).

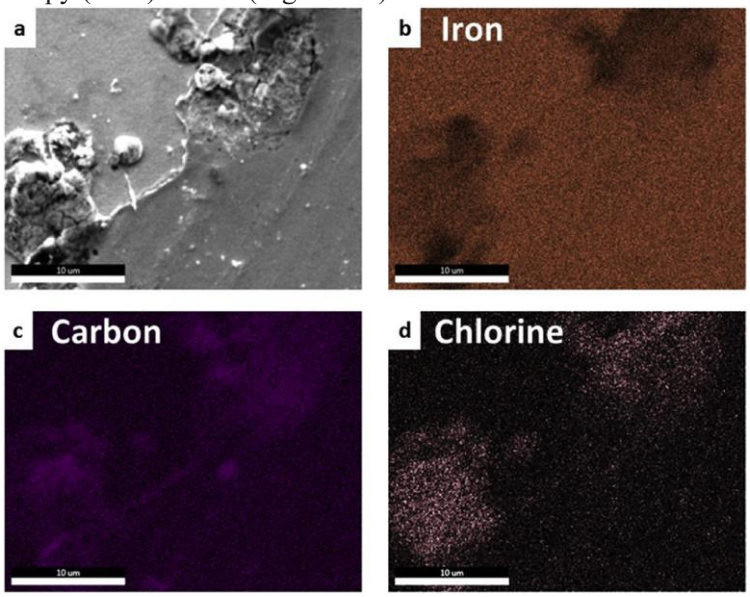

Figure 3.9 *EDS mapping of the CVD-coated iron sample in NaCl solution after 10 h: EDS mapping of a) CVD graphene on iron samples for the graphene tear region for the atomic concentration of (b) iron, (c) carbon,*

and (d) chlorine. The transfer of graphene resulted in the right bottom corner of the sample being partially covered. The analysis confirms a high chlorine presence right at the edge of the graphene flake, (Lee and Berman, 2018).

An alternative solution is to replenish the corrosion-inhibiting properties of the metal surfaces by providing a liquid suspension with a protective coating (i.e., using a nanofluid).

The research on nanolubricant corrosion performance does not seem to be the main interest of tribologist and is rather focused on nano-coated materials as there are no studies conducted on the topic and it is even less in the case of copper corrosion. However, recently Lee, et al. showed that the suspension of silica nanoparticles could benefit not only from higher heat transfer and thermal energy storage rates, but also as corrosion inhibitors of copper substrates (Lee et al., 2019). The study indicates that when silica NPs protect only 10 % of the surface with a nominal diameter of 10 nm, the combined use of the Quartz Crystal Microbalance (QCM) technique and atomic force microscopy suggests a substantial decrease in corrosion rates (up to 4 times), illustrated in Figure 3.10. The negative surface potential of silica NPs preferentially stops negatively charged ions (such as chlorine ions) from entering the metal surface and thereby acts as an impediment to increasing the rate of metal dissolution when the nanoparticles precipitate the copper surface and form surface 'nano-fins'.

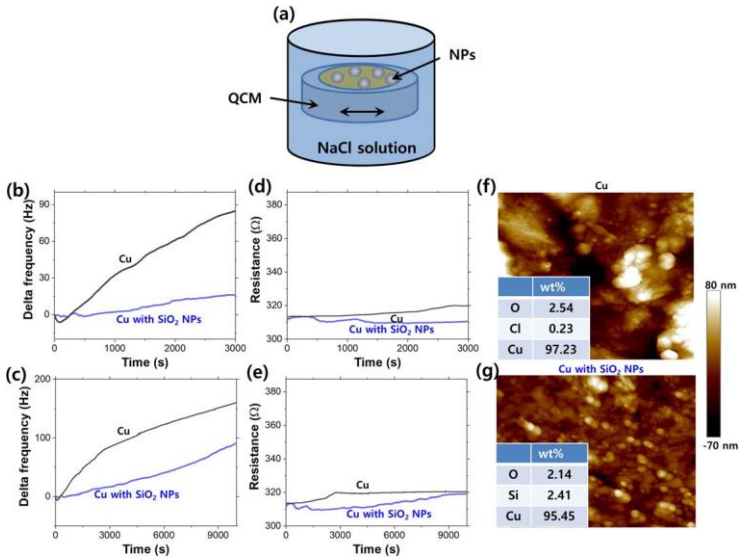

Figure 3.10 *a) Schematic of the QCMexperiment. QCMdelta change in frequency b) and c) and change in resistance d) and (e); analysed in % NaCl solution as a function of time during immersion. Changes in sample morphology after 30 min in a 3 wt% NaCl solution are analysed using AFM:*

f) copper and g) silica nanoparticulate copper. Insets f) and g) summarise the results of the EDS spectra from the samples after 30 minutes of immersion (Lee et al., 2019).

Furthermore, Malshe and Wengyang have patented a dielectric nanolubricant composition based on the addition of modified MoS_2. The addition of dielectric NPs was conducted in various lubricants (Malshe and Zhang, 2018). According to ASTM D130 standards, the dielectric nanolubricant prepared by this method can have a copper corrosion rating of 1B at 100°C.

Alternatively, Carbon-based NPs seems to possess anti-corrosion properties. As 2D-material, graphene not only shears swiftly at the sliding contact interfaces, but also offers corrosion and oxidation protection (Berman, Erdemir and Sumant, 2014). In contrast to graphene, oxidised graphene does not have as good two-dimensional protection, and the presence of oxygen in graphene oxide will cause steel corrosion, thus raising wear (Berman, Erdemir and Sumant, 2014).

An additional option can rely on boron compounds such as boric acid nanopowders, which have been successful in improving A and intense pressure properties, as well as oxidation and thermal stability for corrosion protection (Sawyer et al., 2006; Lovell et al., 2010). It is worth noting that not all NPs have positive effects in resisting corrosion, such an example is IF-WS_2, which is advertised as EP/AW additive for motor oils, gear lubricants, and greases. An out of the box solution can depend on NPs as carriers for other beneficial chemicals towards corrosion. This approach was accomplished in previous experiments, indicating that by using mesoporous NPs as containers filled with corrosion inhibitors, corrosion in metals can be suppressed (Zheludkevich et al., 2007; Borisova, Möhwald and Shchukin, 2011), as shown in Figure 3.11.

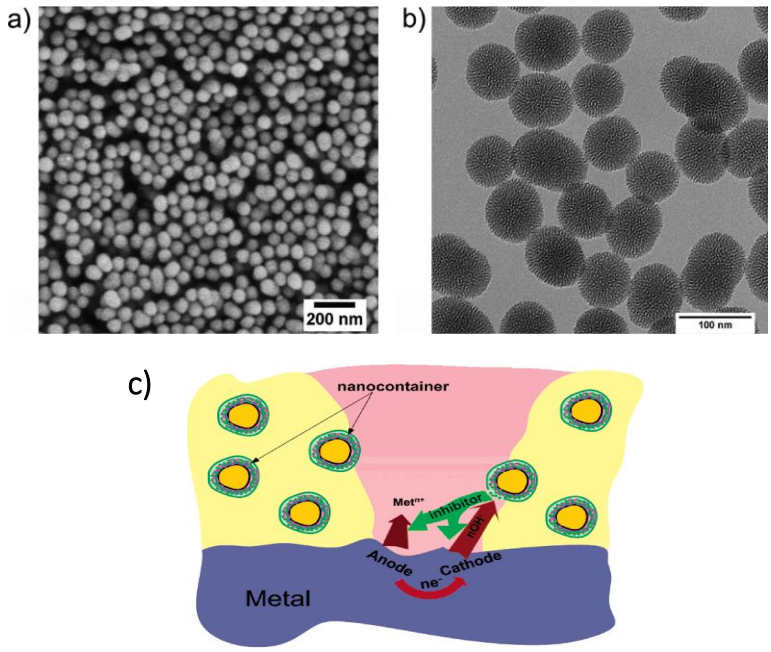

Figure 3.11 *a) Scanning Electron Microscope (SEM), b) TEM micrographs of nanoparticles of mesoporous silica (Borisova, Möhwald and Shchukin, 2011), and (c) Method of the nanocontainers' controllable releasing of the inhibitor and the "smart self-healing" mechanism (Zheludkevich et al., 2007).*

3.7 References

AF MARKET SHARE NEW REGISTRATIONS M1. (2020) [Online] European Alternative Fuels Observatory. Available from : https://www.eafo.eu/vehicles-and-fleet/m1 [Accessed 11/12/20].

AHOLA, J. et al. (2011) Radio-frequency-based detection of electrical discharge machining bearing currents. *IET Electric Power Applications*, 5(4), p. 386.

ALI, M.K.A., HOU, X. and ABDELKAREEM, M.A.A. (2020) Anti-wear properties evaluation of frictional sliding interfaces in automobile engines lubricated by copper/graphene nanolubricants. *Friction*, 8(5), pp. 905–916.

AMBROSE, J. (2020) UK ban on new fossil fuel vehicles by 2030 “not enough” to hit climate targets. *The guardian uk*, 18 Nov.

Annual book of ASTM standards. (1961) ASTM D 288. ASTM.

ASHOUR, M.E. et al. (2017) Novel Tribological Behavior of Hybrid MWCNTs/MLNGPs as an Additive on Lithium Grease. *Journal of Tribology*, 139(4), [Online] Available from: doi.org/10.1115/1.4035345.

ASSOCIATION, C. DEVELOPMENT (2020) *copper.org/environment/sustainable-energy/electric-vehicles*. Available from : https://www.copper.org/environment/sustainable-energy/electric-vehicles [Accessed 11/12/20].

BARRIE, W.L. and LEMIEUX., G.E. (1993) Lubrication and cooling system for a powertrain including an electric motor.

BAUER, W.H., FINKELSTEIN, A.P. and WIBERLEY, S.E. (1960) Flow Properties of Lithium Stearate-Oil Model Greases as Functions of Soap Concentration and Temperature. *A S L E Transactions*, 3(2), pp. 215–224.

BERMAN, D., ERDEMIR, A. and SUMANT, A. V. (2014) Graphene: a new emerging lubricant. *Materials Today*, 17(1), pp. 31–42.

BERMÚDEZ, M.-D. et al. (2009) Ionic Liquids as Advanced Lubricant Fluids. *Molecules*, 14(8), pp. 2888–2908.

BONNETT, A.H. Operating temperature considerations and performance characteristics for IEEE 841 motors. In: *Record of Conference Papers. Industry Applications Society Forty-Seventh Annual Conference. 2000 Petroleum and Chemical Industry Technical Conference (Cat. No.00CH37112)*. IEEE, pp. 77–89.

BORISOVA, D., MÖHWALD, H. and SHCHUKIN, D.G. (2011) Mesoporous Silica Nanoparticles for Active Corrosion Protection. *ACS Nano*, 5(3), pp. 1939–1946.

BOŠKOSKI, P. et al. (2010) Detection of lubrication starved bearings in electrical motors by means of vibration analysis. *Tribology International*, 43(9), pp. 1683–1692.

BOYANTON, H.E. and HODGES, G. (2002) Bearing fluting [motors]. *IEEE Industry Applications Magazine*, 8(5), pp. 53–57.

BOYDE, STEVE. (2002) Green lubricants. Environmental benefits and impacts of lubrication. *Green Chemistry*, 4(4), pp. 293–307.

CHA, C. et al. (2013) Carbon-Based Nanomaterials: Multifunctional Materials for Biomedical Engineering. *ACS Nano*, 7(4), pp. 2891–2897.

CHAN, C.C. (2002) The state of the art of electric and hybrid vehicles. In: *Proceedings of the IEEE*. pp. 247–275.

CHANG, H. et al. (2014) Anti-wear and friction properties of nanoparticles as additives in the lithium grease. *International Journal of Precision Engineering and Manufacturing*, 15(10), pp. 2059–2063.

CHENG, Z.-L. and QIN, X.-X. (2014) Study on friction performance of graphene-based semi-solid grease. *Chinese Chemical Letters*, 25(9), pp. 1305–1307.

CHRISTENSEN, G. et al. (2020) Carbon nanotubes grease with high electrical conductivity. *Synthetic Metals*, 268, p. 116496.

COSTELLO, M.J. Shaft voltages and rotating machinery. In: *Industry Applications Society 38th Annual Petroleum and Chemical Industry Conference*. IEEE, pp. 71–78.

CREVILLEN, A.G., ESCARPA, A. and GARCÍA, C.D. (2018) Chapter 1. Carbon-based Nanomaterials in Analytical Chemistry. In: pp. 1–36.

DASSENOY, F. (2019) Nanoparticles as Additives for the Development of High Performance and Environmentally Friendly Engine Lubricants. *Tribology Online*, 14(5), pp. 237–253.

DOPPELBAUER, M. and WINZER, P. (2016) Shut Up About the Batteries: The Key to a Better Electric Car Is a Lighter Motor. In: *IEEE Energy Conversion Congress and Exposition*.

DUONG, S. et al. (2018) New Approach for Understanding the Oxidation Stability of Neopolyol Ester Lubricants Using a Small-Scale Oxidation Test Method. *ACS Omega*, 3(9), pp. 10449–10459.

FARFAN-CABRERA, L.I. (2019) Tribology of electric vehicles: A review of critical components, current state and future improvement trends. *Tribology International*, 138, pp. 473–486.

FLORES-TORRES, S., HOLT, D.G. and CAREY., J.T. Method for controlling electrical conductivity of lubricating oils in electric vehicle powertrains.

FRANKEL, G.S. (1998) Pitting corrosion of metals. A review of the critical factors. *Journal of the Electrochemical Society*, 145(8), pp. 2970–2970.

FUJITA, H., ITOH, A. and URANO, T. (2019) Newly Developed Motor Cooling Method Using Refrigerant. *World Electric Vehicle Journal*, 10(2), p. 38.

GAFITANU, M.D. et al. (2001) Bearing grease deterioration. *Lubrication Science*, 13(2), pp. 181–191.

GE, X., XIA, Y. and CAO, Z. (2015) Tribological properties and insulation effect of nanometer TiO2 and nanometer SiO2 as additives in grease. *Tribology International*, 92, pp. 454–461.

GONDA, A. et al. (2019) The Influence of Lubricant Conductivity on Bearing Currents in the Case of Rolling Bearing Greases. *Lubricants*, 7(12), p. 108.

GOODARZI, M. et al. (2019) Experimental evaluation of dynamic viscosity of ZnO–MWCNTs/engine oil hybrid nanolubricant based on changes in temperature and concentration. *Journal of Thermal Analysis and Calorimetry*, 136(2), pp. 513–525.

GOW, G. (2007) Ecclesiastes 3: 1, Time for a New Approach? In: *NLGI 74th Annual Meeting*. NLGI.

GOW, G. and CHRISTIERNSSON, A. (1995) Alassca, a complex complex. In: *NLGI*. NLGI, pp. 10–18.

GUO, X. et al. (2016) Effect of Al 2 O 3 Particle Size on Electrical Wear Performance of Al 2 O 3 /Cu Composites. *Tribology Transactions*, 59(1), pp. 170–177.

HE, F., XIE, G. and LUO, J. (2020) Electrical bearing failures in electric vehicles. *Friction*, 8(1), pp. 4–28.

HE, Q. et al. (2017) Effect of nanometer silicon dioxide on the frictional behavior of lubricating grease. *Nanomaterials and Nanotechnology*, 7, p. 184798041772593.

HE, Q., LI, A., WANG, Z., et al. (2018) Tribological behavior of ZnO-Si 3 N 4 nanoparticles-based lubricating grease. *Journal of Experimental Nanoscience*, 13(1), pp. 231–244.

HE, Q., LI, A., GUO, Y., et al. (2018) Tribological properties of nanometer cerium oxide as additives in lithium grease. *Journal of Rare Earths*, 36(2), pp. 209–214.

HEMMAT ESFE, M. and ESFANDEH, S. (2018) Investigation of rheological behavior of hybrid oil based nanolubricant-coolant applied in car engines and cooling equipments. *Applied Thermal Engineering*, 131, pp. 1026–1033.

HOLMBERG, K. and ERDEMIR, A. (2019) The impact of tribology on energy use and CO2 emission globally and in combustion engine and electric cars. *Tribology International*, 135, pp. 389–396.

HOSHINO, MICHIO. (2002) Theory of grease lubricationTechnological trends of grease lubrication. *Japanese journal of tribology*, 47(1), pp. 13–23.

HUANG, Z. et al. (2012) Characterization and application of forced cooling channels for traction motors in HEVs. In: *2012 XXth International Conference on Electrical Machines*. IEEE, pp. 1212–1218.

HWANG, J.G. et al. (2008) Modeling of Streamer Propagation in Transformer Oil-Based Nanofluids. In: *2008 Annual Report Conference on Electrical Insulation and Dielectric Phenomena*. IEEE, pp. 361–366.

IRLE, R. (2019) *Global BEV & PHEV Sales for 2019*. Available from : http://www.ev-volumes.com/news/global-bev-phev-sales-for-2019 [Accessed 11/12/20].

IRTEGOV, Y. et al. (2016) Influence of Copper Nanoparticles on Tribological Properties of Nanolamellar Tungsten Disulfide. *Key Engineering Materials*, 712, pp. 133–136.

IVANOV, M. et al. (2018) Antioxidant Properties of Nanocarbon-based Nanolubricants. *MRS Advances*, 3(47–48), pp. 2881–2886.

JI, X. et al. (2011) Tribological Properties of CaCO3 Nanoparticles as an Additive in Lithium Grease. *Tribology Letters*, 41(1), pp. 113–119.

JING, W. et al. (2017) Synthesis and tribological properties of graphene-copper nanoparticle composites as lithium grease additive. *China Petroleum Processing and Petrochemical Technology*, 19(4), pp. 113–122.

KAMEL, B.M. et al. (2017) Rheological characteristics of modified calcium grease with graphene nanosheets. *Fullerenes, Nanotubes and Carbon Nanostructures*, 25(7), pp. 429–434.

KARKI, A. et al. (2020) Status of Pure Electric Vehicle Power Train Technology and Future Prospects. *Applied System Innovation*, 3(3), p. 35.

KIM, M.-S., LEE, K.-S. and UM, S. (2009) Numerical investigation and optimization of the thermal performance of a brushless DC motor. *International Journal of Heat and Mass Transfer*, 52(5–6), pp. 1589–1599.

KOMATSUZAKL, S., UEMATSU, T. and KOBAYASHL, Y. (2000) Change of grease characteristics to the end of lubricating life. In: *NLGI*. pp. 22–29.

KOZAKO, M. et al. Difference in surface degradation due to partial discharges between polyamide nanocomposite and microcomposite. In: *The 17th Annual Meeting of the IEEE Lasers and Electro-Optics Society, 2004. LEOS 2004.* IEEE, pp. 398–401.

KRAWIEC, S. (2011) On the mechanism of the synergistic effect of PTFE and copper in a lithium grease lubricant. *Industrial Lubrication and Tribology*, 63(3), pp. 171–177.

KUMARA, C., MEYER, H.M. and QU, J. (2019) Synergistic Interactions Between Silver and Palladium Nanoparticles in Lubrication. *ACS Applied Nano Materials*, 2(8), pp. 5302–5309.

LECKNER, J. and WESTBROEK, R. (2017) Polypropylene—a novel thickener technology with many surprises. In: *29th ELGI AGM Helsinki, Finland*. Helsinki, Finland.

LEE, J. et al. (2019) Silica nanoparticles as copper corrosion inhibitors. *Materials Research Express*, 6(8), p. 0850e3.

LEE, J. and BERMAN, D. (2018) Inhibitor or promoter: Insights on the corrosion evolution in a graphene protected surface. *Carbon*, 126, pp. 225–231.

LEE, P.M. and CARPICK, R. (2017) *Tribological opportunities for enhancing America's energy efficiency*.

LI, D., XIE, W. and FANG, W. (2011) Preparation and properties of copper-oil-based nanofluids. *Nanoscale Research Letters*, 6(1), p. 373.

LI, T. et al. (2019) Effect of eco-friendly carbon microspheres on the tribological behavior of lithium lubricating grease. *UPB Sci. Bull. Ser. B*, 81, pp. 57–68.

LI, Z. et al. (2010) Effects of nano-filler addition on partial discharge resistance and dielectric breakdown strength of Micro-Al 2 O 3 Epoxy composite. *IEEE Transactions on Dielectrics and Electrical Insulation*, 17(3), pp. 653–661.

LIM, D.H. and KIM, S.C. (2014) Thermal performance of oil spray cooling system for in-wheel motor in electric vehicles. *Applied Thermal Engineering*, 63(2), pp. 577–587.

LOVELL, M.R. et al. (2010) Influence of boric acid additive size on green lubricant performance. *Philosophical Transactions of the Royal Society A: Mathematical, Physical and Engineering Sciences*, 368(1929), pp. 4851–4868.

LOW, R. et al. (2013) Interfacing two insulation parts in high voltage environment.

LUGT, P.M. (2016) Modern advancements in lubricating grease technology. *Tribology International*, 97, pp. 467–477.

MALSHE, A.P. and ZHANG, W. (2018) Dielectric nanolubricant compositions.

MCHALE, G. et al. (2019) Apparent Contact Angles on Lubricant-Impregnated Surfaces/SLIPS: From Superhydrophobicity to Electrowetting. *Langmuir*, 35(11), pp. 4197–4204.

MEIJER, D. and LANKAMP, H. (1995) Polymer thickened lubricating grease.

MENG, Y., SU, F. and CHEN, Y. (2016) Supercritical Fluid Synthesis and Tribological Applications of Silver Nanoparticle-decorated Graphene in Engine Oil Nanofluid. *Scientific Reports*, 6(1), p. 31246.

MOHAMED, A. et al. (2020) Development and manufacturing an automated lubrication machine test for nano grease. *Journal of Materials Research and Technology*, 9(2), pp. 2054–2062.

MOHAMED, A. et al. (2015) Tribological Behavior of Carbon Nanotubes as an Additive on Lithium Grease. *Journal of Tribology*, 137(1), [Online] Available from: doi.org/10.1115/1.4028225.

MUETZE, A. and BINDER, A. (2006) Don't lose your bearings. *IEEE Industry Applications Magazine*, 12(4), Jul., pp. 22–31.

MUKHERJEE, R., PATRA, A. and BANERJEE, S. (2010) Impact of a Frequency Modulated Pulsewidth Modulation (PWM) Switching Converter on the Input Power System Quality. *IEEE Transactions on Power Electronics*, 25(6), pp. 1450–1459.

NAIDU, S.K., KLAUS, E.E. and DUDA, J.L. (1984) Evaluation of liquid phase oxidation products of ester and mineral oil lubricants. *Industrial & engineering chemistry product research and development*, 23(4), pp. 613–619.

NAKAHAMA, T. et al. (2006) Cooling Airflow in Unidirectional Ventilated Open-Type Motor for Electric Vehicles. *IEEE Transactions on Energy Conversion*, 21(3), pp. 645–651.

NALLUSAMY, S. and LOGESHWARAN., J. (2017) EXPERIMENTAL ANALYSIS ON NANOLUBRICANTS USED IN MULTI CYLINDER PETROL ENGINE WITH COPPER OXIDE AS NANOPARTICLE. *Rasayan Journal of Chemistry*, 3, pp. 1050–1055.

NAZIR, M.H. et al. (2018) Synergistic wear-corrosion analysis and modelling of nanocomposite coatings. *Tribology International*, 121, pp. 30–44.

NIPPES, P.I. (2004) Early Warning of Developing Problems in Rotating Machinery as Provided by Monitoring Shaft Voltages and Grounding Currents. *IEEE Transactions on Energy Conversion*, 19(2), pp. 340–345.

NIU, M. and QU, J. (2018) Tribological properties of nano-graphite as an additive in mixed oil-based titanium complex grease. *RSC Advances*, 8(73), pp. 42133–42144.

PALACIO, M. and BHUSHAN, B. (2010) A Review of Ionic Liquids for Green Molecular Lubrication in Nanotechnology. *Tribology Letters*, 40(2), pp. 247–268.

PANDA, P.K. et al. (2002) Thermal shock and thermal fatigue study of ceramic materials on a newly developed ascending thermal shock test equipment. *Science and technology of advanced materials*, 3(4), p. 327.

PAUL, G. et al. (2019) Tribological behavior of dodecylamine functionalized graphene nanosheets dispersed engine oil nanolubricants. *Tribology International*, 131, pp. 605–619.

PREISINGER, G. (2002) *Cause and effect of bearing currents in frequency converter driven electrical motors: investigations of electrical properties of rolling bearings.*

PUNCKT, C. (2004) Sudden Onset of Pitting Corrosion on Stainless Steel as a Critical Phenomenon. *Science*, 305(5687), pp. 1133–1136.

QIANG, H. et al. (2019) Tribological and rheological properties of nanorods–Al 2 O 3 as additives in grease. *Proceedings of the Institution of Mechanical Engineers, Part J: Journal of Engineering Tribology*, 233(4), pp. 605–614.

RAADNUI, S. and KLEESUWAN, S. (2012) Electrical pitting of grease-lubricated rolling and sliding bearings: a comparative study. In: *Journal of Physics: Conference Series*. p. 012041.

RADULESCU, A. V. and RADULESCU, I. (2006) Rheological models for lithium and calcium greases. *Mechanics*, 59(3), pp. 67–70.

RAPOPORT, L., FLEISCHER, N. and TENNE, R. (2003) Fullerene-like WS2 Nanoparticles: Superior Lubricants for Harsh Conditions. *Advanced Materials*, 15(78), pp. 651–655.

RASHEED, A.K. et al. (2015) Study of graphene nanolubricant using thermogravimetric analysis. In: *Proceedings of Malaysian International Tribology Conference*. pp. 155–156.

RAWAT, S.S. et al. (2019) Pristine and Alkylated MoS2 Nanosheets for Enhancement of Tribological Performance of Paraffin Grease Under Boundary Lubrication Regime. *Journal of Tribology*, 141(7), [Online] Available from: doi.org/10.1115/1.4043606.

ROMANENKO, A. (2017) *Study of inverter-induced bearing damage monitoring in variable-speed-driven motor system*.

ROMANENKO, A., MUETZE, A. and AHOLA, J. (2016) Effects of Electrostatic Discharges on Bearing Grease Dielectric Strength and Composition. *IEEE Transactions on Industry Applications*, 52(6), pp. 4835–4842.

SALMERON, C. and BENJAMIN, G. (2019) *Enabling More Efficient E-Mobility: Grease Development by a Novel Bearing-Grease Test Machine*.

SANDER, J., MCDANIEL, E. and PIANGERELLI., D. (2007) Grease Characterization: Are All Greases Lithium Greases? In: *ubrication and Lubricants*. pp. 431–437.

SAWYER, W.G. et al. (2006) In Situ Lubrication with Boric Acid: Powder Delivery of an Environmentally Benign Solid Lubricant. *Tribology Transactions*, 49(2), pp. 284–290.

SCARLETT, N.A. (1967) Paper 21: Use of Grease in Rolling Bearings. *Proceedings of the Institution of Mechanical Engineers, Conference Proceedings*, 182(1), pp. 585–624.

SENATORE, A. (2020) Editorial: Special Issue "Automotive Tribology." *Lubricants*, 8(4), p. 48.

SEONG, K.-H. et al. (2014) Investigation of Temperature Rise in an Induction Motor Considering the Effect of Loading. *IEEE Transactions on Magnetics*, 50(11), pp. 1–4.

SINGH, J., KUMAR, D. and TANDON, N. (2018) Tribological and Vibration Studies on Newly Developed Nanocomposite Greases Under Boundary Lubrication Regime. *Journal of Tribology*, 140(3), [Online] Available from: doi.org/10.1115/1.4038100.

SINGH, R.K. et al. (2016) Study of a novel phenolic-ester as antioxidant additive in lube, biodiesel and blended diesel. *Journal of Industrial and Engineering Chemistry*, 37, pp. 27–31.
SOLEIMANI, M. et al. (2018) Antioxidants classification and applications in lubricants. In: *LubricationTribology, Lubricants and Additives*. InTech, p. 23.
SUDGES, R.A. (1968) Transistor insulator with self-contained silicone grease supply.
SUNAHARA, K. et al. (2011) Preliminary Measurements of Electrical Micropitting in Grease-Lubricated Point Contacts. *Tribology Transactions*, 54(5), pp. 730–735.
SUZUMURA, J. (2016) *Prevention of Electrical Pitting on Rolling Bearings by Electrically Conductive Grease*.
VENGUDUSAMY, B., ENEKES, C. and SPALLEK, R. (2019) On the film forming and friction behaviour of greases in rolling/sliding contacts. *Tribology International*, 129, pp. 323–337.
WALTHER, H.C. and HOLUB, R.A. (2014) Lubrication of electric motors as defined by IEEE standard 841-2009, shortcomings and potential improvement opportunities. In: *2014 IEEE Petroleum and Chemical Industry Technical Conference (PCIC)*. IEEE, pp. 91–98.
WANG, L. et al. (2007) Tribological investigation of CaF2 nanocrystals as grease additives. *Tribology International*, 40(7), pp. 1179–1185.
WANG, R. et al. (2011) Development and performance characterization of an electric ground vehicle with independently actuated in-wheel motors. *Journal of Power Sources*, 196(8), pp. 3962–3971.
WANG, T. et al. (2020) Impact of Boron Nitride Nanoparticles on the Wear Property of Lithium Base Grease. *Journal of Materials Engineering and Performance*, 29(8), pp. 4991–5000.
WANG, X. and WANG, Z.D. (2008) Particle Effect on Breakdown Voltage of Mineral and Ester Based Transformer Oils. In: *2008 Annual Report Conference on Electrical Insulation and Dielectric Phenomena*. IEEE, pp. 598–602.
WHITE, MICHAEL. (2015) Rolling bearing with integrated electrical shunt.
WILLIAMS, D.E. et al. (1991) Passivity breakdown and pitting corrosion of binary alloys. *Nature*, 350(6315), pp. 216–219.
WU, H. et al. (2017) A study of the tribological behaviour of TiO 2 nano-additive water-based lubricants. *Tribology International*, 109, pp. 398–408.
WU, J. et al. (2018) Efficiency comparison of electric vehicles powertrains with dual motor and single motor input. *Mechanism and Machine Theory*, 128, pp. 569–585.
XIA, X.T. et al. (2010) Influence of ZrO2 Nanoparticle as Additive on Tribological Property of Lithium Grease. *Applied Mechanics and Materials*, 26–28, pp. 83–87.

XIE, G. et al. (2008) Micro-Bubble Phenomenon in Nanoscale Water-based Lubricating Film Induced by External Electric Field. *Tribology Letters*, 29(3), pp. 169–176.

XUE, W. et al. (2007) Preparation of anti-corrosion films by microarc oxidation on an Al–Si alloy. *Applied Surface Science*, 253(14), pp. 6118–6124.

YAN, C. et al. (2019) Friction-Induced Hardening Behaviors and Tribological Properties of 60NiTi Alloy Lubricated by Lithium Grease Containing Nano-BN and MoS 2. *Tribology Transactions*, 62(5), pp. 812–820.

YU, Z.-Q. and YANG, Z.-G. (2011) Fatigue Failure Analysis of a Grease-Lubricated Roller Bearing from an Electric Motor. *Journal of Failure Analysis and Prevention*, 11(2), pp. 158–166.

ZAAROUR, M. et al. (2019) Zeolite Nanocrystals Protect the Performance of Organic Additives and Adsorb Acid Compounds during Lubricants Oxidation. *Materials*, 12(17), p. 2830.

ZHANG, B. et al. (2014) Thermal model of totally enclosed water-cooled permanent magnet synchronous machines for electric vehicle applications. In: *2014 International Conference on Electrical Machines (ICEM)*. IEEE, pp. 2205–2211.

ZHANG, W. et al. (2012) Fundamental understanding of the tribological and thermal behavior of Ag–MoS2 nanoparticle-based multi-component lubricating system. *Wear*, 288, pp. 9–16.

ZHANG, X. et al. (2014) Preparation and tribological properties of Bi nanoparticles as a lithium grease additive. *Optoelectronics and Advanced Materials-Rapid Communications*, 8, pp. 500–505.

ZHAO, G. et al. (2014) Tribological properties of nano-calcium borate as lithium grease additive. *Lubrication Science*, 26(1), pp. 43–53.

ZHELUDKEVICH, M.L. et al. (2007) Anticorrosion Coatings with Self-Healing Effect Based on Nanocontainers Impregnated with Corrosion Inhibitor. *Chemistry of Materials*, 19(3), pp. 402–411.

ZHENG, B. et al. (2020) Friction and wear property of lithium grease contained with copper oxide nanoparticles. *Applied Nanoscience*, 10(4), pp. 1355–1367.

ZHONGYI, H. et al. (2013) Tribological and Antioxidation Synergistic Effect Study of Sulfonate-Modified Nano Calcium Carbonate LORENZ, C. (ed.). *PLoS ONE*, 8(5), p. e62050.

Chapter IV. Graphene-Based Naonosheets as lubricant additives

4.1 Overview

Nowadays, there is a growing demand for highly efficient lubricants. Several aspects define a lubricant's efficiency, including the energy consumption reduction percentage, an increase of machines' service life, eco-friendliness, and long-time performance. Conventional lubrication depends on the choice of different types of liquid lubricants as intermediate means between metal surfaces in contact. The major constituents of a fully formulated lubricant are hydrocarbon molecules, whereas the remaining part is made up of performing additives. These additives include friction and wear modifiers, which for many years have been represented by organic carboxylic acids and phosphorus-based chemicals (Bowden, Gregory and Tabor, 1945; Forbes, 1970; Spikes, 2004).

Lubrication is a complicated phenomenon, and it is most convenient to consider it as a system which is a function of many factors such as the lubricated surface characteristics, chemical and physical interactions between lubricant molecules and surface- friction conditions, thin film dynamics in steady and transient conditions.

In order to improve the effectiveness of such a complex system, nanoparticles can be chosen as lubrication additives, which, even in small amounts, can bring about substantial improvements in physical properties, i.e., thermal, heat dissipation (Sudeep et al., 2014; Taha-Tijerina, Aviña and Diabb, 2019), as well as work as friction modifiers (FM) and anti-wear agents (AW)

(Bakunin et al., 2004; Jiao et al., 2011; Zhang et al., 2012; Sarno et al., 2014). This positive attribute is due to their chemical stability, limited interaction with other additives and non-volatility, resulting in excellent durability in harsh conditions (Spikes, 2015). The latter advantage of nanoparticles is a big drawback for organic traditional FM and AW additives. Therefore, researchers began to study nanoparticles for the reduction and optimization of friction and wear.

In this chapter, the focus has been placed on graphene's (G) main derivatives, graphene oxide (GO) and reduced graphene oxide (rGO), as lubricant additives for friction and wear reduction. The reason for focusing on rGO and GO includes the possibility of their mass production with respect to pristine G (Seiler et al., 2018). There are several differences and contrasts between rGO and GO. The former one has more effective dispersion abilities in non-polar solvents in comparison to GO (Konios et al., 2014) and possesses relatively restored superior mechanical and thermal conductivity properties after reduction (Pei and Cheng, 2012), while the abundant presence of reactive oxygen groups on the GO's surface favours its functionalization for an enhanced dispersion (Li et al., 2014). Regardless of all these differences, both rGO and GO have friction- and wear-reduction properties when added to a lubricant oil.

G is one of the strongest materials (Lee et al., 2008) in the form of a monolayer. Moreover, G's multi-layers are easily sheared (Berman, Erdemir and Sumant, 2014), due to both the weak Van der Waals forces between its sheets (Van, 2018) and its high chemical stability (Van, 2018). These characteristics make it an excellent candidate as a lubricant additive, mainly for friction and wear reduction. In particular, the two-dimensional graphene sheets gained considerable attention as a solid lubricant. Nevertheless, the usage of G and its derivatives as additives in liquid lubricants still requires more comprehensive analyses. These characteristics make it an excellent candidate as a lubricant additive, mainly for friction and wear reduction. Nevertheless, the usage of G and its derivatives as additives in liquid lubricants still requires more comprehensive analyses.

In order to maximize the tribological merits of nanoparticles' utilization as additives in lubricant oils, apart for nanomaterials' size (indeed, the hardness of nanoparticles increases as the particle size decreases (An et al., 2019), and when this hardness becomes higher than the one of the tribo-pair scratching and/or indentation can occur), two factors play a significant role: the nanoparticles' concentration optimization (Lin, Wang and Chen, 2011a) and the requirement of a stable and homogenous- dispersion (Lin, Wang and Chen, 2011a; Kim and Archer, 2011). In particular, the concentration optimization is still far from being standardized and rationalized, since it strongly depends on the characteristics of the base oil, the additive and their mixture.

In the case of G and its derivatives, the aforementioned instability is caused by different factors. First, G and its derivatives exhibit a very large surface

area of ~2590 m^2g^{-1} (Qin et al., 2014), which gives rise to a high interface area and high surface energy within the solvent, pushing the sheets to aggregate in order to reduce this huge energy. Additionally, the sheets tend to re-stack and re-aggregate under Van der Waals interactions (Shen et al., 2009). In the case of non-polar solvents, which constitute the majority of lubricant mediums, the difficulty in forming a stable G suspension is even greater, due to their inert nature.

In summary, this review, after introducing the four main lubrication mechanisms of nanoparticles, such as tribofilm formation due to tribochemical reaction (YU et al., 2008; Tomala et al., 2015), ball bearing (Viesca et al., 2011; Sayuti et al., 2014), mending and the polishing effect (Liu et al., 2004), focuses considerable attention on the adoption of rGO/GO in the field of tribology and includes a critical review dedicated to the optimization of nanoparticles, as well as to nanoadditives' functionalization to give a stable and homogenous suspension.

4.2 rGO/GO lubrication mechanism

As the main interest of this chapter is the adoption of rGO and GO nanosheets in tribology, the focus will be on lamellar structures and their behavior under di_erent conditions. The main lubrication mechanism of lamellar nanoparticles, such as graphene and MoS_2, derives from the formation of a tribo-film which acts as a protective layer between the metal pairs (Xu et al., 2015). Additionally, polishing or smoothing e_ects are also reported in the literature (Eswaraiah, Sankaranarayanan and Ramaprabhu, 2011).

Lin et al., 2011, attributed the outstanding lubrication performance of rGO nanoparticles to their small size and extremely thin laminated structure, allowing the rGO sheets to easily access the contact area, thereby preventing the rough surfaces from coming into direct contact (Lin, Wang and Chen, 2011a). Zhang et al., 2011, explained the rGO tribological mechanism by revealing the formation of a protective layer on the surface of the steel ball specimen at not so high nanoadditive concentrations (i.e., when exceeding a critical value, dry contact occurs), which indicates an enhanced anti-wear performance due to smoothed surfaces with reduced roughness (Zhang et al., 2011). In the study by Mungse et al., 2014, the excellent performance of rGO, whose dispersion in lube oil was enhanced by a modification obtained through a chemical procedure for selective inclusion of long alkyl chains on the edges and defects sites through amide linkage, as a lubricant additive are the results of: (a) the weak Van der Waals interactions between the lamellas of the modified rGO sheets, which make them easy to be sheared under the rolling contact stress; and (b) the continuous supply of the modified rGO sheets on

the contact surfaces due to their stable dispersion in the lube oil (Mungse and Khatri, 2014a).

Kim et al., 2011, demonstrated the importance of graphene as the thinnest solid lubricant that reduces adhesion and friction forces between the contact surfaces at the nano and microscale while protecting the coated surfaces at once (Kim et al., 2011). Additionally, Sarno et al., in 2014, showed that the protection offered to the tribo-interfaces by the laminated structure of reduced GO nanosheets generated during sliding was suitable for reducing friction and wear (Sarno et al., 2014).

Berman et al., 2013, found that, after 400 cycles of sliding contact, ethanol-processed graphene was gradually removed from the wear track; consequently, friction increased until a new dose of graphene was supplied to the contact interfaces. Therefore, for an efficient performance, the long-term dispersion stability of graphene nanosheets in lube oil is essential for their uninterrupted supply to the contact interfaces (Berman, Erdemir and Sumant, 2013).

Mungse et al., 2015, observed that modified GO nanosheets dispersed in lube oil are deposited on the contact interfaces under the sliding tribo-stress, as confirmed by Raman spectroscopy. It was proposed that under the sheared contact, some of the graphene layers are delaminated and then deposited on the contact interfaces. As the sliding goes on, the dispersed modified GO nanosheets in the lube oils easily sheared with the weakly adhered graphene on the contact interfaces of the steel ball and disc (Figure 4.1 a and b), reducing the friction significantly (Mungse, Kumar and Khatri, 2015a). Additionally, in the case of MoS_2 nanosheets, it has been found that, under the sheared contact, delaminated sheets are weakly deposited on the contact interfaces. It was observed that the deposition and then removal of MoS_2 nanosheets from the contact interfaces was a continuous process under the sliding contact stress (Bart, Gucciardi and Cavallaro, 2013). Furthermore, deposited graphene nanosheets on contact interfaces protect the surface against the tribo-damages. Hence, for maintaining the low friction and protection of contact surfaces, the uninterrupted supply of solid lubricant additive is very important. This can be obtained by a thorough dispersion of graphene nanosheets in the lube oil (Mungse, Kumar and Khatri, 2015b). Patel et al., 2019, investigated the tribological effects of highly reduced graphene oxide (H-rGO) nanoplatelets as additives to mineral base oil, aiming to exploit the fewer oxygen groups present between the microlayers, allowing spacing between the surfaces to accommodate the lubricant (Patel and Kiani, 2019). Liñeira del Río et al., 2019, (Liñeira del Río et al., 2019) studied the tribological properties of nanolubricants formed by trimethylolpropane trioleate (TMPTO) or polyalphaolefin (PAO 40) base oils with reduced graphene oxide sheets (rGO) (Schlüter, Mülhaupt and Kailer, 2014; Gupta et al., 2016; Li et al., 2016; N. Ismail and Bagheri, 2017) whose reduction was carried out in order to obtain a good stability of the nanoadditives in the fluids, observing 24% and 20%

friction enhancement for the PAO 40 and the TMPTO base oils, respectively. Mungse et al., 2019, prepared alkylated graphene oxide (GO)/reduced graphene oxide (rGO) by covalent interaction with octadecyltrichlorosilane (OTCS) and octadecyltriethoxysilane (OTES), finding that the variable oxygen functionalities in the GO/rGO and hydrolysis rate of octadecylsilanes governed the grafting density of octadecyl chains on the GO and rGO. In terms of the coefficient of friction and wear scar diameter, the tribological properties revealed a good correlation with the structure of alkylated GO/rGO and their dispersion stability in the poly lube base oil (Mungse et al., 2019).

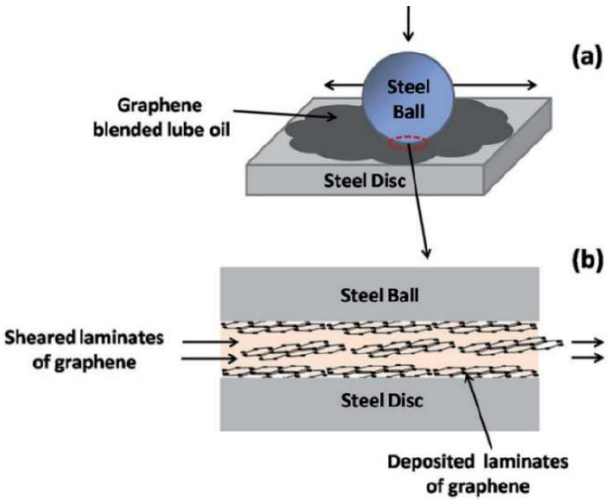

Figure 4.1 *Schematic illustration of the role of graphene nanosheets under the sliding contact (Mungse, Kumar and Khatri, 2015b). (a) The ball-on-disc contact with GO–octadecylamine (ODA) blended lube oil. (b) The image of the contact interfaces was magnified in order to show the deposited and sheared graphene nanosheets, which are responsible for friction and wear reductions.*

4.2.1 rGO/GO Behavior in Different Lubrication Conditions

Most of the studies confirmed the beneficial role of rGO/GO nanosheets in different types of base lubricant oils. With regards to the lubricant film thickness, four different regimes can be recognized: hydrodynamic, boundary, mixed and elastohydrodynamic. Because of the different film thicknesses between tribo-surfaces, nanolubricants were typically explored in two lubrication regimes, characterized by high load and speed. Under these intensive conditions, rGO/GO nanosheets play a significant role in the lubrication process. However, one of the most important factors for the nanosheets to be activated within this thin film is their ability to deposit onto the contacting regions and form a continuous film. This formation requires a

good dispersion capability and, depending on the binding forces, that speeds do not exceed a critical value to be drifted away with the film flow (Yu and Xie, 2012).

4.3 Nanoadditives in Tribology: The Critical Aspects

4.3.1 Optimum Concentration

The optimum concentration of additives in lubricating oils is a function of the amount of particles performing their tribological properties and can decrease with an increased dispersion stability. The enhancement of the lubrication performance which occurs when a small amount of graphene is added is related to the formation of a protective layer between the rubbing surfaces. The utilization of the optimum concentration is of great significance as an excess in loading could result in the formation of a discontinuous oil layer (Zhang et al., 2011). This can deteriorate the anti-wear performance due to the partial dry friction or transition to boundary regions. In Table 4.1, some of the main results regarding this topic are shown (see column 4).

Ref.	Method of stabilization	Optimum Concentration	Lubricant oil	Stability	Tribometer	Load	Speed	Temperature/ time	Wear reduction	Friction reduction
(Zhao et al., 2017)	Mild thermal reduction of graphene oxide achieved by high temperature (700 °C) treatment	0.5 wt%	Base oil PAO 6	25 h	Ball-on-disc	2 N	24 rpm	NA/ 1.5 h	positive effect	30%
(N. A. Ismail and Bagheri, 2017)	Covalent functionalization with organic moiety*	0.01 wt%	Base oil (NA)	1 month	4-ball	400 N	1200 rpm	Room /1 h	30%	16%
(Mungse, Kumar and Khatri, 2015c)	Basal plane modification with Octadecylamine *	0.02 mg mL^{-1}	commercial engine oil 10W-40	1 month	standard steel balls reciprocating ball-on-disc	100 mN	(Micro:1 cm s^{-1}) (standard:3 cm s^{-3})	Room / 1 h	25%	25%
(Lin, Wang and Chen, 2011b)	Stearic and oleic acids (mass ratio 3:5) modification	0.075 wt%	Base oil SN350	NA	4-ball	147 N	1200 rpm	75 ± 2 °C / 1h	0.8 -0.3	0.15 -0.12
(Ali et al., 2018)	Oleic acid surfactant in oil	0.4 wt%	A5 (5W-30)	NA	Bench of ring/line	90-368 N	0.154 -0.6 m/s	Room /NA	22-29%	29-35%
(Mungse and Khatri, 2014b)	Amide linkage for octadecylamine defects edges sites modification*	0.02 mg mL^{-1}	commercial engine oil (10W-40)	1 month	4-ball	392 N	1200 rpm	75 °C/ 1 h	26%	9%
(Ota et al., 2015)	Use of the dispersant: poly isobutylene succinic imide in oil	0.5 wt% (used)	API Gr I and II lube base oils + linear alkyl benzene	1 year	Block-on-ring	900 N	1125 rpm	50-110 °C / 3 h	positive effect	0.07 -0.02
(Dou et al., 2016)	Graphene balls formation by using an aerosol capillary compression approach	0.01–0.1 wt %	Base oil PAO4	20 h	Pin-on-disk/boundary regime	10 N	linear sliding (10 mm/s)	Room/0.5 or 1 h	~85%	20%

***Covalent immobilization**

Table 4.1 *Overview of the main literature results concerning the use of reduced graphene oxide and graphene oxide (rGO/GO) as lubricant additives.*

In particular, Zhao et al. (Zhao et al., 2017) report the preparation of mildly thermally reduced graphene oxide at 700 °C for 5 h, which shows an optimal concentration of 0.5 wt%, beyond which additive aggregation under lubrication conditions highly occurs, leading to a reduced permeation of the as obtained rGO aggregates into the rubbing surfaces. This agglomeration phenomenon at higher concentrations also occurs with chemically modified rGO (N. A. Ismail and Bagheri, 2017) and surfactant-stabilized graphene nanosheets (Ali et al., 2018): beyond the optimum concentration value, the higher the sheets aggregation (which could be caused by additive instability in oil), the more likely that the uninterrupted supply to metal surfaces could be not provided.

In addition, aggregation can also start at the concentration at which lubricating surfaces become saturated with additive nanosheets (Ali et al., 2018). In (N. A. Ismail and Bagheri, 2017), the optimum concentration of the synthesized functionalized reduced graphene in base oil is 0.01 wt%, and the authors clearly explain the reason to choose this optimum amount, since: (1) at lower concentrations (0.005 wt%), rGO can easily disperse, though, due to the shortage of additive, the additive sheets cannot cover the whole metal surfaces with their protective film; (2) at higher concentration (0.015 wt%), the excess sheets will act as debris, producing abrasive-like wear. A similar trend in additive concentration and a similar corresponding explanation can also be formulated for the basal plane octadecylamine functionalized GO (Mungse, Kumar and Khatri, 2015c) and the stearic/oleic acid-modified graphene platelets (Lin, Wang and Chen, 2011b). The latter also showed a similar trend with regard to the load-carrying capacity.

As previously mentioned, Zhang et al. (Zhang et al., 2011) give a more detailed explanation of this phenomenon, which is related to the importance of maintaining the continuity of the oil layer during lubrication. The authors produced oleic acid-modified graphene sheets, observing an optimum concentration of the additive in base oil of 0.02–0.06 wt%. According to them, the optimum corresponds to the amount of graphene sheets on the lubricating surfaces which maximizes the ratio between the oil film thickness and surface roughness, i.e., the maximum shift from a mixed to boundary lubrication regime. At higher concentrations than the optimum one, the graphene sheets pile up between the lubricating surfaces, breaking the continuity of the oil film and determining again a fall into the mixed regime and, eventually, dry contact. More generally, wear and friction decrease with the gradual addition of graphene up to a specific concentration, after which they start to rise, achieving values higher than the ones shown by the free-additives oil (i.e., lubrication governed by solid nanoparticles, “dry lubrication”). It was assumed that friction was a function of three terms, as illustrated in Equation (4.1) (Zhang et al., 2011):

$$F_C = \frac{FC_o A_o + FC_g A_g + FC_f A_f}{A_o + A_g + A_f} \quad (4.1)$$

where A_o, A_g and A_f are the friction area between friction pairs separated by oil-containing graphene, friction area separated only by graphene (dry-contact) and dry-contact area of furrows, respectively. The progressive addition of graphene determines an increase of A_g and a reduction of A_f. This is true until a certain point and results in friction and wear reductions. On the other hand, after that point, A_g increases, generating an abrasive effect with wear and friction that is higher than for pure oil.

Eventually, it is worth mentioning that the morphology and dimensions of additives can also be crucial in determining the effect of additive concentration on tribological performance. For instance, Dou et al. (Dou et al., 2016) produced ultrafine particles consisting of crumpled, paper-ball–like graphene which, unlike more traditional GO/rGO nanosheet additives, show no significant variation in the friction coefficient and wear reduction at both 0.01 wt.% and 0.1 wt.% due to their high self-dispersion and aggregation-resistant properties.

4.3.2 Nanosuspensions: Stability Factors:

Suspension stability is one of the main factors affecting the tribological performances of lubricant oils. This is a topic not fully explored at all.

Suspended nanoparticles are pushed to attract each other, driven by their high surface energy. DLVO theory (Derjaguin and Landau 1941, Verwey and Overbeek 1948) suggests that the stability of a nanofluid suspension is determined by a balance between Van der Waals attractive forces among nanoparticles and the electrical double layer repulsive forces (Yu and Xie, 2012). Van der Waals forces are almost always present, and they result from interactions of the rotating or fluctuating dipoles of atoms and molecules. In the simplest situation, this interaction can be modelled as Equation 4.2 (Trefalt and Borkovec, 2017).

$$W_{v\,dW}(h) = \frac{-H}{12\pi^2} \quad (4.2)$$

Where H is the Hamaker constant, which defines forces strength. In most of the situations, the Hamaker constant is positive, meaning that the Van der Waals force is attractive. Typical values of H are in the range 10−21-10−19 J. Double layer interactions can be approximated as in Equation 4.3 (Trefalt and Borkovec, 2017).

$$\mathrm{W_{dl}(h)} = \frac{2\sigma_+\sigma_-}{\varepsilon_0\varepsilon_k}\exp(-kh) \quad (4.3)$$

Where σ+ and σ− are the surface charge densities per unit area of the right and left surfaces, ϵ0 is the permittivity of vacuum, ϵ the dielectric constant of water, and κ is the inverse Debye length (Trefalt and Borkovec, 2017).

As shown in Figure 4.2, in the state of a random Brownian movement of suspended nanoparticles, the stability is governed by repulsive forces greater than attractive interactions. Electrostatic repulsions between nanoparticles, as well as steric repulsions, (Figure 4.3, a) can generate a stable homogenous suspension (Figure 4.2, b).

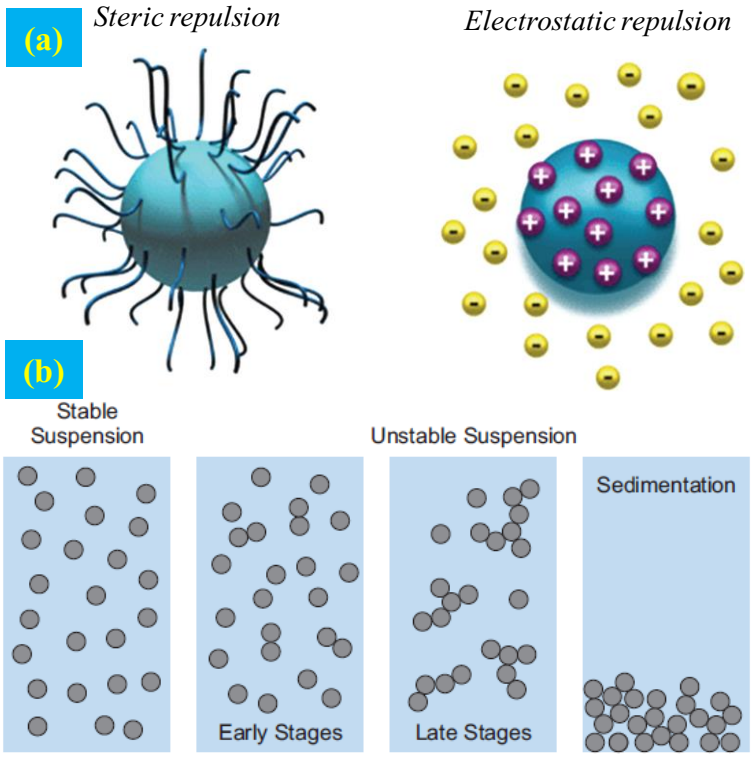

Figure 4.2 *a) Types of colloidal stabilization (Yu and Xie, 2012). Reproduced with permission from [Yu, W.; Xie, H.], [Journal of Nanomaterials]; published by [Hindawi], [2012]. b) Particle aggregates formation: as the aggregation proceeds, the particles form larger and larger clusters and sediments.*

4.4 rGO/GO suspension stabilization techniques

In general, rGO/GO nanosheets can be stabilized by either adding a dispersing agent into the solvent or by surface modification, see Table 4.1 column 2. A depth discussion about these two methods is presented below, along with a detailed description of the stabilization methods reported in the literature for specific dispersion in lubricant base oils.

4.4.1 Dispersing agents

It is a common practice in lubrication to add dispersant molecules that can interact with organic contaminants, generated from aging and oxidation processes, to maintain them in suspension until the filtration point of the lubrication system is reached. They reduce the formation of deposits on metal surfaces and inhibit soot agglomeration via stable micelles formation. Therefore, the utilization of dispersing agents is not a novel technique in the attempt of stabilizing rGO/GO nanosheets suspensions. Dispersants are mainly surfactants with multiple polar groups that enable better interaction with suspended contaminants (Minami, 2017).
Additionally, the surfactant acts as a barrier against re-aggregation phenomena by providing steric or electrostatic repulsions depending on its nature. One of the most outstanding surfactants for dispersing graphene-like materials in lubricant oils is polyisobutylene succinimide. Ota, J. et al., 2015 reported, for this surfactant, an excellent stability performance for one year (Ota et al., 2015). This long-term stability could be explained by the presence of various functional groups in the dispersant that can form multiple numbers of interactions with nanosheets as illustrated in Figure 4.3.

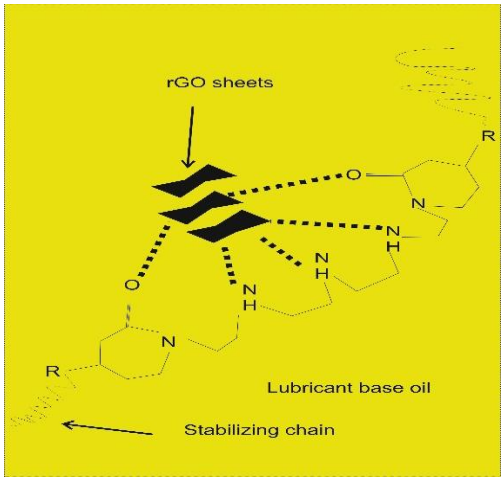

Figure 4.3 *Polyisobutylene succinimide interaction with rGO nanosheets.*

Although dispersant addition seems an optimal method for homogenous suspension, its presence might change the lubricant base oil properties. Surfactants are well known to increase the continuous medium viscosity which can limits lubricant oil usage. Furthermore, dispersants need to be mixed at high concentrations in the industrial base oil, which leaves them prone to harsh mechanical conditions and oxidation, hence declining their stable performance.

Moreover, it is important to distinguish between the utilization of surfactants as a dispersant and their usage as a nonadditive surface modifier, which will be discussed in the following section.

4.4.2 rGO/GO surface modification and functionalization routes

In this section, we describe the main approaches reported in the literature for rGO/GO modification to improve stability in polar and non-polar media. Graphene has two main derivatives, i.e., GO and rGO, produced through harsh chemical oxidation processes, leaving them with a large number of oxygenated functional groups that cannot be completely removed after reduction (Stankovich et al., 2007; A Abdala, 2014). The remaining oxygenated groups are present both on basal planes and edges of GO and mainly on the edges of rGO, as illustrated in Figure 4.4. Oxygen groups on rGO/GO pave the way for their functionalization in contrast to graphene, which is considered an inert material. In the following, graphene surface functionalization is reviewed, often they are unexplored results in the field of lubrication; different possibilities for stabilizing graphene are reported, with particular attention to dispersion in hydrophilic and hydrophobic phases.

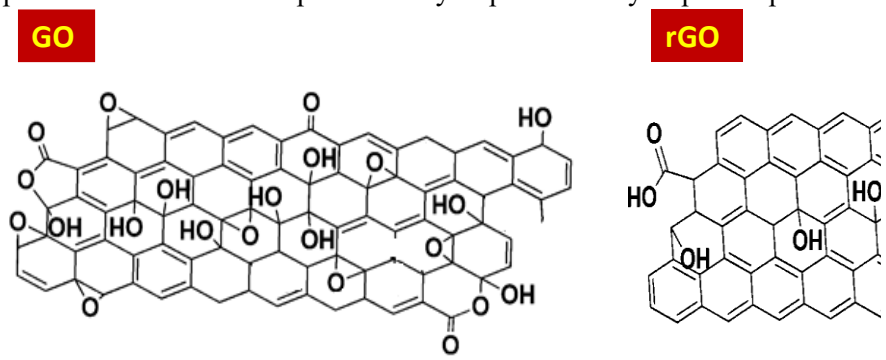

Figure 4.4 *Structural model of single-layer graphene oxide and reduced graphene oxide.*

There is an abundance of literature about the functionalization of graphene and its derivatives for enhanced stability in polar and hydrophilic media. However, the research for improving dispersibility in lipophilic solvents is still scarce. Moreover, it should be noted that the functionalization process can be designed to prevent re-staking phenomena and/or increase interaction with the solvent molecules.

There are different methods to classify the functionalization techniques, which could be based on the nature of the interaction or based on the targeted site or group present on GO and or rGO surface. The latter method seems more practical and comprehensive; that is why it was decided to adopt it in order to summarize the data available in the literature.

• π sites (non-covalent):

One beneficial feature of such modification is that it maintains the native properties of graphene without disturbing sp2 hybridized regions which are responsible for its high mechanical strength and thermal conductivity (Jeon et al., 2011).

• π – π interactions:

The main characteristics of modifiers of this category are the presence of aromatic rings (Grimme, 2008) which interact with the sp2 orbitals on the graphene surface. Furthermore, π – π stacking is more suitable for pristine graphene than rGO and GO due to the absence of oxygen groups that affect sp2 extensions. There is no sufficient information about the performance of such systems in oil medium, but the nearest analogy could be made with studies performed in the hydrophobic chloroform (Wang et al., 2015), where pyrene linked to polymers was utilized for graphene dispersion. Additionally, a study was conducted in chloroform using styrene and 2 vinylpyridine copolymers (Popescu, Tasis and Tsitsilianis, 2014) revealing enhanced graphene stability for concentrations ranging from 0.29-0.219 mgL-1. The surfactants with aromatic rings have the ability to form π – π stackings on the graphitic regions of the sheet surface. In this regard, a comparative investigation was performed between sodium dodecyl sulfonate (SDS) and sodium dodecylbenzene sulfonate (SDBS) (Karachevtsev et al., 2011; Song et al., 2014). Both of them are anionic surfactants with identical alkyl chain length, except the presence of the aromatic ring on the hydrophilic head of SDBS. The results indicated enhanced stability for graphene-like materials under different pH conditions with SDBS. In addition, when SDBS was used as an exfoliating assistant agent, it revealed simultaneous intercalating and stabilizing properties. Furthermore, the stability of graphene exfoliated in the presence of SDBS was higher in the hydrophobic chloroform than in water (Spikes, 2015). However, this is contradictory since SDBS is mainly hydrophilic showing a high hydrophilic-lipophilic balance (HLB = 30).

• Cation– π interactions

This method depends on the interactions between the quadrupole moment of the aromatic ring and a positive charge (Gallivan and Dougherty, 1999; Jeong et al., 2012).

• Hydroxyl groups, Tri-alkoxy groups (covalent)

In this method, a reaction is triggered between hydroxyl groups and tri-alkoxy groups linked to silanes (Hou et al., 2010). The resulted modified GO showed enhanced stability in water.

• Polar groups (non-covalent)

These interactions depend on the formation of hydrogen bonds between the hydroxyl groups of graphene oxide and the oxygen groups in the modifier, as it was reported that hydrogen bonding contributed to the interaction between GO and single-stranded nucleic acids such as DNA and RNA (Park et al., 2013).

• Epoxy (covalent)

The functionalization of graphene oxide surface with epoxy groups is more favorable with respect to other oxygen groups because of their central position. The activation of epoxy groups of GO is initiated by nucleophilic reagents including amines for epoxy ring-opening (Wang et al., 2009). Another root for modification is the use of organosulfur compounds such as potassium thioacetate (Thomas et al., 2014).

• Carboxylic group (covalent)

This group is considered a common target for further GO and rGO modification, in particular with the aim of improving stability in hydrocarbon solvents. The aim of this modification is to form either amides or esters for enhanced reactivities. A common activation agent is thionyl chloride ($SOCl_2$) (Pham, Choi and Jeong, 2010). After this step, amides or esters bonds could be formed with amine or alcohol groups respectively. This method seems to be superior with respect to other methods when considering dispersion in oils, due to the possibility of grafting alkylated modifiers on the sheets. Organic moieties and octadecylamine were used to produce alkylated rGO (Mungse, Kumar and Khatri, 2015c; N. A. Ismail and Bagheri, 2017) and tribological results indicated the formation of relatively stable dispersion in commercial engine oil. They also exhibited a stable suspension for a controlled period of one month with a rGO concentration of 0.02 $mgmL^{-1}$.

In earlier studies, the characterization of different alkyl amines with variable chain length (Cn=8, 12, 18) to modify GO was performed. It was observed that the dispersibility of alkylated graphene in hydrocarbon solvents increased by increasing the chain length, which indicates that a higher interaction with the solvent provided better stability (Choudhary, Mungse and Khatri, 2012).

• Adsorption on different sites

Hydrophobic interaction with alkyls (non-covalent),this is an alternative route for pristine G, rGO and GO stabilization, which consists of non-covalent interaction and adsorption of the aliphatic part of amphiphilic molecules (surfactants) with graphene surface, driven by Van der Waals forces (di Crescenzo et al., 2016). An example of such interactions was confirmed by conductometric surfactant titration (Hsieh et al., 2013). The study reported the adsorption of SDS onto rGO. It was concluded that the adsorption process proceeds through four stages depending on the surfactant concentration. In the first stage, when SDS concentration is less than 12 μM in the bulk solution, SDS monomers initiate to be adsorbed on rGO surface. Following this stage, at a concentration of ~12 μM, a monolayer is formed, completely covering rGO surface. Additionally, the critical surface aggregation concentration (CSAC) for the surface hemicylederical micelles formation on rGO is around 1.5 mM, which is considered as a saturation concentration and any increment in this SDS concentration leads to micelles formation in the bulk phase. Such a system showed superior stability for two years with an SDS concentration

of 40 μM, e.g. two orders of magnitude below CSAC. What is more, it could be observed that the utilization of this technique in the oil phase would favor the second stage of adsorption, as the hydrophilic parts of the surfactant have no affinity for the bulk phase.

Other types of surfactants including the non-ionic oleic and stearic acids, were utilized as modifiers (Eswaraiah, Sankaranarayanan and Ramaprabhu, 2011). The mechanism of these surfactants consists of providing steric barriers around graphene in order to limit aggregation phenomena between nanosheets in industrial base oils, which resulted in improved stability for rGO concentrations up to 0.4 wt%.

- In-situ synthesis of nanoparticles (non-covalent)

This technique is based on the formation of relatively smaller nanoparticles on the surface of rGO/GO to act as re-staking inhibitors. Different studies adopted different nanoparticles, including magnesium phyllosilicate (Achari et al., 2013), yet with a common goal, e.g., to improve stability in water. However, to the best of our knowledge, still, no studies can be found with oil as a bulk phase. Thus, more investigation is required.

4.4.3 Description of the stability methods for dispersion in lubricant base oils

The number of studies on stability utilizing G in lubricant oil additives is still limited. In this section, data available in the literature regarding the techniques thus far utilized for stabilization are reported.

Lin, J.et al., 2011 chemically modified graphene in reactions with stearic and oleic acids under reflux conditions (Lin, Wang and Chen, 2011b). The modified graphene plates (MGP) revealed improvement in stability in base oil confirmed by ultraviolet-visible spectroscopy (UV-Vis). A tribological enhancement occurred when only 0.075 wt% of MGP dispersed in base oil led to improvements in wear resistance and load-carrying capacity of the equipment. In a different study, Zhang, W., 2011 modified rGO only with oleic acid and with a lower range of optimum concentrations of 0.02-0.06 wt% which contributed to friction and wear reduction of 17% and 14% respectively (Zhang et al., 2011). Furthermore, Ali, M. et al., 2018 utilized oleic acid as a dispersing agent by mixing ~2% of it with rGO and lubricant oil to form a stable mixture (Ali et al., 2018). The mixture remained homogenous for a measured period of one month. The friction and wear dropped considerably of 29-35% and 22-29% respectively, at 0.4 wt% of graphene concentration.

Regarding covalent modification, Mungse, H. P., 2015 designed a single-step approach to link the long alkyl chain of octadecyl molecules to the basal plane of graphene oxide in a simultaneous reduction of oxygen (Mungse, Kumar and Khatri, 2015c). The reported controlled stability is for one month in base oil (Figure 4.5) due to Van der Waals interactions between the

octadecyl chains grafted on graphene and the alkyl chains of lube oil with a 25 % reduction of both friction and wear. Another covalent functionalization of GO was conducted by Ismail, N. A., & Begheri, S. 2017 with aromatic moieties by using Copper-Catalyzed Azide-Alkyne Cycloaddition (CuAAC) via Click chemistry. Results showed that with only 0.01 wt% of functionalized graphene added to the base oil, friction and wear reduced significantly of 16% and 30% respectively (N. A. Ismail and Bagheri, 2017).

Ota. J.et. al. 2015 utilized commercial polyisobutylene succinic imide dispersant in various lube oils to disperse 0.5 wt% of graphene. Results indicated superior stability for one year with positive enhancement in both friction and wear reduction. It should be noted that this dispersant needs to be added in relatively greater amounts to show its positive effects (Ota et al., 2015).

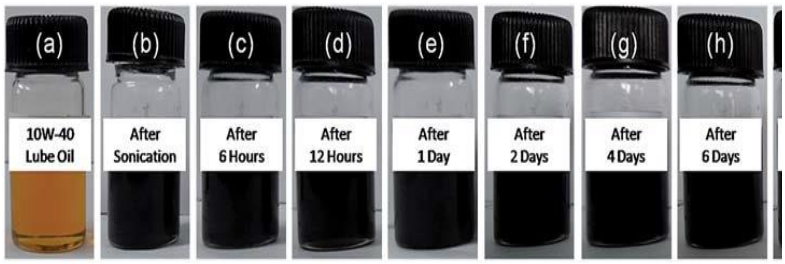

Figure 4.5 *Photos of (a) 10W-40 lube oil and (b–k) dispersions of GO–ODA nanosheets in 10W-40 lube oil at different times (up to one month). Time is reported on each bottle. Concentration of GO–ODA nanosheets: 0.04 mg* mL^{-1} *(Mungse, Kumar and Khatri, 2015c).*

An alternative route to modify graphene is to change its morphology, as it was indicated by Duo, X. et. al. 2016. Their method consists of crumpling G sheets into ball-like particles by a capillary compression approach. The crumpled balls revealed high stability for 20 hours in contrast to rGO plane sheets. This method originates from the analogy according to which crumpled papers do not stick together. Tribological tests of base oil mixed with these balls showed extreme wear reduction of ~85% and friction reduction of 20 %, regardless of their relatively big average size of ~500 nm (Ali et al., 2018). Table 1 summarizes literature studies utilizing rGO/GO as tribo-additives in different base oils, including the adopted modification methods, the measured stability, and tribo-conditions.

Eventually, the stability of GO in commercial oil can be enhanced also through a thermal reduction treatment at 700 °C, as reported by Zhao et al. (Karachevtsev et al., 2011).

4.5 Discussion

On the basis of what the valley's profile above and from the conclusions of the different studies, it can be postulated that rGO/GO nanosheets can reduce wear and friction. Wear reduction is obtained by deposition and film formation, while friction reduction is more related to the shear and lamination of the sheets on the contacting surfaces. Nevertheless, the two phenomena are interrelated and work in sync. In this context, it is of high importance to form a homogenous suspension, for a continuous nanosheets supply after deposition and shearing (Figure 4.6).

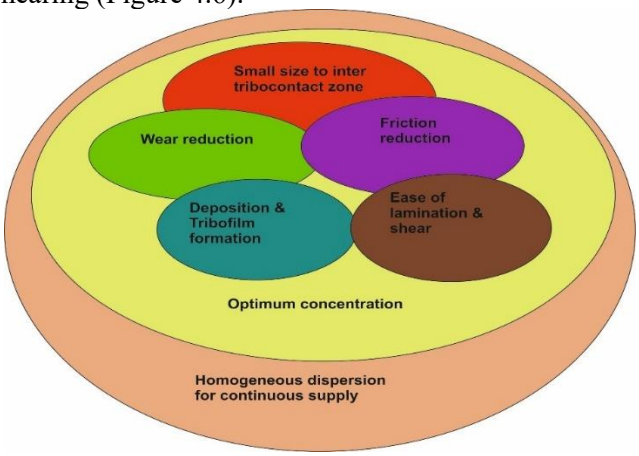

Figure 4.6 *Relationships between the different factors contributing to the best tribological results.*

On the other hand, despite the consistent performance of rGO/GO nanolubricants in reducing wear and friction, there are still remaining obstacles to overcome. Moreover, the fact that every new system deserves renewed attention, and more precisely, every graphene/base combination needs a dedicated effort, e.g., nano-carbons used in different laboratories have not precisely the same surface properties, does not help. Additionally, anti-friction and anti-wear additives are only a part of the delicate balance of components that will constitute the final formulation. For industrialization, it would be desirable that additives do not modify the base rheological properties. Indeed, otherwise, a re-modulation of the entire formulation would probably be required. This aspect is almost never explored in literature, in which little attention has been devoted to the rheology of the formulations or to the analysis of completely formulated oils. In particular, aspects such as the tendency to aggregate as well as the optimum concentration remain hot topics.

The reaggregation of nanosheets in lubricating oils is one of the most urgent issues. The two-dimensional rGO/GO nanosheets exhibit very high surface energy with high diffusive properties, enabling them to form a

protective layer and helping to mend the micro-cracks on the rubbing surface. However, these properties are also the main cause of poor suspension. Reaggregation of the sheets can even deteriorate the pure base oil properties due to the formation of a non-equivalent distribution of the sheets themselves, as conceptualized in Figure 4.7. Another important issue in order to ensure the best tribological performance is to find the optimum additive concentration. Too few nanosheets may not be sufficient to cover the rubbing surfaces, whereas too many sheets present in the oil can increase reaggregation and formation of a non-continuous oil film due to large aggregates, as shown in Figure 8c. Regarding enhanced stability, rGO/GO surface modification seems more attractive than using a dispersing agent, because of the possible effects of the dispersant on the bulk properties of the lubricating oil. For instance, the addition of dispersant can increase the viscosity, thus affecting the viscosity index of the oil, which is a crucial parameter for oil usage. Additionally, it can affect the nanosheet's capability to diffuse towards the interacting surfaces, as a consequence of the increased viscosity.

More in general, rGO/GO nanoadditives are still in need of a more comprehensive study and characterization regarding long-term stability and working mechanism.

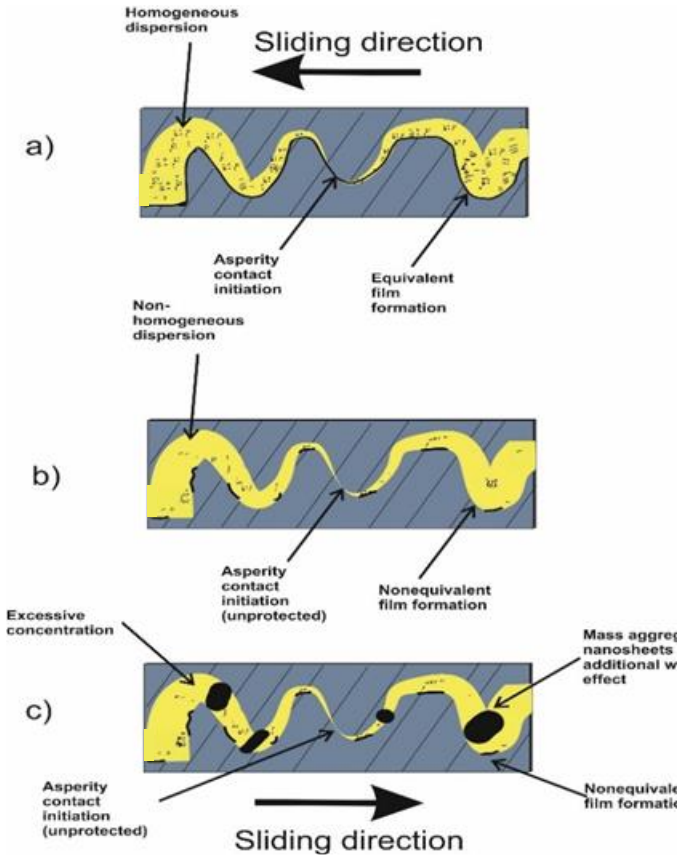

Figure 4.7 *rGO/GO suspension and tribofilm formation between two rubbing surfaces sliding in opposite directions (a), homogenous suspension with the optimum concentration (b), non-homogenous state, excessive concentration (c).*

In this scenario, a recent way, which inherently possesses the solution to many of the critical aspects listed above, consists of the use of carbon quantum dots (CQDs), see Figure 4.8. CQDs are surface-functionalized and easily modifiable 0D material, which can be easily dispersed and able to repair wear scars and form tribofilms, above all by not signficantly changing the oil color and rheological properties of the oil (Ye et al., 2018).

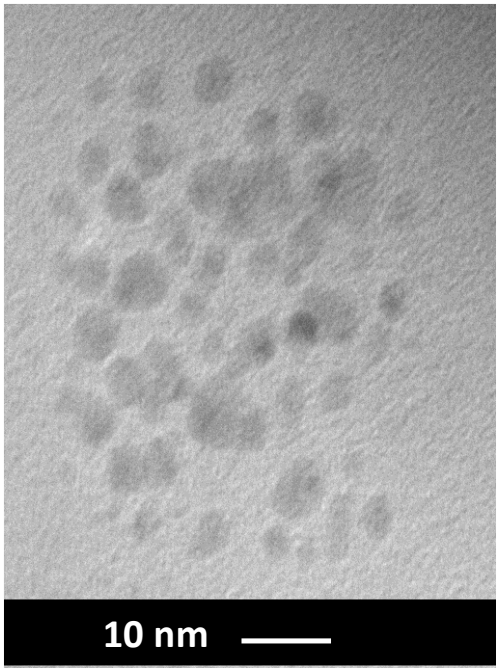

Figure 4.8 *Transmission electron microscope image of CQDS formed by a facile hydrothermal carbonization of citric acid in a relatively low temperature at 200°C.*

4.6 References

A ABDALA, A. (2014) Applications of Graphene in Catalysis. *Journal of Biofertilizers & Biopesticides*, 05(01), [Online] Available from: doi.org/10.4172/2157-7544.1000132.

ACHARI, A. et al. (2013) Amphiphilic aminoclay–RGO hybrids: a simple strategy to disperse a high concentration of RGO in water. *Nanoscale*, 5(12), p. 5316.

AN, L. et al. (2019) Effect of nanoparticle size on the mechanical properties of nanoparticle assemblies. Nanoscale, 11(19), pp. 9563–9573.

ALDANA, P.U. (2016) *Tungsten disulfide nanoparticles as lubricant additives for the automotive industry*.

ALI, M.K.A. et al. (2018) Novel approach of the graphene nanolubricant for energy saving via anti-friction/wear in automobile engines. *Tribology International*, 124, pp. 209–229.

BAKUNIN, V.N. et al. (2004) Synthesis and Application of Inorganic Nanoparticles as Lubricant Components – a Review. *Journal of Nanoparticle Research*, 6(2/3), pp. 273–284.

BART, J.C.J., GUCCIARDI, E. and CAVALLARO, S. (2013) Lubricants: properties and characteristics. In: *Biolubricants: science and technology*. pp. 24–73.

BERMAN, D., ERDEMIR, A. and SUMANT, A. V. (2013) Few layer graphene to reduce wear and friction on sliding steel surfaces. *Carbon*, 54, pp. 454–459.

BERMAN, D., ERDEMIR, A. and SUMANT, A. V. (2014) Graphene: a new emerging lubricant. *Materials Today*, 17(1), pp. 31–42.

BOWDEN, F.P., GREGORY, J.N. and TABOR, D. (1945) Lubrication of Metal Surfaces by Fatty Acids. *Nature*, 156(3952), pp. 97–101.

CHOUDHARY, S., MUNGSE, H.P. and KHATRI, O.P. (2012) Dispersion of alkylated graphene in organic solvents and its potential for lubrication applications. *Journal of Materials Chemistry*, 22(39), p. 21032.

DI CRESCENZO, A. et al. (2016) Optimizing the Interactions of Surfactants with Graphitic Surfaces and Clathrate Hydrates. *Langmuir*, 32(26), pp. 6559–6570.

DOU, X. et al. (2016) Self-dispersed crumpled graphene balls in oil for friction and wear reduction. *Proceedings of the National Academy of Sciences*, 113(6), pp. 1528–1533.

ESWARAIAH, V., SANKARANARAYANAN, V. and RAMAPRABHU, S. (2011) Graphene-Based Engine Oil Nanofluids for Tribological Applications. *ACS Applied Materials & Interfaces*, 3(11), pp. 4221–4227.

FORBES, E.S. (1970) Antiwear and extreme pressure additives for lubricants. *Tribology*, 3(3), pp. 145–152.

GALLIVAN, J.P. and DOUGHERTY, D.A. (1999) Cation-pi interactions in structural biology. *Proceedings of the National Academy of Sciences*, 96(17), pp. 9459–9464.

GEIM, A.K. (2009) Graphene: Status and Prospects. *Science*, 324(5934), pp. 1530–1534.

GRIMME, S. (2008) Do Special Noncovalent π–π Stacking Interactions Really Exist? *Angewandte Chemie International Edition*, 47(18), pp. 3430–3434.

GUPTA, B. et al. (2016) Energy efficient reduced graphene oxide additives: Mechanism of effective lubrication and antiwear properties. *Scientific Reports*, 6(1), p. 18372.

HOU, S. et al. (2010) Formation of highly stable dispersions of silane-functionalized reduced graphene oxide. *Chemical Physics Letters*, 501(1–3), pp. 68–74.

HSIEH, A.G. et al. (2013) Adsorption of Sodium Dodecyl Sulfate on Functionalized Graphene Measured by Conductometric Titration. *The Journal of Physical Chemistry B*, 117(26), pp. 7950–7958.

ISMAIL, N. and BAGHERI, S. (2017) Lube Oil Wear Reduction via Organic Tribofilms. *Lubricants*, 5(3), p. 30.

ISMAIL, N.A. and BAGHERI, S. (2017) Highly oil-dispersed functionalized reduced graphene oxide nanosheets as lube oil friction modifier. *Materials Science and Engineering: B*, 222, pp. 34–42.

JEON, I.-Y. et al. (2011) Functionalization of Carbon Nanotubes. In: *Carbon Nanotubes - Polymer Nanocomposites*. InTech.

JEONG, SEUNG YOL et al. (2012) Highly Concentrated and Conductive Reduced Graphene Oxide Nanosheets by Monovalent Cation-π Interaction: Toward Printed Electronics. *Advanced Functional Materials*, 22(15), pp. 3307–3314.

JIAO, D. et al. (2011) The tribology properties of alumina/silica composite nanoparticles as lubricant additives. *Applied Surface Science*, 257(13), pp. 5720–5725.

KARACHEVTSEV, V.A. et al. (2011) Comparative study on protection properties of anionic surfactants (SDS, SDBS) and DNA covering of single-walled carbon nanotubes against pH influence: luminescence and absorption spectroscopy study. *Materialwissenschaft und Werkstofftechnik*, 42(1), pp. 41–46.

KIM, D. and ARCHER, L.A. (2011) Nanoscale Organic−Inorganic Hybrid Lubricants. *Langmuir*, 27(6), pp. 3083–3094.

KIM, K.-S. et al. (2011) Chemical Vapor Deposition-Grown Graphene: The Thinnest Solid Lubricant. *ACS Nano*, 5(6), pp. 5107–5114.

KONIOS, D. et al. (2014) Dispersion behaviour of graphene oxide and reduced graphene oxide. *Journal of Colloid and Interface Science*, 430, pp. 108–112.

LEE, C. et al. (2008) Measurement of the Elastic Properties and Intrinsic Strength of Monolayer Graphene. *Science*, 321(5887), pp. 385–388.

LI, J. et al. (2014) The Preparation of Graphene Oxide and Its Derivatives and Their Application in Bio-Tribological Systems. *Lubricants*, 2(3), pp. 137–161.

LI, Y. et al. (2016) Highly Exfoliated Reduced Graphite Oxide Powders as Efficient Lubricant Oil Additives. *Advanced Materials Interfaces*, 3(22), p. 1600700.

LIN, J., WANG, L. and CHEN, G. (2011a) Modification of Graphene Platelets and their Tribological Properties as a Lubricant Additive. *Tribology Letters*, 41(1), pp. 209–215.

LIN, J., WANG, L. and CHEN, G. (2011b) Modification of Graphene Platelets and their Tribological Properties as a Lubricant Additive. *Tribology Letters*, 41(1), pp. 209–215.

LIÑEIRA DEL RÍO, J.M. et al. (2019) Tribological properties of dispersions based on reduced graphene oxide sheets and trimethylolpropane trioleate or PAO 40 oils. *Journal of Molecular Liquids*, 274, pp. 568–576.
LIU, G. et al. (2004) Investigation of the Mending Effect and Mechanism of Copper Nano-Particles on a Tribologically Stressed Surface. *Tribology Letters*, 17(4), pp. 961–966.
MINAMI, I. (2017) Molecular Science of Lubricant Additives. *Applied Sciences*, 7(5), p. 445.
MUNGSE, H.P. et al. (2019) Alkylated graphene oxide and reduced graphene oxide: Grafting density, dispersion stability to enhancement of lubrication properties. *Journal of Colloid and Interface Science*, 541, pp. 150–162.
MUNGSE, H.P. and KHATRI, O.P. (2014a) Chemically Functionalized Reduced Graphene Oxide as a Novel Material for Reduction of Friction and Wear. *The Journal of Physical Chemistry C*, 118(26), pp. 14394–14402.
MUNGSE, H.P. and KHATRI, O.P. (2014b) Chemically Functionalized Reduced Graphene Oxide as a Novel Material for Reduction of Friction and Wear. *The Journal of Physical Chemistry C*, 118(26), pp. 14394–14402.
MUNGSE, H.P., KUMAR, N. and KHATRI, O.P. (2015a) Synthesis, dispersion and lubrication potential of basal plane functionalized alkylated graphene nanosheets. *RSC Advances*, 5(32), pp. 25565–25571.
MUNGSE, H.P., KUMAR, N. and KHATRI, O.P. (2015b) Synthesis, dispersion and lubrication potential of basal plane functionalized alkylated graphene nanosheets. *RSC Advances*, 5(32), pp. 25565–25571.
MUNGSE, H.P., KUMAR, N. and KHATRI, O.P. (2015c) Synthesis, dispersion and lubrication potential of basal plane functionalized alkylated graphene nanosheets. *RSC Advances*, 5(32), pp. 25565–25571.
OTA, J. et al. (2015) Graphene dispersion in hydrocarbon medium and its application in lubricant technology. *RSC Advances*, 5(66), pp. 53326–53332.
PARK, J.S. et al. (2013) Desorption of single-stranded nucleic acids from graphene oxide by disruption of hydrogen bonding. *The Analyst*, 138(6), p. 1745.
PATEL, J. and KIANI, A. (2019) Effects of Reduced Graphene Oxide (rGO) at Different Concentrations on Tribological Properties of Liquid Base Lubricants. *Lubricants*, 7(2), p. 11.
PEI, S. and CHENG, H.-M. (2012) The reduction of graphene oxide. *Carbon*, 50(9), pp. 3210–3228.
PHAM, T.A., CHOI, B.C. and JEONG, Y.T. (2010) Facile covalent immobilization of cadmium sulfide quantum dots on graphene oxide nanosheets: preparation, characterization, and optical properties. *Nanotechnology*, 21(46), p. 465603.
POPESCU, M.-T., TASIS, D. and TSITSILIANIS, C. (2014) Ionizable Star Copolymer-Assisted Graphene Phase Transfer between Immiscible Liquids: Organic Solvent/Water/Ionic Liquid. *ACS Macro Letters*, 3(10), pp. 981–984.
QIN, Z. et al. (2014) Effect of Wrinkles on the Surface Area of Graphene: Toward the Design of Nanoelectronics. *Nano Letters*, 14(11), pp. 6520–6525.

SARNO, M. et al. (2014a) Oil Lubricant Tribological Behaviour Improvement Through Dispersion of Few Layer Graphene Oxide. *Journal of Nanoscience and Nanotechnology*, 14(7), pp. 4960–4968.

SAYUTI, M. et al. (2014) Investigation on the morphology of the machined surface in end milling of aerospace AL6061-T6 for novel uses of SiO2 nanolubrication system. *Journal of Cleaner Production*, 66, pp. 655–663.

SCHLÜTER, B., MÜLHAUPT, R. and KAILER, A. (2014) Synthesis and Tribological Characterization of Stable Dispersions of Thermally Reduced Graphite Oxide. *Tribology Letters*, 53(1), pp. 353–363.

SEILER, S. et al. (2018) Effect of friction on oxidative graphite intercalation and high-quality graphene formation. *Nature Communications*, 9(1), p. 836.

SHEN, J. et al. (2009) Synthesis of Amphiphilic Graphene Nanoplatelets. *Small*, 5(1), pp. 82–85.

SONG, Y. et al. (2014) Preparation and Characterization of Surfactant-Exfoliated Graphene. *Bulletin of the Korean Chemical Society*, 35(7), pp. 2009–2012.

SPIKES, H. (2015) Friction Modifier Additives. *Tribology Letters*, 60(1), p. 5.

SPIKES, H. (2004) The History and Mechanisms of ZDDP. *Tribology Letters*, 17(3), pp. 469–489.

STANKOVICH, S. et al. (2007) Synthesis of graphene-based nanosheets via chemical reduction of exfoliated graphite oxide. *Carbon*, 45(7), pp. 1558–1565.

SUDEEP, P.M. et al. (2014) Nanofluids based on fluorinated graphene oxide for efficient thermal management. *RSC Advances*, 4(47), p. 24887.

TAHA-TIJERINA, J., AVIÑA, K. and DIABB, J.M. (2019) Tribological and Thermal Transport Performance of SiO2-Based Natural Lubricants. *Lubricants*, 7(8), p. 71.

THOMAS, H.R. et al. (2014) Sulfur-Functionalized Graphene Oxide by Epoxide Ring-Opening. *Angewandte Chemie International Edition*, 53(29), pp. 7613–7618.

TOMALA, A. et al. (2015) Interaction Between Selected MoS2 Nanoparticles and ZDDP Tribofilms. *Tribology Letters*, 59(1), p. 26.

TREFALT, G. and BORKOVEC, M. (2017) *Overview of DLVO Theory*. Available from : http://www.colloid.ch/index.php?name=dlvo [Accessed 05/01/20].

VAN, N.H. (2018) EFFECT OF LONG-CHAIN ALKYLAMINE ON THE DISPERSIBILITY AND TRIBOLOGICAL PROPERTIES OF ALKYL-GRAPHENE IN LUBRICANT OIL. *Vietnam Journal of Science and Technology*, 56(2A), pp. 163–173.

VIESCA, J.L. et al. (2011) Antiwear properties of carbon-coated copper nanoparticles used as an additive to a polyalphaolefin. *Tribology International*, 44(7–8), pp. 829–833.

WANG, G. et al. (2009) Synthesis and characterisation of hydrophilic and organophilic graphene nanosheets. *Carbon*, 47(5), pp. 1359–1364.

WANG, H. et al. (2015) Synthesis of pyrene-capped polystyrene by free radical polymerization and its application in direct exfoliation of graphite into

graphene nanosheets. *Journal of Polymer Science Part A: Polymer Chemistry*, 53(18), pp. 2175–2185.

XU, Y. et al. (2015) Synergistic lubricating behaviors of graphene and MoS2 dispersed in esterified bio-oil for steel/steel contact. *Wear*, 342–343, pp. 297–309.

YE, M. et al. (2018) Friction-induced transfer of carbon quantum dots on the interface: Microscopic and spectroscopic studies on the role of inorganic–organic hybrid nanoparticles as multifunctional additive for enhanced lubrication. *Tribology International*, 127, pp. 557–567.

YU, F. et al. (2017) Dispersion stability of thermal nanofluids. *Progress in Natural Science: Materials International*, 27(5), pp. 531–542.

YU, H. et al. (2008) Tribological properties and lubricating mechanisms of Cu nanoparticles in lubricant. *Transactions of Nonferrous Metals Society of China*, 18(3), pp. 636–641.

YU, W. and XIE, H. (2012) A Review on Nanofluids: Preparation, Stability Mechanisms, and Applications. *Journal of Nanomaterials*, 2012, pp. 1–17.

ZHANG, W. et al. (2012) Fundamental understanding of the tribological and thermal behavior of Ag–MoS2 nanoparticle-based multi-component lubricating system. *Wear*, 288, pp. 9–16.

ZHANG, W. et al. (2011) Tribological properties of oleic acid-modified graphene as lubricant oil additives. *Journal of Physics D: Applied Physics*, 44(20), p. 205303.

ZHAO, J. et al. (2017) Mild thermal reduction of graphene oxide as a lubrication additive for friction and wear reduction. *RSC Advances*, 7(3), pp. 1766–1770.

Chapter V. Experimental exposure on the influence of surfactant modification of Nanocarbons and their tribological performance

5.1 Overview

Lubricating oils are of fundamental importance today to ensure the proper operation of machinery by shielding them from damage caused by wear, friction and heat. While additives may be applied to the base oil to improve tribological properties, the existing lubricants have hit their performance limits. However, nanoscale regulation has lately been identified as a crucial factor in the further development of the additive formulation in terms of minimizing wear and friction, energy consumption and environmental sustainability.

In this research, mineral oil-based lubricants, usually used for industrial gears, and synthetic oils such as polyalphaolefins (PAO) and Group III base oils, commonly used in manual and automatic transmissions in the automotive sector, were chosen. Carbon-based nanomaterials are able to ensure good tribological performance among nano-additives, due to their inert structure without any dangling bonds and their excellent mechanical properties, resulting in a reduction of friction and wear even under heavy load conditions and for long-term operations (Grierson and Carpick, 2007). Carbon nanotubes (CNTs) can be considered as promising materials for lubricant nano-additives applications (Kałużny et al., 2017; Singh and Bhowmick, 2020). For example, single-walled carbon nanotubes (SWNTs) were added at a very low

concentration (1 wt %) to a PAO-based oil, leading to a major reduction in friction and wear in the boundary lubrication regime (Joly-Pottuz et al., 2004).

In addition, an optimum concentration of 0.5 wt. % of multi-walled carbon nanotubes (MWNTs) in industrial mineral base oil has contributed to a substantial improvement in the load-bearing capability and anti-wear efficiency of the lubricant (Bhaumik, 2013). Analogously, graphene, a two-dimensional composite with a honeycomb crystalline structure of sp2 hybridized carbon atoms, is also capable of having a major anti-wear and anti-friction contribution, as well as a very high thermal conductivity and enhancement of convective heat transfer phenomena in base oil. At present, graphene-based materials have been seen as a desirable alternative to conventional lubricant additives, especially due to their chemical inertness, exceptional mechanical strength and ease of sliding between various layers due to the presence of weak intermolecular forces of Van der Waals. In several of the previous studies on nanoscale graphene, it has been seen that its tribological activity stems from its structural properties, such as the stacking of its multiple layers, rather than the chemical nature of its sliding surfaces (Shahnazar, Bagheri and Abd Hamid, 2016a).

It was found that multi-layer graphene mixed with PAO2 oil at a very low concentration of 0.05 wt % was able to reduce the coefficient of friction and the diameter of the wear scar by the development of a protective tribofilm on metal surfaces (Guo and Zhang, 2016). In addition, graphene oxide (GO) nanosheets in Group I mineral oil have been shown to improve anti-friction and anti-wear properties as a result of GO's small dimensions and very thin laminate structure, which defines the low shear stress between sliding surfaces (Sarno et al., 2014).

Presently, the major problem related to the introduction of chemical inert carbon-based additives, such as CNTs and graphene-based compounds, is the difficulty of obtaining a stable dispersion of these additives in base oils, which can also lead to a decrease in their tribological output within a limited period of time following their preparation (Shahnazar, Bagheri and Abd Hamid, 2016b). Various studies have been conducted (Chen et al., 2005; Zhang et al., 2011), and even though some results are interesting and step forwards have been done, long term stability still requires additional efforts. Two approaches can be followed to improve nano-additives stability, the use of a dispersant or a surface modification by surfactants. A lot of research has been performed around the possibility to use surfactants in a wide range of applications, also other than lubrication, such as: oil and impurities recovery, de-hydration (or hydration), detergents processes, for pharmaceuticals, etc (Bagheri and Khalili, 2017a). Mixtures of surfactants can theoretically boost the ability to change interfacial properties (Bagheri and Khalili, 2017a). In addition, the presence of a synergistic mixture of surfactants reveals more effectively the development of micelle and surface modifications (Zhang and Zhu, 2010). Simultaneous application, e.g. of two surfactants, by means of interactions

between the two different organisms with different synergistic properties, can more readily contribute to the creation of micelle, i.e. the overcoming of repulsion forces, common for ion molecules; or steric hindrances, as in the case of non-ionic molecules. In addition, various functionalities can lead to the generation of multi-contact points on mixed activity surfaces, favouring interaction and dispersibility (Bagheri and Khalili, 2017b).

Till now, in the domain of lubrication, while research efforts have been effectively devoted to this issue, little or no attention has been paid to avoiding the alteration of specific properties, e.g. viscosity and viscosity index, after the addition of a dispersant or surfactant. Moreover, not only are the properties of the lubricating oil highly dependent on these factors, but also, considering the delicate combination of multiple components in the final formulation, it would be better to use new additives which do not conflict with the rheological properties of the base oil. This is especially valid in view of future industrialisation, where, instead, any alteration due to new additions may involve the re-modulation of the whole composition, leading to one of the key resistances of the industrial sector to the introduction of nano-additives.

Carbon nanotubes and graphene-based nanocarbons, synthesized by simple and scalable methods, such as catalysed chemical vapor deposition (CCVD), chemical exfoliation and solvent-based exfoliation, have been widely defined for the enhancement of anti-friction and anti-wearing properties of lubricating oils by the use of stable nano-additives and without significantly altering oil viscosity. A systematic study of their stability in the presence of a low amount of dispersant/surfactants (Kundu, Kumar and Mishra, 2015), and tribological activity has been documented. Tribological testing revealed a substantial decrease in friction and wear, as shown by the excellent performance of the synthesized nanomaterials.

5.2 Materials and methods

5.2.1 Lubricant bases for formulations

Two different bases were chosen in this study:
ETRO IV (GROUP III) base, which commercial name after addition of additional additives, for fully formulated oil, is SYNPLUS-75W-90 of RILUB SPA (Table 5.1). In the following section, SYNPLUS 75W-90. SN150 and DS150 mixture (GROUP I-GROUP II), which commercial name after addition of additional additives, for fully formulated oil, is EUBUSH 220 of RILUB SPA, Table 5.1. In the following, see EUBUSH 220.

Table 5.1 *Nanoparticles, surfactants combinations, and designated IDs.*

ID	Sample	Surfactant/dispersant
1	CN1	1,8 diaminonaphthalene
2	CN2	1,8 diaminonaphthalene
3	CN3	1,8 diaminonaphthalene
4	CN4	1,8 diaminonaphthalene
6	GO	1,8 diaminonaphthalene
7	rGO	1,8 diaminonaphthalene
8	FLG	1,8 diaminonaphthalene
10	CN1	SDBS
11	CN2	SDBS
12	CN3	SDBS
13	CN4	SDBS
14	GO	SDBS
15	rGO	SDBS
16	FLG	SDBS
17	CN1	SDBS and Tween 80
18	CN2	SDBS and Tween 80
19	CN3	SDBS and Tween 80
20	CN4	SDBS and Tween 80
21	GO	SDBS and Tween 80
22	rGO	SDBS and Tween 80
23	FLG	SDBS and Tween 80
24	CN1	HiTEC®646E Performance Additive - Polyisobutylene Succinimides
25	CN2	HiTEC®646E Performance Additive - Polyisobutylene Succinimides
26	CN3	HiTEC®646E Performance Additive - Polyisobutylene Succinimides
27	CN4	HiTEC®646E Performance Additive - Polyisobutylene Succinimides
28	GO	HiTEC®646E Performance Additive - Polyisobutylene Succinimides
29	rGO	HiTEC®646E Performance Additive - Polyisobutylene Succinimides
30	FLG	HiTEC®646E Performance Additive - Polyisobutylene Succinimides

Synthesized samples were dispersed in SYNPLUS 75W-90 with and without dispersants/surfactants, whereas stability in EUBUSH 220 was quite high, therefore no further dispersants were added to the latter oil.
Synthesized samples were distributed in SYNPLUS 75W-90 with and without dispersants/surfactants, while stability in EUBUSH 220 was very high, so no more dispersants were applied to the latter liquid.

For clarification purposes, the following text will differentiate four classes of synthesized nanomaterials, see Table 5.1, based on the type of dispersant they were combined with. As for the first group, nanocarbons were combined with 1,8 diaminonaphthalene (weight ratio 1:8) in 100 mL of bi-distilled water, sounded for 20 minutes, and finally dried at 80 °C. In the second group,

50 mg of nanocarbons and 500 mg of SDBS were mixed in 100 mL of distilled water, sonicated at 45 °C for 20 minutes and air-dried for 24 hours.

After that, they were centrifuged at 7500 rpm for 30 minutes and dried at 80 °C. In the third category, 50 mg of nanocarbons, 250 mg of SDBS and 250 mg of Tween 80 were combined in 100 mL of bi-distilled water, sounded at 45 °C for 20 minutes and air-dried for 24 hours. Afterwards, they were centrifuged at 7500 rpm for 30 minutes and dried at 80 °C. As for the last PS category, dispersions were prepared using nanocarbons at three different percentages (0.05 wt.%, 0.1 wt.%, and 1 wt.%) and 2 wt.% of the industrial dispersion. Since combining dispersants and nanocarbons, the as-prepared nanomaterials were combined with the two base oils at three different percentages: 0.05 wt.%, 0.1 wt.%, and1 wt.%. The desired volume of nanocarbons was first sonicated in 25 mL of oil for 60 min and then combined with the remaining portion of the base oil using a homogenizer (Silverson Homogenizer L5M).

UV-Vis spectroscopy combined with intermittent centrifugation was conducted to test dispersion stability. Next, the prepared samples were scattered in SYNPLUS 75W-90. As described above, since the visual stability in EUBUSH 220 is substantially high even without dispersants, measurements were carried out in order to determine stability only in SYNPLUS 75W-90. After dispersion via a homogenizer into the base oil, dispersions were precipitated through centrifugation at 1000 rpm for 30 min. The absorbance of the supernatant developed after centrifugation was then assessed using the UV-Vis spectrophotometer. Eventually, the absorbance ratio between pre-centrifugation and post-centrifugation (named A ratio in this study) was determined taking advantage of the proportionality between absorbance and concentration via the Lambert-Beer equation.

5.2.2 Carbon nanotubes preparation

Four samples of MWNTs were produced by ethylene or acetylene catalytic chemical vapor deposition (CCVD) on a Co/Fe-based catalyst, prepared by wet impregnation using an aqueous solution containing cobalt and iron acetate and gibbsite powder (Δ-Al (OH)3) and then dried at 140 °C for 12 h (Sarno et al., 2012). The synthesis was carried out in a continuous flow microreactor fed by a reagent-nitrogen gas mixture, see Figure S1. The adopted reactor consists of a quartz tube (internal diameter of 16 mm, length of 300 mm) loaded with a catalyst with a particle size of between 40 and 90 μm. The reactor is heated by an electrical oven, the temperature of which is controlled by a temperature controller (Eurotherm 2408). Cylinder gases (99.99 pure ethylene, 99.5 acetylene and 99.99 pure nitrogen) flow rates to be mixed in the inlet stream at 15 v/v per cent were recorded and kept constant by means of a mass flow controller (MFC).

In the first place, the catalyst was preheated at 70 °C/min to the synthesis temperature (700 °C for ethylene and 600 °C for acetylene) below the nitrogen flow. A mixture of ethylene/nitrogen or acetylene/nitrogen was then fed to the reaction system for about 10 minutes or 30 minutes to produce carbon nanotubes.

Four samples were produced in detail: CN1 and CN2 under ethylene/nitrogen flow at 700°C for 10 and 30 minutes respectively; CN3 and CN4 under acetylene/nitrogen flow at 600°C for 10 and 30 minutes respectively. After each synthesis, the gas flow was stopped, the reactor cooled down to room temperature under the nitrogen flow and the composite powder was obtained. As previously reported, a multi-step procedure was followed for purification.

5.2.3 Graphene Oxide (GO) and Reduced Graphene Oxide (rGO)

Preparation

Graphene Oxide (GO) nanosheets were obtained from graphite powder (synthetic 99.9 per cent of Sigma Aldrich) using the modified Hummers method.

In the first place, graphite oxide was produced from graphite powder, which was added to a water-free mixture of concentrated sulfuric acid and potassium permanganate. Second, by an additional sonication step, the oxidized graphite layers were exfoliated and the graphene oxide sample was obtained. In addition, another sample was prepared using the same procedure and then reduced to 98°C in aqueous vitamin C solution for an hour to obtain reduced graphene oxide (rGO) nanosheets (Fernández-Merino et al., 2010).

5.2.4 Solvent-Exfoliated Graphene Preparation

In order to obtain the last sample, graphite flakes (200 grams, graphite Alfa Aesar, natural,-325 mesh, 99.8 per cent) were sonicated in a 100 mg/ml N-methylpyrrolidone (spectrophotometric grade > 99.0 per cent) solution for 4 h at the highest instrument capacity (Hernandez et al., 2008).

The apparatus consists of an ultrasonic homogenizer fitted with titanium tips of varying diameters to be used depending on the amount of liquid required, the modular capacity and the form of flow cell. The looking result was a greyish and homogeneous liquid. Downstream of the sonication, a few-layer graphene (FLG) was retrieved after centrifugation and by filtration of the supernatant to a 20 nm aluminum pore membrane, resulting in homogeneous dispersion.

5.2.5 characterization techniques

5.2.5.1 chemical/physical characterization techniques

Scanning electron microscope (SEM), and Transmission electron microscopy (TEM) by means of a FEI Tecnai 200 kV electron microscope was used for understanding the morphological characteristics of samples. The absorbance of the supernatant produced after centrifugation was then evaluated through Thermo-Scientific UV–vis Evolution Q60 spectrophotometer. Thermogravimetric analysis (TGA) and Derivative Thermogravimetry analysis (DTG) were performed through a SDTQ 600 Analyzer (TA Instruments) under the following conditions: heating rate of 10 ºC/min, from room temperature up to 450 ºC under air flow. Finally, Raman spectra were obtained by means of a Renishaw inVia spectrometer at a wavelength of 514 nm.

5.2.5.2 tribological test description

The tribometer adopted in this analysis is the Ducom TR-BIO-282 (as seen in Figure 5.1) with a set-up for reciprocating sliding tests in both dry and lubricated contacts, with specimens of several shapes/sizes to allow a wide variety of contact pressures to be applied. The investigated tribopair consists of an upper steel ball in reciprocating motion and a lower steel disc flooded in a temperature-controlled lubricant bath with electrical resistances as a heating source. The upper element of the tribopair is an X45Cr13 polished steel ball (diameter of 6 mm, 52–54 HRC), whilst the lower element is an X210Cr12 steel disc (thickness of 6 mm, diameter of 25 mm, roughness Ra of 0.30 μm, 60 HRC).

The contact normal force, varying in the range 0-20 N, was generated through a dead weight-based lever system. The average Hertzian pressure measured at the ball/disc interface with a normal load of 19 N was equal to 1.17 GPa; therefore, the maximum attainable contact pressure was 1.76 GPa (Theses conditions guaranteed boundary conditions). The lubricant bath covered the disk, with a volume of 10 mL in order to avoid starvation. After temperature reached a constant value, a load was applied. For each test, new ball and disk were adopted. Tests were carried out at both room temperature and 80°C, and the lubricant average temperature was maintained constant by means of a NiCr-Ni thermocouple in the oil reservoir and an electric resistance driven by a digital controller.

The data reported in the following were obtained at 25 °C, unless otherwise indicated. The sliding motion, characterized by a triangular speed profile, was set with the following parameters: 10 Hz of frequency and 5 mm of stroke. The resulting maximum sliding speed in each stroke reached 240 mm/s,

whereas the average speed is equal to 120 mm/s, with an average approximate λ ratio of 1.

Figure 5.1 *Ducom TR-BIO-282 tribometer setup.*

5.2.5.2 Surface analysis

The worn surface of the steel ball was examined using a confocal profiler (Figure 5.2) to measure the wear scar diameter (WSD), the contact surface roughness, and to produce a ball worn surface topography. The confocal imaging system produces high-contrast images by removing out-of-focus radiation. The sample is screened vertically in steps such that each point on the surface passes through the focus. The height of the surface at each pixel position is calculated by detecting the peak of the narrow axial response. Since only local surface areas are illuminated at the same time, an in-plane raster scan is needed to produce an axial response (i.e. a confocal image) at each vertical phase.

Figure 5.2 *Confocal profiler ''Sensofar Neox PLu''.*

5.3 Results and discussion

5.3.1 Carbon nanotubes characterization

Figures 5.3, a and b show SEM images of the CNTs produced through ethylene for 10 and 30 minutes respectively. SEM analysis reveals a morphology consisting of bundles of tubes anchored to the catalyst with a length of about 50 μm and 200 μm, respectively. Similarly, SEM images of the CNTs produced by means of acetylene for 10 minutes and 30 minutes are shown in Figure 5.3, c and d. They also have separate lengths (40 μm and 180 μm, respectively). A typical TEM image of the nanotubes generated by CCVD was shown in Figure 5.3, e. TEM results show two types of multi-walled CNTs, one with an average external diameter of 14 nm and an average internal diameter of 6 nm produced at 700 °C from ethylene, and different dimensions are produced with an average external diameter of around 25 nm and an

average internal diameter of 8 nm when the reagent acetylene at 600 °C. Figure 5.3, f shows a typical Raman spectrum of produced CNT, in which the typical G band is present at about 1580 cm^{-1} and the D band at about 1330 cm^{-1}(Maurin et al., 2001). The presence of the D band can be attributed to terminal defects of nanotubes and is strongly influenced by their bending. A longer synthesis time leads to a higher order, probably due to a longer exposure to a high temperature (Sarno et al., 2012).

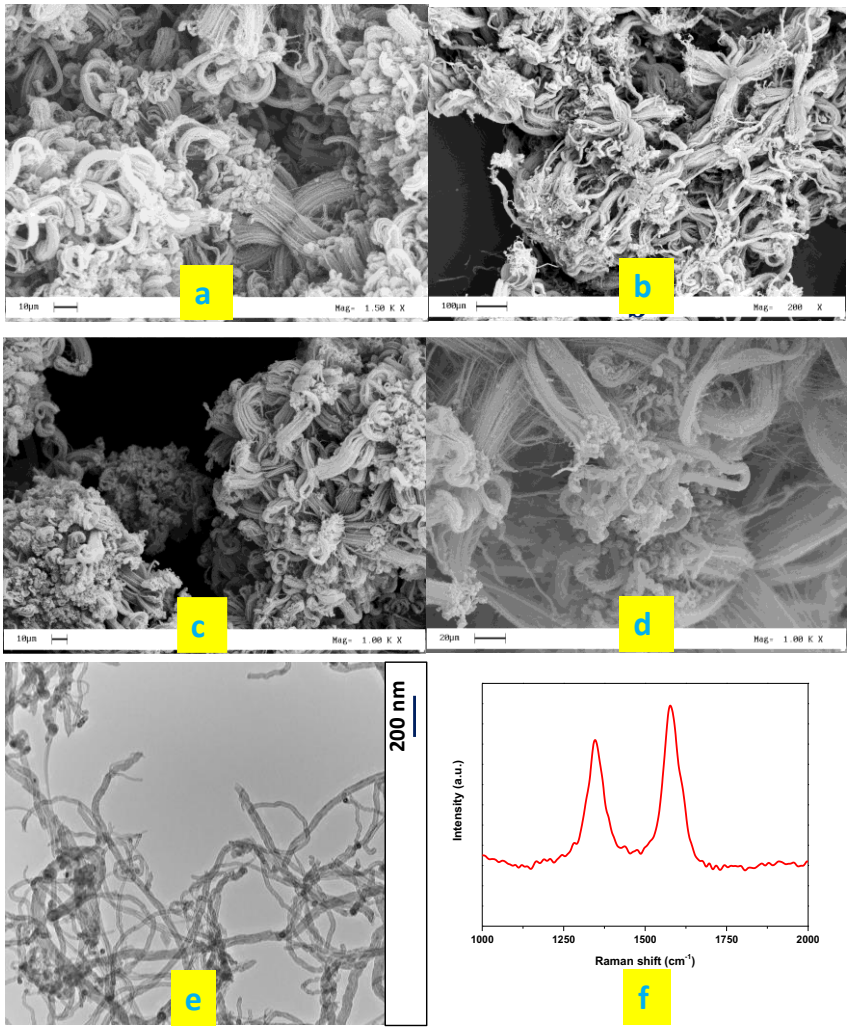

Figure 5.3 *SEM images of the produced CNTs: for ethylene CVD, at 700°C and after 10 minutes, CNTs mean length 50 µm (a); for ethylene CVD, at 700°C and after 30 min, CNTs mean length 200 µm (b); for acetylene CVD, at 600°C and after 10 minutes, CNTs mean length 40 µm (c); for acetylene*

CVD, at 600°C and after 30 min, CNTs mean length 180 μm (d). A TEM image of CN2 (e). Raman spectrum of CN2 in the region 1000-2000 cm-1 (f).

5.3.2 GO and rGO characterization

Figures 5.4, a and b demonstrate the thermal decomposition activity of the GO and rGO airflows, respectively. For graphene oxide, it can be found that there are weight losses in three major areas. Between room temperature and around 125 °C, the loss observed can be due to physically adsorbed water. The second weight loss, located in the range 125 -210 ° C, is mainly due to a simultaneous release of water and of CO_2 of the carbon atoms originating from the oxyfunctional groups (Muge Acik et al., 2010). Ali et al. (Ali et al., 2009) suggested that the elimination of CO_2 increases hydrophobicity which leads to a co-elimination of the water bounded to the hydrophilic sites. Furthermore, at higher temperatures, a small weight loss caused by the oxidation of the carbonaceous network occurs.

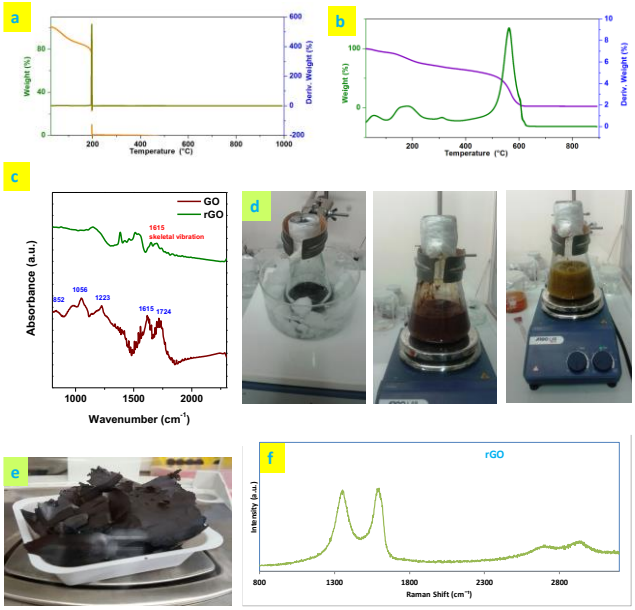

Figure 5.4 *TG-DTG of graphene oxide and reduced graphene oxide (a, b). IR spectra of GO and rGO (c). Photos of different synthesis steps (d). Photo of the produced graphene oxide (e). Raman spectrum of rGO (f).*

Reduced graphene oxide, on the other hand, shows higher thermal stability. The primary weight loss happens in the 400-600 °C range and the overall weight loss ends at 650 °C. Water loss at low temperatures is less important

than for GO, although water loss at higher temperatures due to the presence of H_2O between the layers is certainly not present, indicating a good reduction. Figure 5.4, c shows the IR spectrum of GO. The spectrum exhibits a peak at about 1800 cm^{-1}, representative of carbonyl groups (C=O), and at 1724 cm^{-1}, due to the presence of C=O bonds from carboxyl groups (Eigler, Dotzer and Hirsch, 2012). The signal at 1615 cm^{-1} is related to the vibrations of C=C bonds, while the 1414 cm^{-1} signal corresponds to the vibration connected to the deformation of O-H bonds from carboxylic groups. C-O vibrations from several groups, mainly epoxy and hydroxyl groups, are present in the range 800-1300 cm^{-1} and it is possible to identify distinct peaks at about 852, 966, 1056 and 1223cm^{-1} (Stankovich et al., 2006). In particular, the bands at 852 and 1221 cm^{-1} can be attributed to the vibrations of epoxy groups (Stankovich et al., 2006). The peak at 1056 cm^{-1} could also originate from the vibration of the C-C skeleton (M. Acik et al., 2010). The IR spectrum of the reduced graphene oxide, which is shown in Figure 5.4, c, too, has fewer peaks than the one of graphene oxide. In particular, the latter spectrum shows, no peaks related to C=O bonds, epoxy groups, and carboxyl groups. Furthermore, the peak generated by the C-C skeleton vibration (1615 cm^{-1}) is present, and the two new bands at 1385 cm^{-1} and 1460 cm^{-1} are related to the flexural vibration of C-H bonds (Ali et al., 2009), probably due to the presence of residual ascorbic acid.

Figures 5.4, d and 5.3, e give evidence of the different steps GO formation, i.e. mixture after addition of sulfuric acid to graphite powder, inside the ice bath; mixture after addition of distilled water; mixture after the addition of hydrogen peroxide. The photo in Figure 5.4, e shows the typical aspect of the produced GO. Figure 5.4, f shows the Raman spectrum at 514 nm of the synthesized graphene-based materials. The spectrum, which is overall a typical spectrum of reduced graphene oxide (Sarno et al., 2017), exhibits the two most characteristic peaks of graphene, which correspond to the D band at 1360 cm^{-1} and the G band at 1585 cm^{-1} (M. Acik et al., 2010).

Lastly, Figures 5.5 show TEM images at low and high magnification of the synthesized graphene, thus suggesting a good level of exfoliation of the sample as well as the presence of a number of layers not higher than 5.

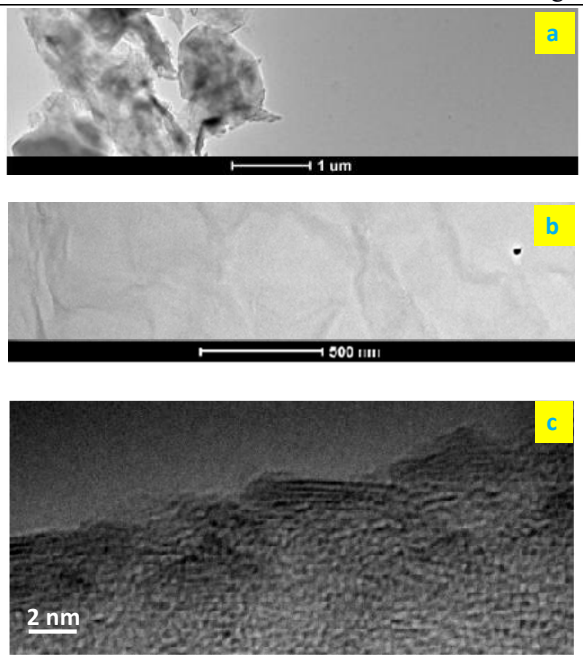

Figure 5.5 *TEM images of the produced rGO at different magnifications (a, b, c).*

5.3.3 Graphene from exfoliation characterization

A scheme of the FLG production process is shown in Figure 5.6, a. The TEM image in Figure 5.6, b confirms the existence of the graphene nanosheets produced. A statistical distribution of the thickness of the graphene flakes was generated and shown in Figure 5.6, c as a result of an analysis of a large number of TEM images by paying close attention to the uniformity of the edges of flakes. In addition, the sheets are of a lateral size in the order of microns.

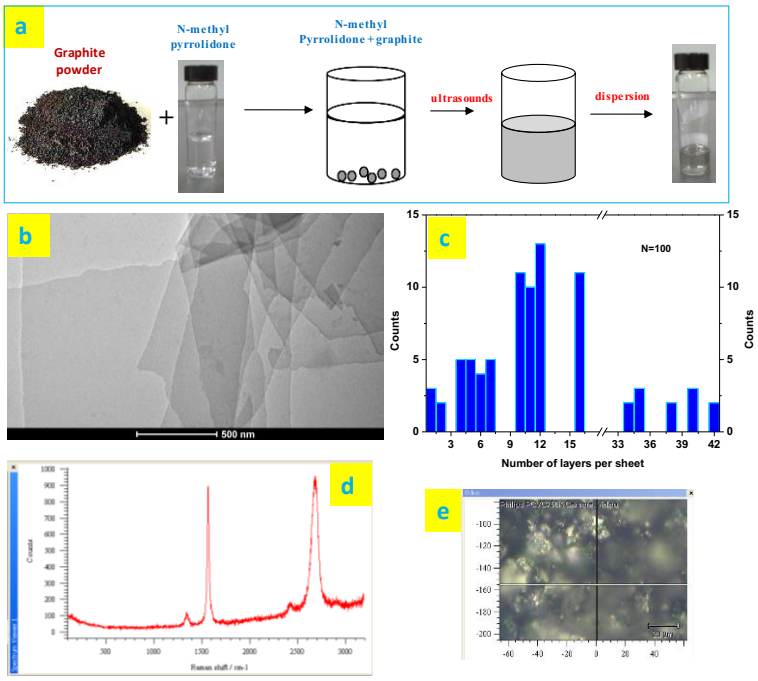

Figure 5.6 *Scheme of the FLG synthesis procedure (a). A typical TEM image of FLG (b); and, relative histogram of number of layers per sheets distribution (c). Typical Raman Spectrum of FLG (d); and corresponding optical microscopy image (e).*

Figure 5.6, d shows the Raman spectra of the graphene nanosheets formed after exfoliation. In specific, the characteristic Raman bands are 1582 cm^{-1} (G-band) and around 2700 cm^{-1} (G-band or 2D-band). A weak D band, due to disorder or borders, can be detected at roughly half the frequency of the 2D band (at around 1350 cm^{-1}). On the other hand, the Raman spectrum of graphene sheets reveals a sharp and extreme 2D band profile, indicating the creation of a few layers of graphene.

5.3.4 Lubricant preparation and stability dispersion tests

In general, stability in EUBUSH 220 was found to be very high, which is why stability in Synplus 75W-90 was evaluated in the presence of various surfactant/dispersant agents.

In particular, the ratio A obtained under UV-Vis for GO, rGO and FLG at different concentrations was stated in Figure 5.7. Indeed, the stabilization of carbon nanotubes is very difficult due to the extreme de-bundling and strong contact of Van der Waals.

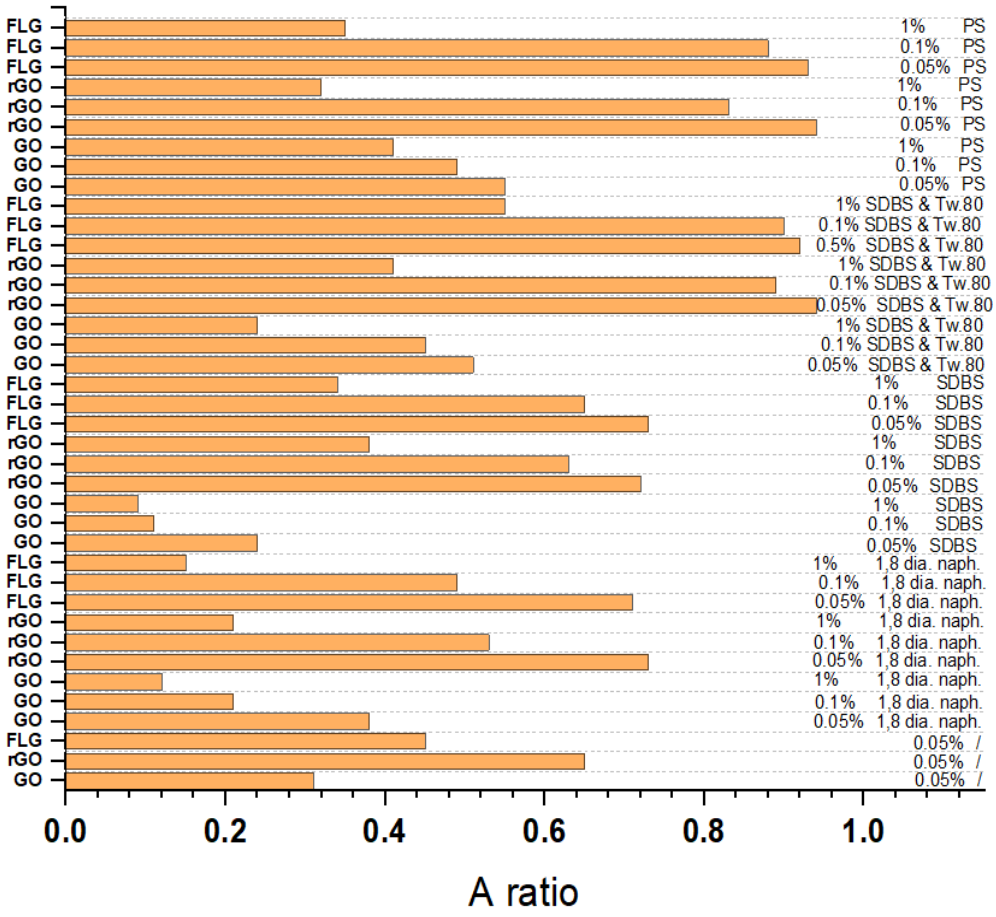

Figure 5.7 *Stability of surfactant/dispersant assisted and free formulations.*

Firstly, graphene-based formulations without dispersants have been analyzed, see the first lines of Figure 5.7. Dispersion experiments reveal the following: GO disperses worst due to its high hydrophilicity; rGO disperses best due to its increased hydrophobicity; eventually, FLG, being thicker (contains a fraction of a larger number of layers), disperses worse than rGO.

Dispersants can be used to increase stability. A dispersant with its polar head may be bound to solid particles. The polar head is chemically bound to a very long hydrocarbon tail, which leaves the dispersant submerged in oil. This mechanism, which is usually used to suspend impurities, such as soot, sludge, or others, can be used here to hold nano-additives in suspension. Surfactants function in the same manner in practice. Here, certain surfactant

molecules have been checked with the goal of helping to spread well and disrupting as little as possible the lubricant composition, which is such a delicate balance.

It was observed that 1,8 diaminonaphthalene is able to improve dispersion at low concentrations. Moreover, the use of “strongly” surfaces anchoring molecules significantly allows improvement, also in the case of the heavier FLG. This is not the case for GO hydrophilic enriched surfaces, which disperse worst in the presence of ionic SDBS surfactant. On the other hand, increased stability was observed in the presence of the synergistic combination of anionic-non ionic surfactants, which generally show more easily formation of micelles (Zhang and Zhu, 2010).

In Figure 5.8, the evolution of the relative concentration as a function of time for FLG in SYNPLUS 75W-90, and, in the presence of SDBS +Tween 80 surfactants or PS dispersant, is shown. It can be observed that stability in both cases is strongly dependent on concentration. The combination of the two surfactants ensures higher stability for all the 20 hours of investigation.

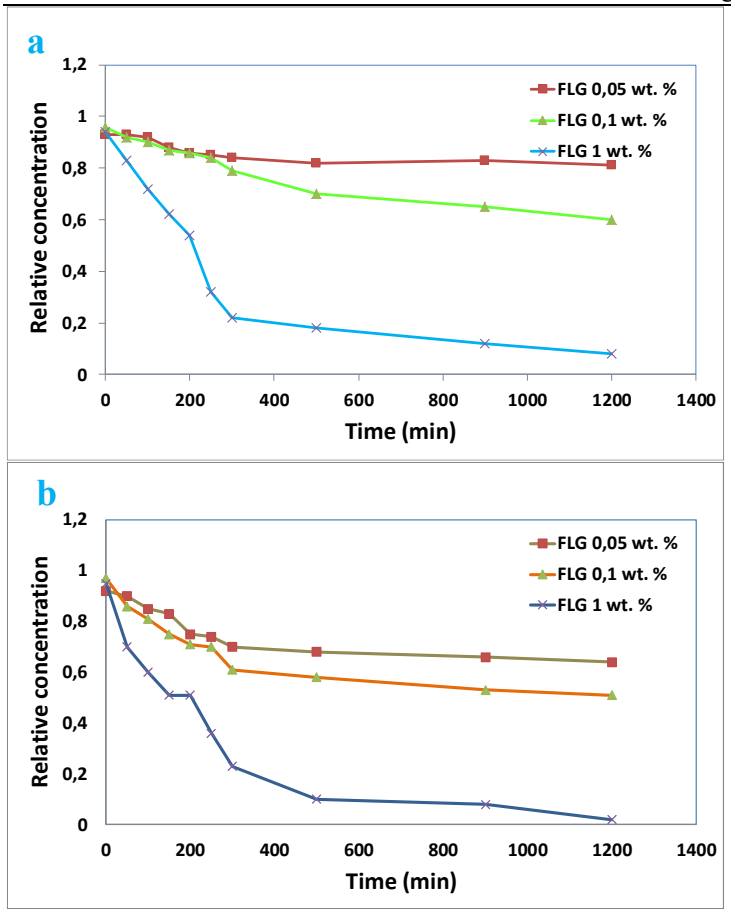

Figure 5.8 *Relative concentration vs time increase of FLG in SYNPLUS 75W-90, in the presence of: SDBS+Tween 80 surfactant (a); and PS blending (b).*

Rheological properties, such as dynamic viscosity, are important features of the final lubricant composition. Viscosity does not alter as a function of the incorporation of surfactants and nano-additives. In specific, in Figure 5.9, the viscosity of: SYNPLUS 75W-90 alone; SYNPLUS 75W-90 loaded with 2 wt. % PS; SYNPLUS 75W-90 loaded with 2 wt. % of PS and a presence of 0.1 wt. %.1 wt. % FLG, are reported. The experimental data clearly evidence that the low surfactant concentration does not modify significantly viscosity. Moreover, it results unchanged even after nano-carbons addition.

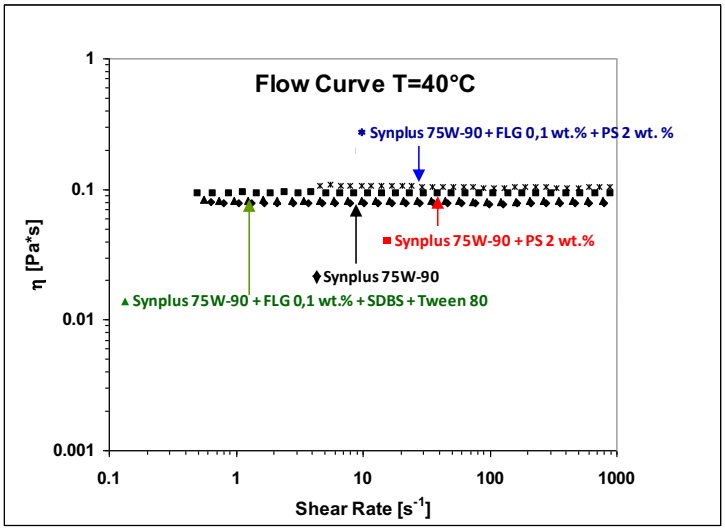

Figure 5.9 *Viscosity vs. shear rate: for SYNPLUS 75W-90; for SYNPLUS 75W-90 + 2 wt. % PS; for 0.1 wt. % loaded FLG in SYNPLUS 75W-90 + 2 wt. % PS; for 0.1 wt. % loaded FLG in SYNPLUS 75W-90 + 1 wt. % (SDBS + Tween 80).*

5.3.5 Tribological characterization

The results of the tribological tests performed on SYNPLUS 75W-90 are summarized in Table 5.2. Reductions, of Coefficient of Friction (CoF) and Wear Scar Diameter (WSD). The WSD is reported only for the ball side as the wear on the disk was not noticeable for the control sample. The results were recorded for the synthesized dispersant and surfactants-enhanced graphene-based materials in SYNPLUS 75W-90 at three different concentrations (0.05 wt%, 0.1 wt%, and 1 wt%). As shown in Table 5.2, the solvent-exfoliated few-layer graphene exhibits the best tribological performance, showing a mean reduction during 160 min operation of CoF and WSD, at the ambient temperature, of 22 % and 19 %, respectively.

This can be explained as a consequence of the larger and defect-free FLG generating protective films. At 80°C the reductions are of 20 % and 17 % respectively, at an optimum concentration of 0.1 wt. %, highlighting the role of the nano-additive, which, indeed, at higher temperatures where the base viscosity decreases, locally precipitates on the metal surfaces in contact by protecting them. The promising results obtained with FLG are also a good outcome in light of the more complex and difficult GO/rGO production on a large scale.

Table 5.2 *COF (%) and mean wear scar diameter reduction (%) for different formulations.*

ID	Sample	Nanoadditive concentration	Surfactant/dispersant	COF reduction [%]	Mean wear scar diameter reduction [%]
29	**GO**	**0.05%**	**SDBS and Tween 80**	**5**	**3**
30	**GO**	**0.1%**	**SDBS and Tween 80**	**8**	**4**
31	**GO**	**1%**	**SDBS and Tween 80**	**2**	**1**
32	**rGO**	**0.05%**	**SDBS and Tween 80**	**9**	**11**
33	**rGO**	**0.1%**	**SDBS and Tween 80**	**11**	**14**
34	**rGO**	**1%**	**SDBS and Tween 80**	**6**	**5**
35	**FLG**	**0.05%**	**SDBS and Tween 80**	**18**	**8**
36	**FLG**	**0.1%**	**SDBS and Tween 80**	**22**	**19**
37	**FLG**	**1%**	**SDBS and Tween 80**	**5**	**8**
41	**GO**	**0.05%**	**PS**	**6**	**4**
42	**GO**	**0.1%**	**PS**	**9**	**4**
43	**GO**	**1%**	**PS**	**3**	**2**
44	**rGO**	**0.05%**	**PS**	**10**	**10**
45	**rGO**	**0.1%**	**PS**	**14**	**15**
46	**rGO**	**1%**	**PS**	**8**	**6**
47	**FLG**	**0.05%**	**PS**	**17**	**13**
48	**FLG**	**0.1%**	**PS**	**15**	**14**
49	**FLG**	**1%**	**PS**	**13**	**9**

The wear scar diameter reduction (%) and the friction coefficient, in SYNPLUS 75W-90, with SDBS and Tween 80 surfactants, were reported in Figure 5.10, for FLG 0.1 wt. % and 0.05 wt. %, showing the influence of time on the lubricant performance.

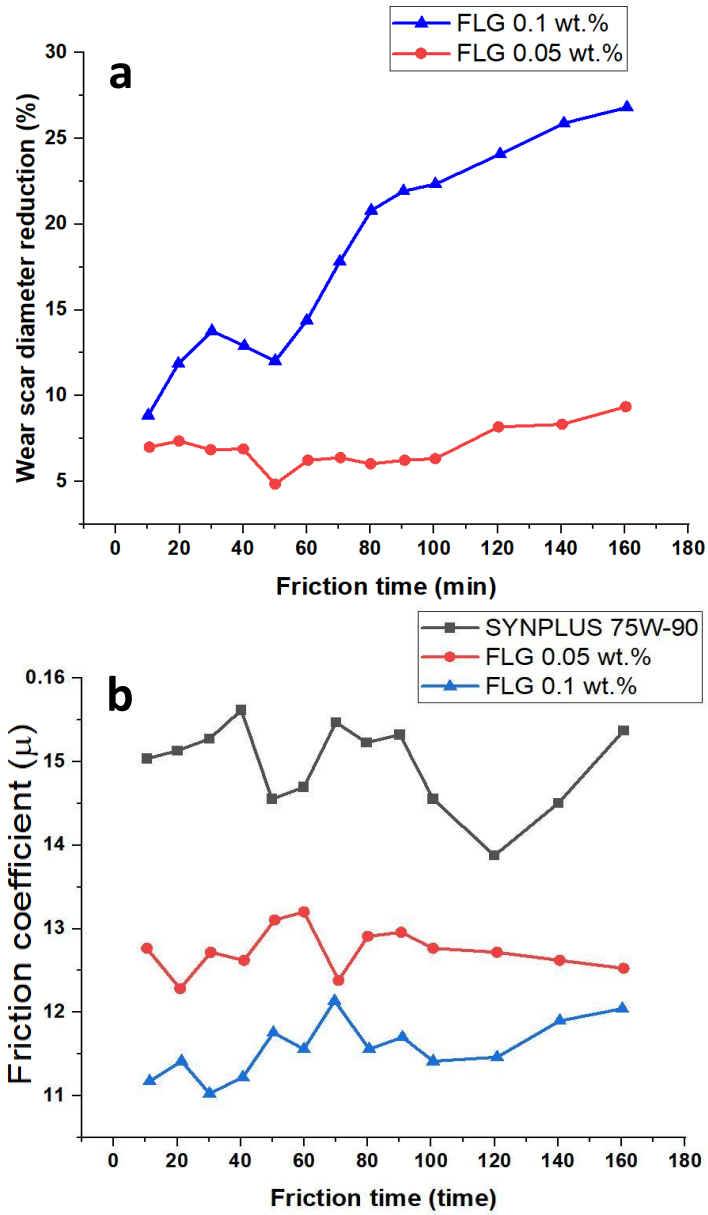

Figure 5.10 *SYNPLUS 75W-90 alone, and with FLG, at two different concentrations, in the presence of SDBS+Tween 80 surfactant, evolution under friction time increase: wear scar diameter reduction % (a); friction coefficient (b).*

A comparison between the two FLG loaded oil at 0.1 wt. % (Figure 5.10), was shown in Figure 5.11. The reductions are rather similar, highlighting the role of the additive. In Figure 5.12, the CN1 loaded oils were compared. The

results show the same trend, even if the reductions are smaller, probably due to the CNTs worst dispersion. However, also, in this case, the friction profiles show a low dependence on time, probably due to a shear-induced dispersion.

ID		Nanoadditive concentration	Base oil	Surfactant/ dispersant
1	FLG	0.1%	Synplus 75W-90	SDBS + Tween 80
2	FLG	0.1%	Eubush220	/

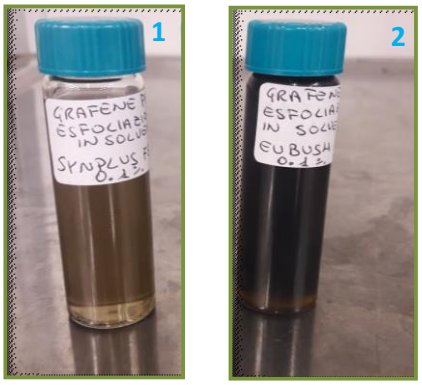

Figure 5.11 *Photos of the two oil at 0.1 wt. % of FLG in SYNPLUS 75W-90 + SDBS + Tween 80 (1); and EUBUSH 220 (2).*

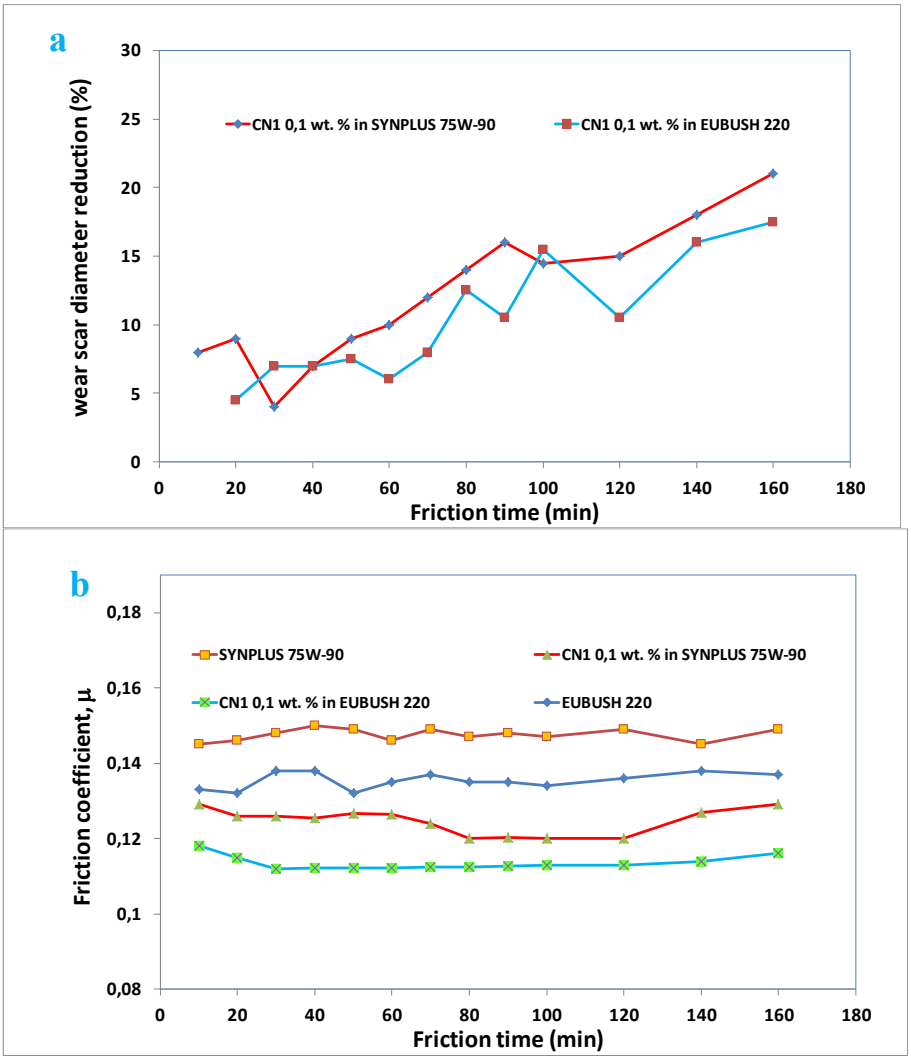

Figure 5.12 *SYNPLUS 75W-90 alone and EUBUSH 220 alone, with CN1, at 0.1 wt. %, evolution under friction time increase: wear scar diameter reduction % (a); friction coefficient (b). SDBS+Tween 80 surfactant mixture was added in the case of SYNPLUS 75W-90.*

The wear scars after 80 minutes of testing in the presence of SYNPLUS 75W-90 alone, at 25 ° C and 80 ° C, were shown in Figures 5.13, a, and 5.13, b, respectively. Moreover, in Figures 5.13, c and 11d the wear scar diameters and surface roughness, as obtained by profilometer images for SYNPLUS 75W-90 with 0.1 wt. % FLG and 1 wt. % surfactants, at 25 ° C and 80 ° C, respectively, were reported. The addition of FLG determines not only a reduction of the wear scar diameters but also a significant reduction of the surface roughness. The rubbing surfaces lubricated by the nano-carbons

loaded oils result smooth, this is likely due to the formation of a film during sliding. In Figures 5.13, c and d, FLG nanosheets on the rubbing surfaces, as darker and more prominent areas, can be observed.

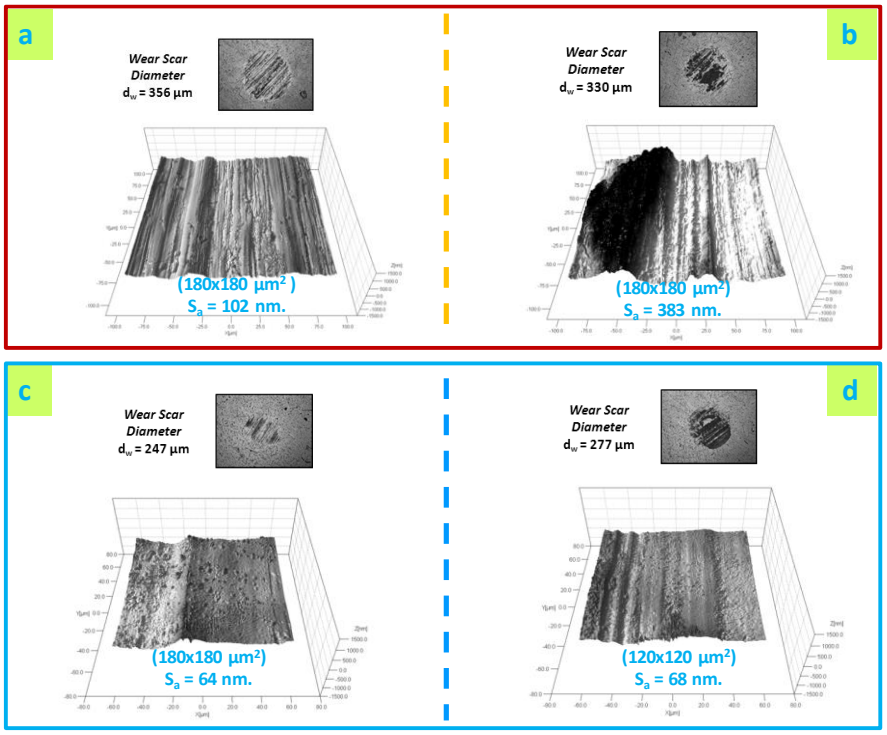

Figure 5.13 *Worn surfaces of steel balls: with SYNPLUS 75W-90 at 25 °C (a) and 80 °C (b); with 0.1 wt. % loaded FLG in SYNPLUS 75W-90 + 1 wt. % (SDBS + Tween 80), at 25 °C (c) and 80 °C (d).*

To better understand the role of the FLG, Raman spectroscopy was also used after tribological tests. In Figure 5.14a, the image of a worn surface after lubrication with FLG at 0.1 mass% dispersed in the presence of SDBS and Tween 80 is shown. Micro-Raman spectrometer was further used to analyse the worn surface, trying to identify carbon deposition. Raman spectra collected in some areas of the image in Figure 5.14a are reported in Figures 5.14b, c and d. It was found that in darker areas, the characteristic peaks of carbon, D and G bands at about 1350 and 1590 cm-1 are clearly visible, Figures 5.14b and c.

On the other hand, they are less intense in lighted areas, Figure 5.14d. These observations can draw the consideration that carbon derived by FLG deposits on the contact surfaces, helping lubrication. Furthermore, the Raman spectra recorded on the worn surfaces after tribological tests, show an increased ID/IG ratio, also suggesting a major role of tribology for exfoliation

and deposition phenomena. Moreover, the reduced roughness after tests in the presence of FLG assisted tribology, indicating the ability of FLG to also repair surfaces, can be likely attributed to the high lateral sizes of the original FLG, which also after fragmentations, retains sizes able to bridge the grains against crack propagations.

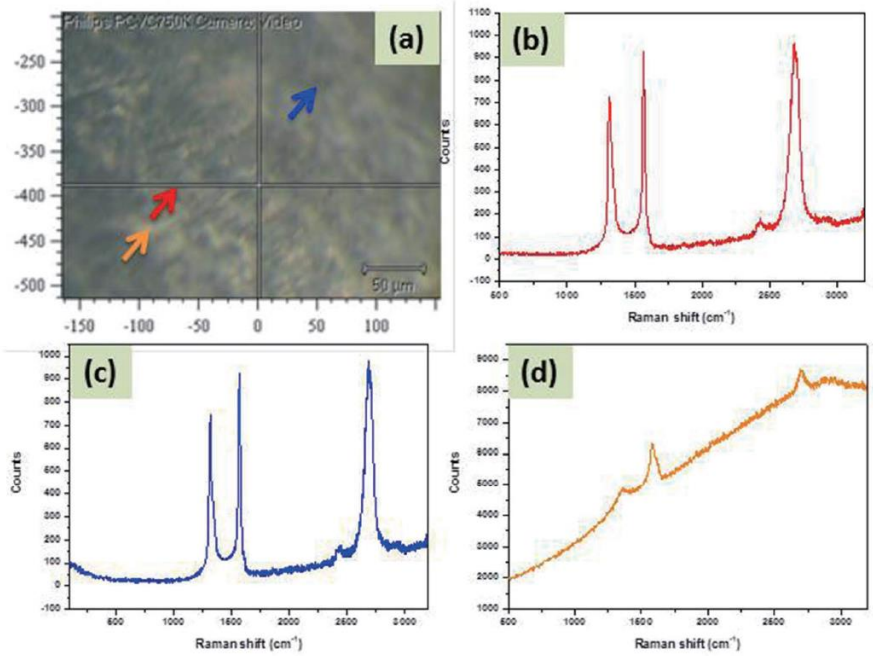

Figure 5.14 *Raman characterization on the worn surface after the tribological test.*

In summary, carbon nanotubes and graphene-based nano-carbons were synthesized through simple and scalable processes, such as catalysed chemical vapor deposition (CCVD), chemic.al exfoliation, and solvent-based exfoliation. After an extensive characterization of the samples, a systematic study of their stability in Group I and Group III base oils, with and without a low quantity of dispersant/surfactants, was carried out, revealing that the combination of SDBS and Tween 80 surfactants enables the highest stability. This enhanced which, indeed, at higher temperatures locally precipitates on the metal surfaces in contact by protecting them. The remarkable performance achieved with FLG, which remains stable also over a long test time, is a very good result when taking into consideration the more difficult GO/rGO production on a large scale. What is more, the dependence of viscosity on the shear rate for different samples was recorded, confirming that the low surfactant concentration and the nano-carbons presence in the base oil do not lead to any significant modification of this rheological parameter. Eventually, not only a reduction of the wear scar diameters but also a high reduction of

the surface roughness was measured both at room temperature and 80°C, due to the addition of the 0.1mass% FLG sample. This promising result, likely due to the formation of a protective film generated by the nano-additive during sliding, confirms its superior tribological performance.

5.5 References

ACIK, MUGE et al. (2010) The Role of Intercalated Water in Multilayered Graphene Oxide. *ACS Nano*, 4(10), pp. 5861–5868.

ACIK, M. et al. (2010) Unusual infrared-absorption mechanism in thermally reduced graphene oxide. *Nature Materials*, 9(10), pp. 840–845.

ALI, F. et al. (2009) Chemical route to the formation of graphene. *Current Science*, 97(5).

BAGHERI, A. and KHALILI, P. (2017a) Synergism between non-ionic and cationic surfactants in a concentration range of mixed monolayers at an air–water interface. *RSC Advances*, 7(29), pp. 18151–18161.

BAGHERI, A. and KHALILI, P. (2017b) Synergism between non-ionic and cationic surfactants in a concentration range of mixed monolayers at an air–water interface. *RSC Advances*, 7(29), pp. 18151–18161.

BHAUMIK, S. (2013) Extreme pressure property of Carbon Nano Tubes (CNT) based nanolubricant. *Journal of Chemical Engineering and Materials Science*, 4(8), pp. 123–127.

CHEN, C.S. et al. (2005) Modification of multi-walled carbon nanotubes with fatty acid and their tribological properties as lubricant additive. *Carbon*, 43(8), pp. 1660–1666.

EIGLER, S., DOTZER, C. and HIRSCH, A. (2012) Visualization of defect densities in reduced graphene oxide. *Carbon*, 50(10), pp. 3666–3673.

FERNÁNDEZ-MERINO, M.J. et al. (2010) Vitamin C Is an Ideal Substitute for Hydrazine in the Reduction of Graphene Oxide Suspensions. *The Journal of Physical Chemistry C*, 114(14), pp. 6426–6432.

GRIERSON, D.S. and CARPICK, R.W. (2007) Nanotribology of carbon-based materials. *Nano Today*, 2(5), pp. 12–21.

GUO, Y.-B. and ZHANG, S.-W. (2016) The Tribological Properties of Multi-Layered Graphene as Additives of PAO2 Oil in Steel–Steel Contacts. *Lubricants*, 4(3), p. 30.

HERNANDEZ, Y. et al. (2008) High-yield production of graphene by liquid-phase exfoliation of graphite. *Nature Nanotechnology*, 3(9), pp. 563–568.

JOLY-POTTUZ, L. et al. (2004) Ultralow friction and wear behaviour of Ni/Y-based single wall carbon nanotubes (SWNTs). *Tribology International*, 37(11–12), pp. 1013–1018.

KAŁUŻNY, J. et al. (2017) Lubricating performance of carbon nanotubes in internal combustion engines – engine test results for CNT enriched oil. *International Journal of Automotive Technology*, 18(6), pp. 1047–1059.

KUNDU, P., KUMAR, V. and MISHRA, I.M. (2015) Modeling the steady-shear rheological behavior of dilute to highly concentrated oil-in-water (o/w) emulsions: Effect of temperature, oil volume fraction and anionic surfactant concentration. *Journal of Petroleum Science and Engineering*, 129, pp. 189–204.

MAURIN, G. et al. (2001) Segmented and opened multi-walled carbon nanotubes. *Carbon*, 39(8), pp. 1273–1278.

SARNO, M. et al. (2012) Evaluating the effects of operating conditions on the quantity, quality and catalyzed growth mechanisms of CNTs. *Journal of Molecular Catalysis A: Chemical*, 357, pp. 26–38.

SARNO, M. et al. (2014) Oil Lubricant Tribological Behaviour Improvement Through Dispersion of Few Layer Graphene Oxide. *Journal of Nanoscience and Nanotechnology*, 14(7), pp. 4960–4968.

SARNO, M. et al. (2017) SC-CO 2 -assisted process for a high energy density aerogel supercapacitor: the effect of GO loading. *Nanotechnology*, 28(20), p. 204001.

SHAHNAZAR, S., BAGHERI, S. and ABD HAMID, S.B. (2016a) Enhancing lubricant properties by nanoparticle additives. *International Journal of Hydrogen Energy*, 41(4), pp. 3153–3170.

SHAHNAZAR, S., BAGHERI, S. and ABD HAMID, S.B. (2016b) Enhancing lubricant properties by nanoparticle additives. *International Journal of Hydrogen Energy*, 41(4), pp. 3153–3170.

SINGH, H. and BHOWMICK, H. (2020) Lubrication characteristics and wear mechanism mapping for hybrid aluminium metal matrix composite sliding under surfactant functionalized MWCNT-oil. *Tribology International*, 145, p. 106152.

STANKOVICH, S. et al. (2006) Synthesis and exfoliation of isocyanate-treated graphene oxide nanoplatelets. *Carbon*, 44(15), pp. 3342–3347.

ZHANG, M. and ZHU, L. (2010) Effect of SDBS–Tween 80 mixed surfactants on the distribution of polycyclic aromatic hydrocarbons in soil–water system. *Journal of Soils and Sediments*, 10(6), pp. 1123–1130.

ZHANG, W. et al. (2011) Tribological properties of oleic acid-modified graphene as lubricant oil additives. *Journal of Physics D: Applied Physics*, 44(20), p. 205303.

Chapter VI. Novel study of carbon quantum dots/poly (methyl methacrylate) nanocomposites as a green lubricant oil additive

6.1 Overview

Among nano-additives, carbon-based nanomaterials are capable of ensuring high anti-wear and anti-friction performance (Grierson and Carpick, 2007) as a result of their afore mentioned mirits. However, the inert structure of nano-carbons and their solid nature, especially for 1D and 2D materials, makes their long-time dispersions in lubricant oil extremely challenging (Shahnazar, Bagheri and Abd Hamid, 2016). With the aim of increasing carbon nano-additives stability, surface-modification processes have been proposed, even though they still hinder large-scale applications because of their high cost, complexity and, even more, poor effectiveness (Chen et al., 2005; Lin, Wang and Chen, 2011; Zhang et al., 2011; Ota et al., 2015).

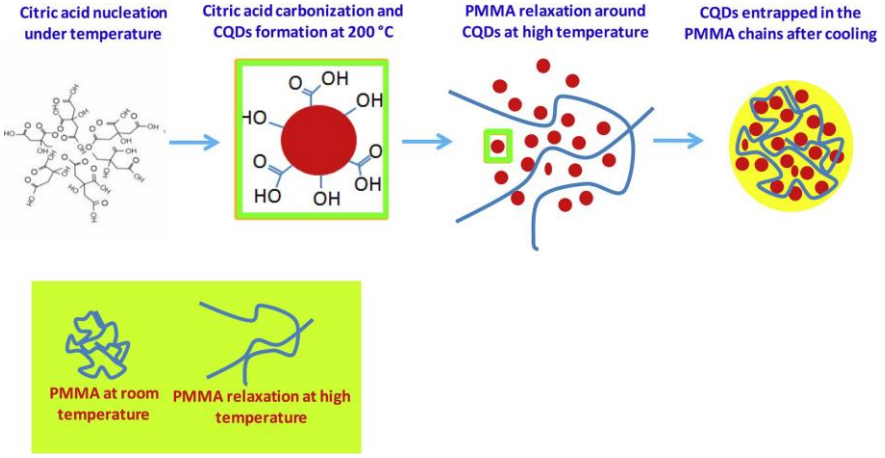

Figure 6.1 *Illustrative representation of formation and entrapment of CQDs within PMMA structure.*

Carbon quantum dots (CQDs) can be regarded as a new type of nano-carbons consisting of quasi-spherical particles with ultra-small sizes and unique optical and electronic properties. Since their accidental discovery by Xu et al., in 2004 (Lin, Wang and Chen, 2011), CQDs have been receiving a significant research focus. Other than sizes below 10 nm, they often exhibit a polar nature due to the presence of functionalized hydroxyl and carboxyl groups on their surface and are highly biocompatible and environmental friendly (Chen et al., 2005; Ota et al., 2015). An additional advantage of CQDs is the ease of synthesis as they can be prepared from natural carbonaceous sources under both severe and mild conditions, for instance through carbonization of various fruit juices, vegetables, fruit peels, plant parts and citric acid (Bottini et al., 2006; Krysmann, Kelarakis and Giannelis, 2012; Jia, Li and Wang, 2012; Dong et al., 2012; De and Karak, 2013; Jiang et al., 2013; Gao et al., 2014). As lubricant additives, in virtue of their ultra-small size and "naturally" functionalized structure, CQDs exhibit enhanced tribological properties, even though they stably disperse only in polar solvents (Bourlinos et al., 2008; Wang et al., 2011).

Indeed, the polar nature of CQDs poses the question of their compatibility with non-polar hydrocarbon oils, such as polyalphaolefin (PAO) and mineral oils, which highly hampers the future usage of CQDs with them. In this direction, a few attempts have been made so far (Barros and Prieto-Rodriguez, 2008; Tu et al., 2020), yet there is still the need to search for simpler synthesis procedures which do not involve the usage of harmful substances. On the other hand, in order to obtain complete and effective lubricant formulations, researchers often seek for additives which can be multifunctional as well as compatible with different chemicals in a formulation, both with other additives as well as the base fluid. Within this context, the development of multifunctional additives with wear-and friction-reducing properties as well

as viscosity index-improving behavior, which do not interfere either with each other or with the base oil, yet exhibit beneficial synergistic interactions, would be of high significance. Poly (methyl methacrylate) (PMMA) is considered as one of the most efficient viscosity index (VI) improvers for base lubricant oils, i.e. able to significantly reduce the lubricant oil viscosity dependence on temperature variations. Non-polar oil-compatible PMMA is traditionally synthesized through free radical polymerization of alkyl methacrylate monomers.

According to the most widely reported mechanism of the capability of such a polymer to act as viscosity modifier, PMMA increases the base oil viscosity proportionately with temperature due to the expansion of its long molecular chains with increasing temperatures (Selby, 1958). Indeed, chains occupying a larger volume possess higher resistance to flow, hence greater viscosity (Aziz, Abdullah, et al., 2019a). As far as literature is concerned, few papers have been published on the preparation of CQDs/PMMA nanocomposites (Bouknaitir et al., 2019; Maxim et al., 2020), in which two step synthesis mechanisms were employed to obtain CQDs, subsequently incorporated in a polymer matrix to give nanocomposites films. In particular, Aziz et al. (Aziz, Abdullah, et al., 2019a) reported the preparation, for applications in optoelectronic devices, of PMMA/CQDs nanocomposite films in two steps: (1) synthesis of CQDs by hydrothermal treatment using glucose, H3PO4 and NaOH as well as chloroform in the purification step; (2) preparation of the nanocomposite using a solution casting procedure carried out by mixing PMMA/acetone and CQDs/acetone solutions. Similarly, Maxim et al. (Maxim et al., 2020) reported an improvement of the light harvesting performance in perovskite solar cells by adopting CQDs-embedded PMMA thin films obtained in a two-steps procedure:

Phosphorus-doped CQDs were prepared at 200ºC for 1 h starting from Na_2HPO_4 and dextrose; (2) afterwards, CQDs with sizes around 3–7 nm were mixed with PMMA in chlorobenzene. Eventually, Bouknaitir et al. (Bouknaitir et al., 2019) studied the optical and the dielectric properties of nanocomposite based on the incorporation of CQDs in PMMA at several filler loading. The CQDs were synthesized at a temperature up to 300ºC, in the presence of octadecene acting as non-coordinating solvent. The nanocomposite was prepared by drop-casting a PMMA/chloroform solution and the prepared CQDs onto glass slides. Herein, a novel method was devised to improve the sustainability and simplicity of CQDs synthesis process, which thus far involved harmful molecules, with enhanced CQDs dispersion stability in non-polar lubricant oils. The method relies on simultaneously obtaining an effective multifunctional nano-additive for tribological applications. The production of PMMA/ CQDs composites, consisting of CQDs covered by an extremely thin layer of PMMA, was proposed for the first time by means of a one-step, mild temperature, oleic acid citric acid-based *green* synthesis. In particular, no harmful oleic acid was chosen as solvent of the one-step *green*

process, contributing to drastically reduce detrimental environmental impact in favour of an improved simplicity and, therefore, feasibility in view of process industrialization.

The synthesis of CQDs occurred during the thermal expansion of PMMA molecular chains, followed by nanoparticles entrapment within the polymer body after cooling. The resulting product is an oil-compatible polymer matrix which will locally release anti-friction and anti-wear CQDs under lubrication conditions. After an extensive characterization, tribological tests were carried out in a commercial mineral oil, confirming the enhanced performance of the sample.

6.2 Materials and methods

6.2.1 PMMA/CQDs composite, CQDs and t-PMMA preparation and dispersion in oil

Citric acid (CA, purity grade ≥99.5%), crystalline poly (methyl methacrylate) (PMMA) and oleic acid (OA, purity grade 90%) were all purchased from Sigma Aldrich. As for the PMMA/CQDs composite, 5 g of CA were dissolved in 50 ml of bi-distilled water and mixed with 100 ml of OA, which is used a solvent to guarantee the proper reaction environment. Afterwards, 0.5 g of PMMA in powder form was added to the mixture, which was then heated up to 200 ºC for 2 h and under magnetic stirring in an open flask. The flask was maintained opened to allow water evaporation. The synthesis of CQDs occurred during the thermal expansion of PMMA molecular chains, followed by nanoparticles entrapment within the polymer body after cooling (as shown in Figure 6.1). Furthermore, for comparison reasons, two other samples were synthesized: a treated PMMA sample and a PMMA-free carbon quantum dots sample, named as t-PMMA and CQDs in the following study, respectively. As for t-PMMA, it was prepared with the same procedure without the addition of CA. On the other hand, CQDs were obtained with both OA and CA without the addition of PMMA. After reaction occurred, the three mixtures were cooled down to room temperature and then underwent centrifugation at 7500 rpm and 5 ºC. The resulting solid particles were rinsed with ethanol for several times and eventually dried for 24 h at 60 ºC. After synthesis, PMMA/CQDs and t-PMMA were both dispersed at 0.1 wt% into a VG 220 base oil (Mineral oil, viscosity index ¼ 93, density at 15 ºC=891.1 kg/m3) by means of a 400 W tip sonicator at for 2 h at maximum power. CQDs do not disperse well in the oils because of their polar nature. In Figure 6.2, the pictures of the base oil VG 220 and the PMMA/CQDs composite dispersed in VG 220 are shown.

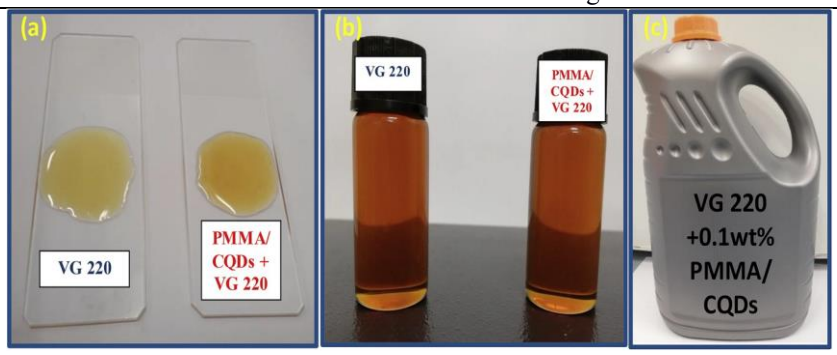

Figure 6.2 *Photos: of pure VG 220 oil and PMMA/CQDs dispersed in VG 220 oil (a) and (b); of one tank containing added oil for high volume tribological characterization.*

6.2.2 PMMA/CQDs composite, CQDs and t-PMMA characterization

The physical and chemical characterization techniques utilized in this experiment were the same as mentioned in chapter V. In addition, FT-IR analysis was carried out through a Vertex 70 apparatus (Bruker Corporation) by adopting the KBr technique. Particle size distribution of nanosheet dispersion was determined using a dynamic light scattering (DLS) instrument (HPPS ET - Malvern Instruments).

6.2.3 Tribological test description

In order to perform tribological tests, a Ducom TR-BIO-282 tribometer was adopted. In detail, the equipment consists of a tribopair composed by an upper steel ball (X45Cr13 polished steel ball, 52–54 HRC, diameter of 6 mm) in reciprocating motion and a lower X210Cr12 steel disc (60 HRC, roughness Ra of 0.30 μm, diameter of 25 mm, thickness of 6 mm) completely flooded in a lubricant bath. Reciprocating sliding tests were performed with a normal load equal to 19 N and an initial average Hertzian contact pressure of 1.17 GPa at 25 ºC and 80 ºC. Afterwards, normal pressure was in
creased to 58 N and average Hertzian contact pressure to 1.76 GPa and measurements performed at 25 ºC (Sarno, Spina and Senatore, 2019; Sarno et al., 2019). Such test conditions were chosen to explore the anti-friction and anti-wear behaviour of CQDs as mineral oil additive in both boundary and mixed lubrication regimes. With sliding motion set at 5 mm stroke and 10 Hz as frequency, boundary regime at zero-speed inversion points moves to mixed conditions in each stroke by sweeping the Stribeck number in the range [0, 7.38 10^{-12} m] at room temperature, and [0, 1.85 10^{-12} m] at 80 ºC; the transition to fully thin-film lubrication regime is expected at around 1.0 – 10^{-11} m, outside of the domain of the test herein discussed.

6.3 Results and discussion

6.3.1 Characterization results

TEM analysis was adopted for a better understanding of CQDs morphology with and without the presence of PMMA. Figure 6.3 a, b and c show TEM images of the CQDs at different magnifications, revealing semi-spherical particles with an average diameter of 3 nm, as clarified by the particle size distribution in Figure 6.3 d. Furthermore, in the presence of PMMA, the synthesized CQDs have smaller average diameters (Figure 6.4). Moreover, it is possible to observe the higher distance between each individual particle (Figure 6.4 b). Hydrodynamic diameters in solution were determined by DLS. The DLS technique measures Brownian motion (the random movement of particles due to the bombardment by the solvent molecules which surround them) and relates this to the size of the particles. The size of a particle is calculated from the translational diffusion coefficient by using the Stokes-Einstein equation (Guguła and Bredol, 2014).

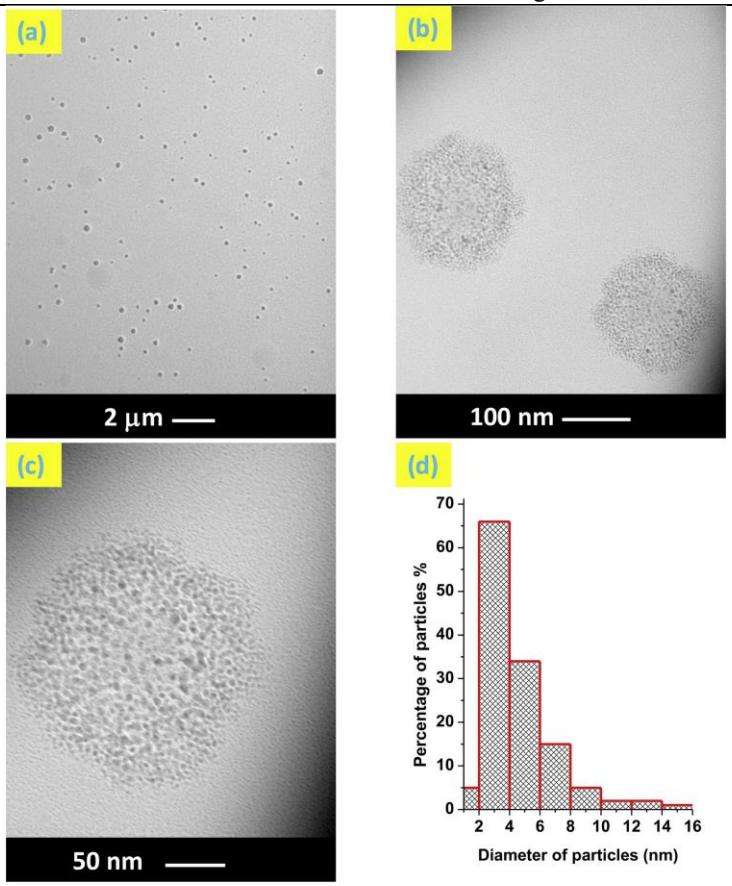

Figure 6.3 *TEM images of the formed CQDs at different magnifications: 2 μm scale bar (a); 100 nm scale bar (b); and 50 nm scale bar (c). The particle size distribution of the formed dots (d).*

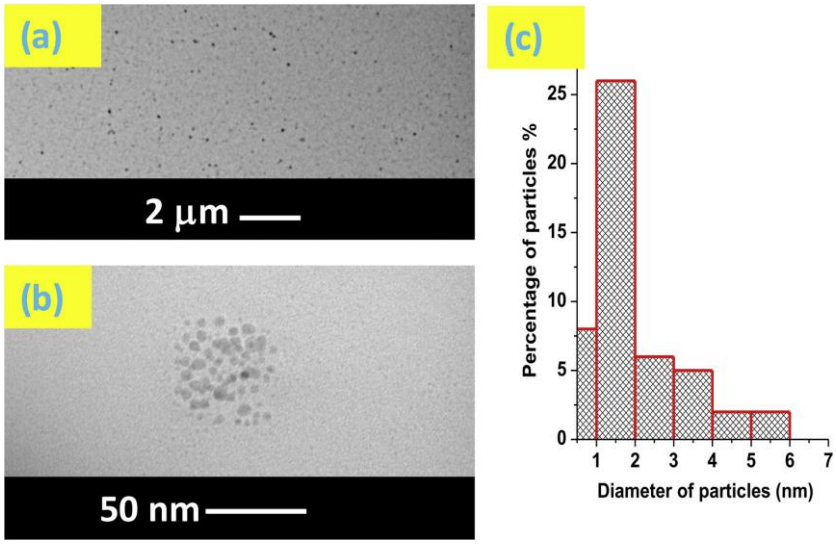

Figure 6.4 *TEM images of the PMMA/CQDs at different magnifications: 2 µm scale bar (a); 50 nm scale bar (b). The particle size distribution of the formed CQDs (c).*

The hydrodynamic diameters are in the range 1–18 nm for CQDs centered at 3 nm and in the range 3–10 nm centered at 4 nm for the PMMA-covered CQDs (Figure 6.5). These results are consistent with the microscopy observations, indicating a mean shell of PMMA of about 2 nm covering the dots.

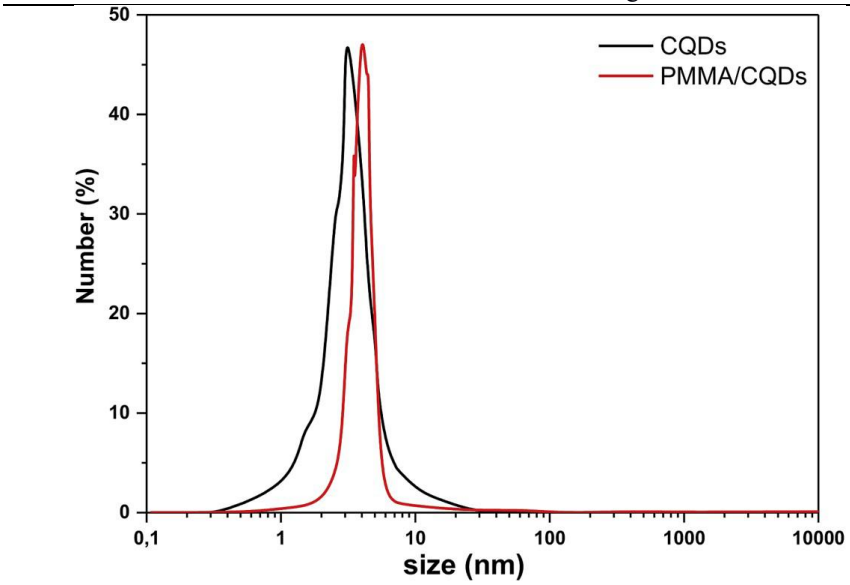

Figure 6.5 *PSD of CQDs and PMMA/CQDs as determined by DLS technique.*

The typical UV–Vis spectrum of the CQDs is reported in Figure 6.6 a, showing that the main absorption band can be seen at 340 nm, which suggests the formation of quantum dots with a size in the range 2–4 nm (Bhunia et al., 2013) in agreement with TEM analysis. In Figure 6.6 b and c, the spectra of t-PMMA and of PMMA/CQDs are reported. The absorption band displayed by the pure treated PMMA is around 274 nm, that corresponds to the n-π* electronic transition bands (El-Zaher and Osiris, 2005) exerted by the non-bonding electrons (Aziz et al., 2017). On the other hand, the shift of PMMA absorbance in the presence of CQDs to a higher wavelength (297 nm) indicates the formation of CQDS in the PMMA matrix that can be likely attributed to either the interaction between the quantum dots and the polymer chains or the formation of extra defects in the energy band gap (Aziz, Hassan, et al., 2019). In addition, Figure 6.6 d shows the behaviour of pure ethanol (on the left) and CQDs dispersed in ethanol (on the right) while being exposed to a UV lamp: contrarily to the one on the left, the sample on the right exhibits fluorescence properties, thus confirming the successful formation of carbon quantum dots.

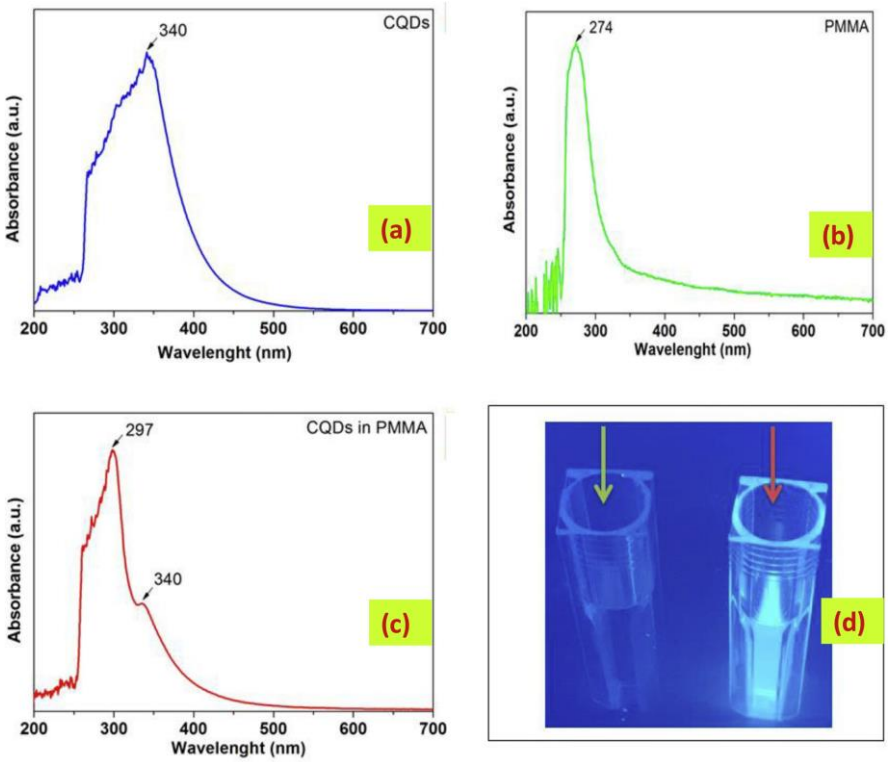

Figure 6.6 *UV–vis spectra of the different samples (a) for CQDs, (b) for the t-PMMA and (c) for PMMA/CQDs; (d) the picture represents ethanol (yellow arrow, on the left) and CQDs dispersed in ethanol (red arrow, on the right), evidencing the fluorescence properties of the latter.*

The FT-IR spectral investigation was conducted and the results shown in Fig. 6.7. Both spectra of CA and PMMA/CQDs composite display stretching vibrations over 1700 cm^{-1} which are dur to carboxylic free groups of CA (green spectrum) and –COOH on the surface of CQDs (blue spectrum). On the other hand, PMMA shows a band at 1730 cm^{-1} due to ester carbonyl stretching, which is no more visible in the spectrum of PMMA/CQDs, suggesting a shift as previously reported for PMMA and carbon quantum dots nanocomposite films formed by solution casting method (Aziz, Abdullah, et al., 2019b). This phenomenon can indicate a polymer conformational change at molecular level (Ahmed, 2009). PMMA/CQDs composite revealed C– – C bond vibrations at 1460 cm^{-1}. The bands at 2928 cm^{-1} and 2858 cm^{-1} are due to –CH3 and –C2H2– groups, respectively. Moreover, stretching vibrations at 3498 cm^{-1} strongly present in CA, are entirely disappeared in the PMMA/CQDs composite, indicating the complete dehydration and decomposition of CA during reaction.

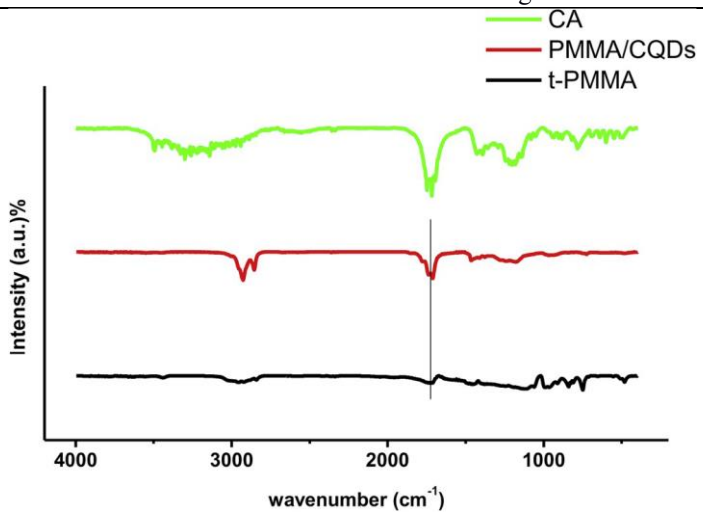

Figure 6.7 *FT-IR spectra of citric acid, PMMA/CQDs and t-PMMA.*

The analyses of the thermograms of PMMA/CQDs and of t-PMMA are reported in Figure 6.8. The thermogravimetric profile of PMMA/CQDs exhibits a first weight loss of ~55 wt % (onset at 167.9 ºC), probably due to CQDs (Ye et al., 2018). On the other hand, the presence of CQDs stabilizes PMMA, whose weight loss occurs in the temperature range 322 ºC–431 ºC, at higher temperatures than PMMA alone.

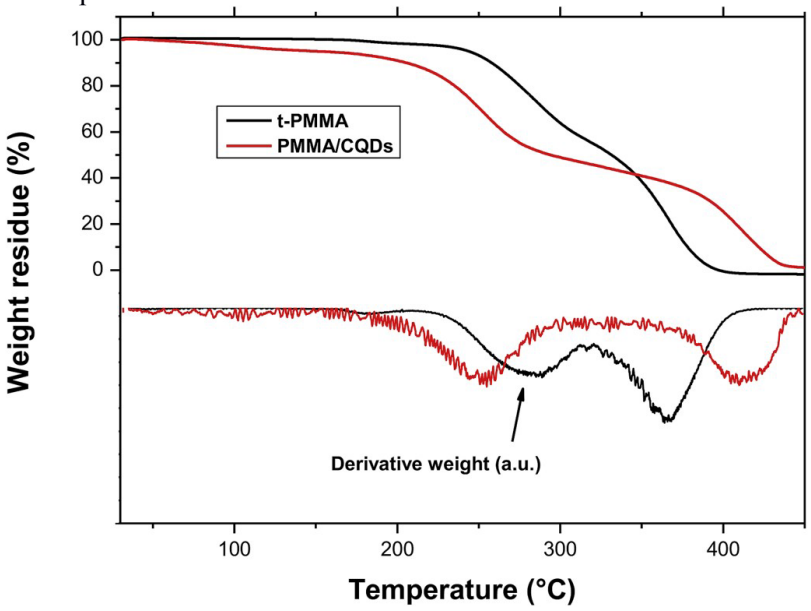

Figure 6.8 *TGA and DTG graphs of PMMA/CQDs and t-PMMA.*

Moreover, viscosities of both pure VG 220 oil and 0.1 wt% PMMA/ CQDs in VG 220 oil were recorded at both 100 ºC and 40 ºC and values were reported in Figure 6.9. As can be seen, no significant modifications of viscosity could be detected between the two samples, which confirmed that the presence of small percentages of the nanocomposite in the oil did not significantly modify its rheological property.

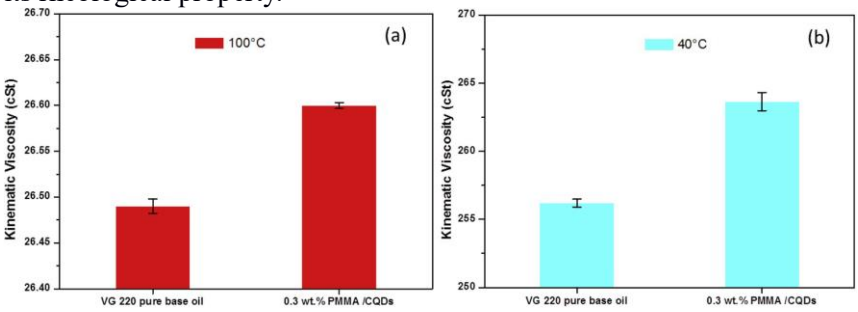

Figure 6.9 *Kinematic viscosities at a) 100 ºC and b) 40 ºC for both 0.3 wt % PMMA/CQDs þVG 220 and pure VG 220.*

6.3.2 Tribological performance

The friction and wear performance of VG 220 base oil, along with VG 220 with 0.1 wt% of PMMA/CQDs and VG 220 with 0.1 wt% of t-PMMA, are shown in Figure 6.10. The additive concentrations were selected on the basis of the optimum concentration of nano-additives in various studies on nano-lubricants (Luo et al., 2014; Wan et al., 2015; Yu, Liu and Zhou, 2019) and with a view to promoting stability and modifying as little as possible the base oil, which must still be added in a delicate balance with other components, e.g. antioxidant and antifoam improvers, etc. What is more, tribological tests were not performed on CQDs sample because of its weak dispersion in oil. In particular, the coefficient of friction (CoF) and wear scar diameter (WSD) values of the pure base oil with PMMA/CQDs and t-PMMA, measured under ambient temperature and low-load tests conditions, are reported in Figure 6.10 a. As also summarized in Figure 6.11, which includes further evaluations at 0.3 wt% and 0.5 wt% of PMMA/CQDs in oil, at the optimum concentration of 0.3 wt%, minimum CoF and WSD values were recorded of 20.2% and 41.6% reductions, respectively. It is worth noticing that these remarkable values were recorded under mixed lubrication conditions in which, because of the relatively high thickness of oil between lubricated mechanical parts, the anti-wear and anti-friction properties of the additive cannot be fully exploited and enhanced as in the boundary lubrication regime often explored in literature.

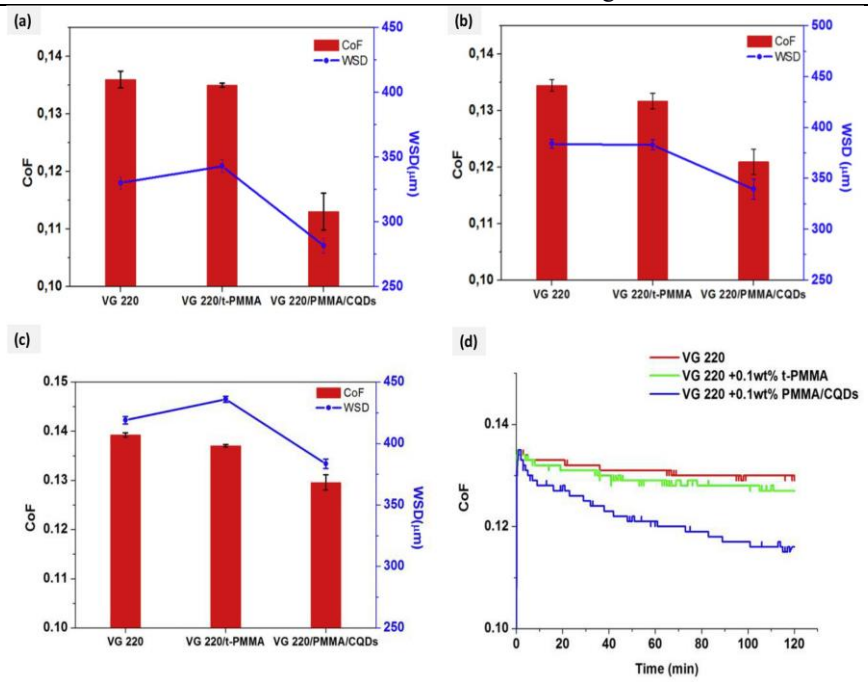

Figure 6.10 *The reciprocating tribometer results of the 1-h mean CoF and WSD values for pure base oil VG 220, 0.1 wt % PMMA-t and 0.1 wt % PMMA/CQDs at: (a) 25 ºC and at 19 N, 1.17 GPa, (b) 80 ºC and at 19 N, 1.17 GPa; and (c) 25ºC and at 58 N, 1.76 GPa. (d) CoF versus time results for the three different samples at 25 ºC, at 19 N, 1.17 GPa.*

A similar trend was observed when the test temperature was raised up to 80 ºC (Figure 6.10 b): a minor improvement in tribological performance, but more significant at this high temperature in which the reduction of the oil viscosity highlights the role of the nanoadditive, with a reduction of 10% and 12% in CoF and WSD, respectively, for 0.1 wt % PMMA/ CQDs in oil was observed.

In order to better understand the role of the nanoadditive on the load carrying capacity, the Hertzian pressure was increased to 1.76 GPa for the same reciprocating test (Figure 10c). In detail, the load carrying capacity was higher for the 0.1 wt % PMMA/CQDs in comparison with the other two samples, with a reduction of 8% in both CoF and WSD. The variation of CoF versus time was reported in Figure 6.10 d at room temperature for a duration of 120 min. The CoF of pure base oil was fluctuating in a uniform manner with average constant values every 20 min time intervals. As the CoF starts to decline, it suddenly bounces back again to maintain relatively the same values of the previous period. McFarlane, J. S., & Tabor, D. explained this behaviour in terms of “asperity junction growth” (Wan et al., 2015) that occurs when the normal load is high enough on the asperities causing a partial absence of the

lubricating media. Additionally, the asperities under load suffer from thermal softening and are pulled off under motion of contacting pairs forming wear debris conjunctions, hence increasing CoF. This behavior can also be observed in the case of t-PMMA sample, but as for the PMMA/CQDs sample there is a gradual reduction in CoF as a function of time as well. Initially, the values of CoF are higher than the ones at the end of the test: this can be attributed to the lack of interactions in the *tribo-zone* with PMMA/CQDs at the beginning. Mungse at al. described a similar phenomenon and the suggested reason is the enhanced dispersion of nanoparticles over time which ensures a continuous supply to the *tribo-interface* and the formation of a uniform *tribo-film* once a certain shear condition is reached (Anon, 1959).

The wear scars after 60 min of test for the 0.1 wt % PMMA/CQDs þ VG 220 oil and the pure VG 220 oil, at ambient temperature, 80 ºC and at a high normal pressure of 21 N at 25 ºC are shown in Figure 6.11. Moreover, the surface roughness obtained by a Profilometer for the corresponding wear scars is also reported. From the Figure, it can be stated that the presence of the nanocomposite did not only reduce the WSD under all the three conditions, but also significantly smoothened the surfaces after the test.

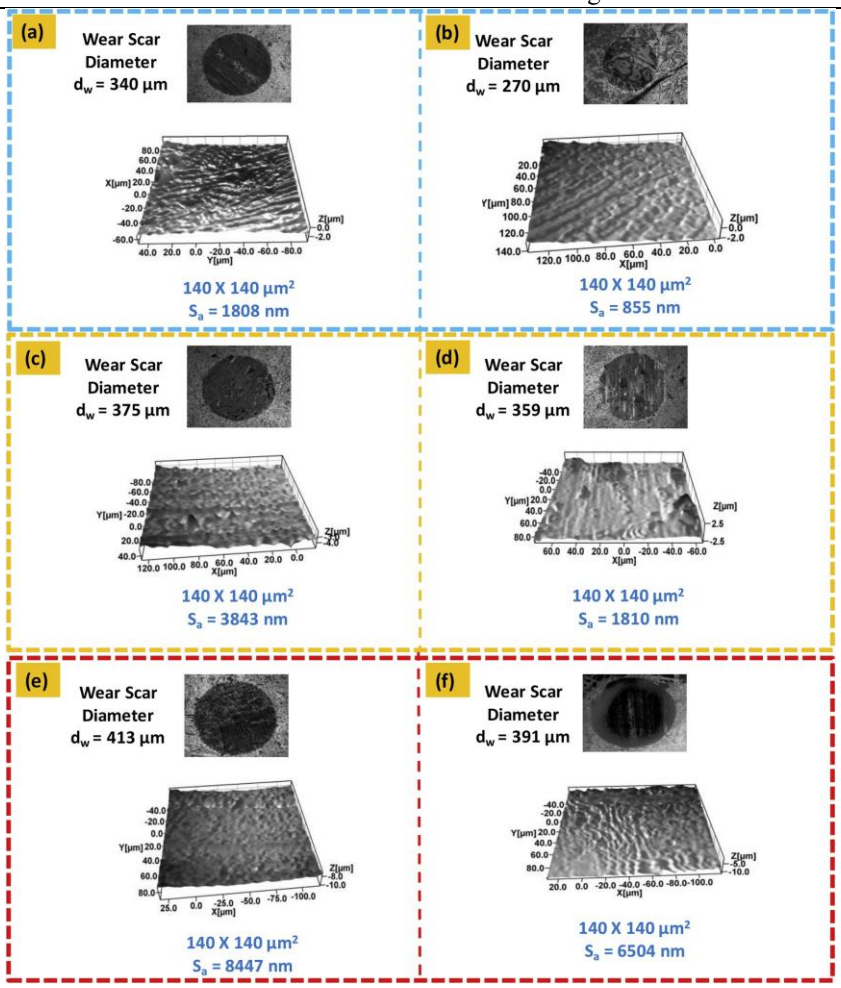

Figure 6.11 *Worn surfaces of steel balls with: (a) VG 220 and (b) 0.1 wt % PMMA/CQDs at 25 ºC and at 19 N, 1.17 GPa; VG 220 (c) and 0.1 wt % PMMA/CQDs (d) at 80ºC and at 19 N, 1.17 GPa; (e) VG 220 and (f) 0.1 wt % PMMA/CQDs at 25 ºC and at 58 N, 1.76 GPa.*

In Figure 6.12 a, the image of a worn surface lubricated with 0.1 wt % PMMA/CQDs at 25 ºC and at 19 N, 1.17 GPa is shown. Micro-Raman spectrometer was further used to analyze the worn surface, trying to identify carbon forms which can be formed by the CQDs. Raman spectra collected in some areas of the image in Figure 6.12 a are reported in Figure 6.12 b, c and 12d. In particular, a band at about 700 cm^{-1} can be seen in the light areas, which can be attributable to iron oxides, indicating oxidation on the steel surface, Figure 6.12 b. It was found that in darker areas, the characteristic peaks of carbon, D and G bands at about 1350 and 1590 cm^{-1}, are clearly visible, Figure 6.12 c. On the other hand, they are less intense in lighted areas,

Fig 6.12 d. No well-defined peaks from PMMA were detected on the worn surface. These observations can draw the consideration that carbon derived by CQDs, variously distributed deposits on the contact surfaces, helping lubrication and avoiding oxidation.

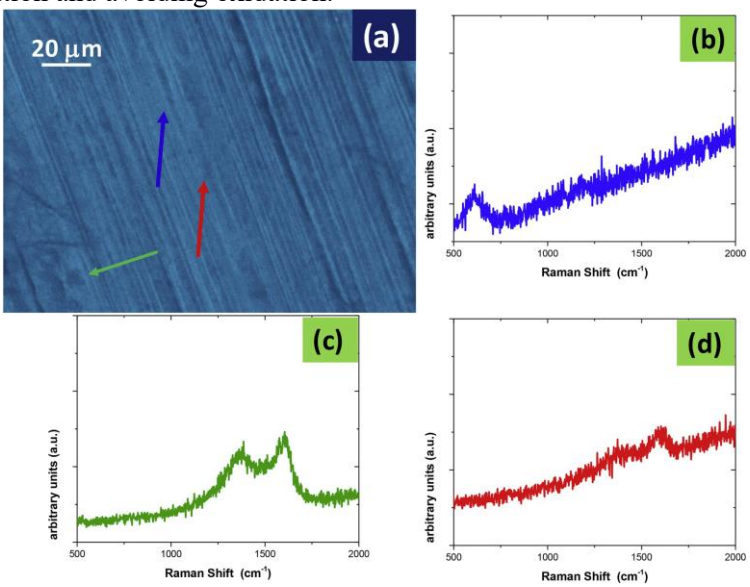

Figure 6.12 *Image of the worm surface lubricated by 0.1 wt % PMMA/CQDs at 25 ºC and at 19 N, 1.17 GPa (a). Raman spectra collected in the areas indicated by the arrows (b,c,d).*

Eventually, considering the aforementioned results, the PMMA/ CQDs composite was able to enhance the tribological performance of the pure commercial oil as a consequence of: a) the release of the entrapped CQDs from the polymer structure under lubrication conditions; and, b) the subsequent efficient lubricating mechanism of the quantum dots, free to interact with their hydrophilic groups with the metal surface to lubricate. A comprehensive scheme of the lubrication mechanism is shown in Figure 6.13. The metal surface, due to emission of low-energy electrons, is, during friction, positively charged and suitable to adsorb CQDs functionalities. As suggested by the behavior showed under time increase, at the initial stage, CQDs act as bearing balls, decreasing friction, while continuous deposition results in the formation of a protective film reducing the direct contact between the friction pairs. Further analyses have been planned and are required to completely clarify the lubrication mechanism utilising different surfaces roughness that is comparable to the average size of the nano-spheres. This technique may elucidate the specific behaviour of the ball-bearing effect of the nano-balls.

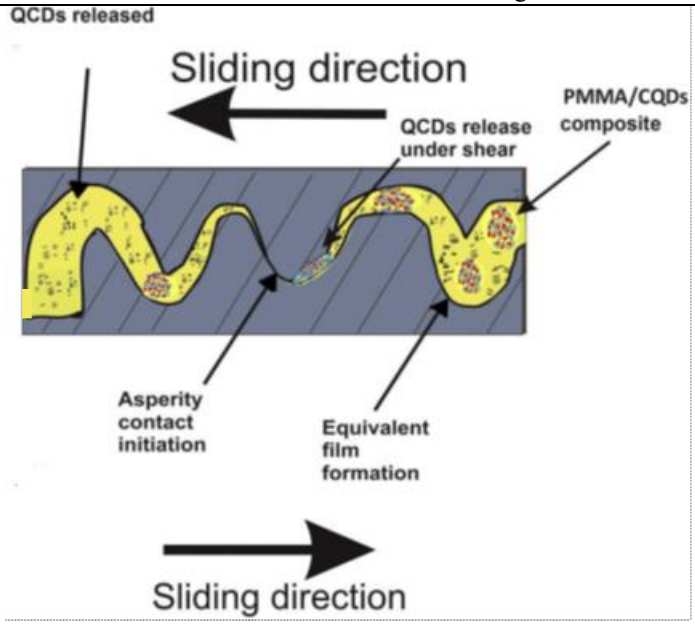

Figure 6.13 *Proposed tribological mechanism of the PMMA/CQDs nanocomposite.*

6.5 References

AHMED, R.M. (2009) Optical Study on Poly(methyl methacrylate)/Poly(vinyl acetate) Blends. *International Journal of Photoenergy*, 2009, pp. 1–7.

AZIZ, S.B., ABDULLAH, O.GH., et al. (2019a) Effect of carbon nano-dots (CNDs) on structural and optical properties of PMMA polymer composite. *Results in Physics*, 15, p. 102776.

AZIZ, S.B., ABDULLAH, O.GH., et al. (2019b) Effect of carbon nano-dots (CNDs) on structural and optical properties of PMMA polymer composite. *Results in Physics*, 15, p. 102776.

AZIZ, S.B. et al. (2017) Fabrication of polymer blend composites based on [PVA-PVP] (1−x) :(Ag 2 S) x (0.01 ≤ x ≤ 0.03) with small optical band gaps: Structural and optical properties. *Materials Science in Semiconductor Processing*, 71, pp. 197–203.

AZIZ, S.B., HASSAN, A.Q., et al. (2019) Structural and Optical Characteristics of PVA:C-Dot Composites: Tuning the Absorption of Ultra Violet (UV) Region. *Nanomaterials*, 9(2), p. 216.

BARROS, C.P. and PRIETO-RODRIGUEZ, J. (2008) A revenue-neutral tax reform to increase demand for public transport services. *Transportation Research Part A: Policy and Practice*, 42(4), pp. 659–672.

BHUNIA, S.K. et al. (2013) Carbon Nanoparticle-based Fluorescent Bioimaging Probes. *Scientific Reports*, 3(1), p. 1473.

BOTTINI, M. et al. (2006) Isolation and Characterization of Fluorescent Nanoparticles from Pristine and Oxidized Electric Arc-Produced Single-Walled Carbon Nanotubes. *The Journal of Physical Chemistry B*, 110(2), pp. 831–836.

BOUKNAITIR, I. et al. (2019) Optical and dielectric properties of PMMA (poly(methyl methacrylate))/carbon dots composites. *Polymer Composites*, 40(S2), pp. E1312–E1319.

BOURLINOS, A.B. et al. (2008) Surface Functionalized Carbogenic Quantum Dots. *Small*, 4(4), pp. 455–458.

CHEN, C.S. et al. (2005) Modification of multi-walled carbon nanotubes with fatty acid and their tribological properties as lubricant additive. *Carbon*, 43(8), pp. 1660–1666.

DE, B. and KARAK, N. (2013) A green and facile approach for the synthesis of water soluble fluorescent carbon dots from banana juice. *RSC Advances*, 3(22), p. 8286.

DONG, Y. et al. (2012) Polyamine-functionalized carbon quantum dots for chemical sensing. *Carbon*, 50(8), pp. 2810–2815.

ELOMAA, O. et al. (2015) Graphene oxide in water lubrication on diamond-like carbon vs. stainless steel high-load contacts. *Diamond and Related Materials*, 52, pp. 43–48.

EL-ZAHER, N.A. and OSIRIS, W.G. (2005) Thermal and structural properties of poly(vinyl alcohol) doped with hydroxypropyl cellulose. *Journal of Applied Polymer Science*, 96(5), pp. 1914–1923.

GAO, S. et al. (2014) A green one-arrow-two-hawks strategy for nitrogen-doped carbon dots as fluorescent ink and oxygen reduction electrocatalysts. *Journal of Materials Chemistry A*, 2(18), p. 6320.

GRIERSON, D.S. and CARPICK, R.W. (2007) Nanotribology of carbon-based materials. *Nano Today*, 2(5), pp. 12–21.

GUGUŁA, K. and BREDOL, M. (2014) Transparent CuInS2 PMMA Nanocomposites Luminescent in the Visible and NIR Region. *Zeitschrift für Naturforschung B*, 69(2), pp. 217–223.

JIA, X., LI, J. and WANG, E. (2012) One-pot green synthesis of optically pH-sensitive carbon dots with upconversion luminescence. *Nanoscale*, 4(18), p. 5572.

JIANG, F. et al. (2013) Eco-friendly synthesis of size-controllable amine-functionalized graphene quantum dots with antimycoplasma properties. *Nanoscale*, 5(3), p. 1137.

Junction growth in metallic friction: the role of combined stresses and surface contamination. (1959) *Proceedings of the Royal Society of London. Series A. Mathematical and Physical Sciences*, 251(1266), pp. 378–393.

KRYSMANN, M.J., KELARAKIS, A. and GIANNELIS, E.P. (2012) Photoluminescent carbogenic nanoparticles directly derived from crude biomass. *Green Chemistry*, 14(11), p. 3141.

LIN, J., WANG, L. and CHEN, G. (2011) Modification of Graphene Platelets and their Tribological Properties as a Lubricant Additive. *Tribology Letters*, 41(1), pp. 209–215.

LUO, T. et al. (2014) Tribological properties of Al2O3 nanoparticles as lubricating oil additives. *Ceramics International*, 40(5), pp. 7143–7149.

MAXIM, A.A. et al. (2020) PMMA Thin Film with Embedded Carbon Quantum Dots for Post-Fabrication Improvement of Light Harvesting in Perovskite Solar Cells. *Nanomaterials*, 10(2), p. 291.

MIN, C. et al. (2018) Unique synergistic effects of graphene oxide and carbon nanotube hybrids on the tribological properties of polyimide nanocomposites. *Tribology International*, 117, pp. 217–224.

MUTHUVEL, S., NARESH BABU, M. and MUTHUKRISHNAN, N. (2020) Copper nanofluids under minimum quantity lubrication during drilling of AISI 4140 steel. *Australian Journal of Mechanical Engineering*, 18(sup1), pp. S151–S164.

OTA, J. et al. (2015) Graphene dispersion in hydrocarbon medium and its application in lubricant technology. *RSC Advances*, 5(66), pp. 53326–53332.

QIU, W. et al. (2010) Experimental study of the Raman strain rosette based on the carbon nanotube strain sensor. *Journal of Raman Spectroscopy*, 41(10), pp. 1216–1220.

SARNO, M. et al. (2019) A Tribochemical Boost for Cu Based Lubricant Nano-Additive. *Key Engineering Materials*, 813, pp. 292–297.

SARNO, M., SPINA, D. and SENATORE, A. (2019) One-step nanohybrid synthesis in waste cooking oil, for direct lower environmental impact and stable lubricant formulation. *Tribology International*, 135, pp. 355–367.

SELBY, T.W. (1958) The Non-Newtonian Characteristics of Lubricating Oils. *A S L E Transactions*, 1(1), pp. 68–81.

SHAHNAZAR, S., BAGHERI, S. and ABD HAMID, S.B. (2016) Enhancing lubricant properties by nanoparticle additives. *International Journal of Hydrogen Energy*, 41(4), pp. 3153–3170.

SINGH, R.K. et al. (2017) Performance evaluation of alumina-graphene hybrid nano-cutting fluid in hard turning. *Journal of Cleaner Production*, 162, pp. 830–845.

TU, Z. et al. (2020) Tribological behaviors of Ni-modified citric acid carbon quantum dot particles as a green additive in polyethylene glycol. *Friction*, 8(1), pp. 182–197.

UMAR, M., MUFTI, R.A. and KHURRAM, M. (2018) Effect of flash temperature on engine valve train friction. *Tribology International*, 118, pp. 170–179.

WAN, Q. et al. (2015) Tribological Behaviour of a Lubricant Oil Containing Boron Nitride Nanoparticles. *Procedia Engineering*, 102, pp. 1038–1045.

WANG, F. et al. (2011) Highly Luminescent Organosilane-Functionalized Carbon Dots. *Advanced Functional Materials*, 21(6), pp. 1027–1031.

YE, M. et al. (2018) Friction-induced transfer of carbon quantum dots on the interface: Microscopic and spectroscopic studies on the role of inorganic–

organic hybrid nanoparticles as multifunctional additive for enhanced lubrication. *Tribology International*, 127, pp. 557–567.

YU, R., LIU, J. and ZHOU, Y. (2019) Experimental Study on Tribological Property of MoS2 Nanoparticle in Castor Oil. *Journal of Tribology*, 141(10), [Online] Available from: doi.org/10.1115/1.4044294.

ZHANG, W. et al. (2011) Tribological properties of oleic acid-modified graphene as lubricant oil additives. *Journal of Physics D: Applied Physics*, 44(20), p. 205303.

Conclusions

This Ph.D. dissertation aims at providing a scientific contribution to the Tribology community regarding optimised green nanolubricants utilisation in transmissions lubrication, from the industrial, point of view, and the theoretical challenges. Here, this study's main findings are outlined to provide the reader with an overall conclusion from the manuscript.

Literature and practical observations were made in Chapter II regarding advantages of nanoparticles in protecting gears against micropitting wear compared to EP conventional additives. Furthermore, the addition of nanomaterials as solid lubricant additives may further reduce the content of traditional AW, AF and EP additives in lubricating oils. This will have a greener impact on the environment, as most conventional additives are poisonous and harmful. However, more studies and investigations are required to ensure operational safety and sustainable production when synthesising nanoadditives.

Chapter III was concerned with the future potentials of nanolubricants use in electric vehicles. This scan was conducted in a literature review that highlights the different attributes and pre-existing challenges regarding the use of nanolubricants as a novel class of lubrication dedicated to EVs. The method conducted in this study relies on critically discussing and coupling theoretical research knowledge with practical information. The following key points are the main conclusions arrived: 1) pristine NPs (without surface modification) seem to be the best pick to avoid the adverse effects of NPs-thickeners interactions, leading to an incompatibility that can destroy grease's structure; 2) NPs can be used to face harmful electrical current discharged by both enhancing insulating or conductivity of lubricants. Therefore, choosing the functional objective of NPs is essential when utilising it as AEDA. When NPs are desired to increase the breakage voltage of a lubricant, the focus should be on the particles' size, as smaller sizes are more effective in electron trapping. Meanwhile, to increase lubricants' electrical conduciveness, it seems that surface-functionalised NPs are more efficient than pristine NPs; 3) regarding copper corrosion protection induced by NPs, it seems that silica-based

lubricants are superior. Besides, nanolubricants can outperform nano-coating in the prevention of pocket-trapping of the corrosive substance under nano-layering; and 4) the rise in nanolubricants thermal conductivity relies primarily on the concentration of the suspended NPs and the environment's temperatures, in a proportional increment which can be advantageous in EVs conditions. Simultaneously, relative to other forms of NPs, carbon-based NPs have excellent properties for increasing thermal conductivity, as proved from the literature scan in Chapter I. Proposed future research may utilise magnetic and electric fields in EVs powertrains to control the behaviour of surface charged NPs, which can result in controlled lubrication for optimum tribological results.

Chapter IV was dedicated to review reduced graphene oxide/graphene oxide (rGO/GO) nanosheets in tribology. Graphene-based nanosheets surface functionalisation is studied, including unexplored findings in the field of lubrication. From the literature it can be concluded that rGO/GO nanosheets can minimise wear and friction. Wear reduction is accomplished by deposition and film-forming, while friction reduction is related to the shearing and lamination of the sheets on the contacting surfaces. However, the two phenomena are interrelated and operate in sync. In general, it is of the utmost importance to form a homogenous suspension for a continuous supply of nanosheets after deposition and shearing.

Experimental exposure concerning NPs surfactant modification use was conducted in Chapter V, in which carbon nanotubes and graphene-based nanocarbons have been synthesised by effective, environment friendly, and scalable methods, such as catalysed chemical vapor deposition (CCVD), chemical exfoliation and solvent-based exfoliation. Following thorough characterisation of the materials, a rigorous review of their stability in Group I-II mixture and Group III base oils, with and without a low volume of dispersant/surfactant, has been carried out, showing that the combination of SDBS and Tween 80 surfactants offers the best stability for 20 hours of investigation of solvent-exfoliated thin-layer graphene (FLG) in the baseline.

This enhanced stability results from the synergistic relationship between anionic and non-ionic surfactants, which promotes the forming of micelles around nanosheets by resolving repulsion interactions between ions as steric repulsions between neutral molecules. Tribological tests showed a significant reduction in CoF and WSD, particularly for 0.1 wt.% of the larger, defect-free, few-layer graphene sample in both base oils due to the broader protective film formed by the nanoadditive relative to the other samples. The remarkable performance achieved with FLG, which remains stable over a long test time, is an excellent result when considering the more difficult GO/rGO production on a large scale. Moreover, dependence of viscosity on shear rate for different samples was acquired, confirming that the low surfactant concentration and

the nano-carbons presence in the base oil do not lead to any significant modification of this rheological parameter.

Eventually, a reduction of the wear scar diameters and a high reduction of the surface roughness were measured both at room temperature and 80°C, due to the addition of the 0.1 wt % FLG sample. This encouraging finding, possibly due to forming a protective film formed by the nanoadditive during sliding, confirms its superior tribological effectiveness.

A novel experimental investigation was achieved in Chapter VI. PMMA/CQDs composite, consisting of carbon quantum dots, 1–2 nm average diameter, entrapped in a PMMA matrix, was prepared through a one-step, mild temperature, oleic acid- and citric acid-based green synthesis. PMMA not only ensures CQDs long-time stability in non-polar commercial oils but, at the same time, allows the release of CQDs under lubricated equipment's operating conditions. Tribological tests carried out in a VG 220 commercial mineral oil confirmed the synthesised sample's high anti-wear and anti-friction performance. CQDs, acting as bearing balls on the positively charged surface, decrease friction, whereas continuous deposition results in the formation of a protective film, which significantly reduces the direct contact between the friction pairs. In this context, it is of high importance the CQDs homogenous suspension, for a continuous supply after deposition and shearing. Viscosity measurements at 40 ºC and 100 ºC confirmed that the presence of small percentages of the nanocomposite in the oil did not significantly change its rheological property. This is particularly interesting because it does not interfere with the physical properties of the base oil, as well as with the delicate balance of the final industrial formulations. Obviously, by increasing the PMMA amount, an improvement of the VI of the fully-formulated oil is expected to occur, which can affect only positively the CQDs dispersion.

List of symbols

a	Contact area
E	Young module
E^*	Reduced module
F_f	Friction force
F_k	Kinetic friction force
F_N	Normal force
F_s	Static friction force
H	Material's hardness
h_{min}	Minimum film thickness
K	Wear rate
P	Contact pressure
$P(r)$	Pressure distribution
r	Young radius
R_a	Surface roughness
s	Movement distance
V	Worn volume
VI	Viscosity index
α	Coefficient of viscosity-pressure
ϵ	Dielectric constant of water
$\epsilon 0$	Permittivity of vacuum
η	Lubricant viscosity
η_0	Lubricant's viscosity is at ambient pressure and constant temperature
κ	Inverse of Debye length
μ	Coefficient of friction
ν	Sliding velocity
$\sigma(r)$	Radial stress
$\sigma+$, and $\sigma-$	Surface charge densities per unit area of the right and left surfaces

Appendix

In this section TEM images of PMMA/CQDs composites of different analysed samples are reported.

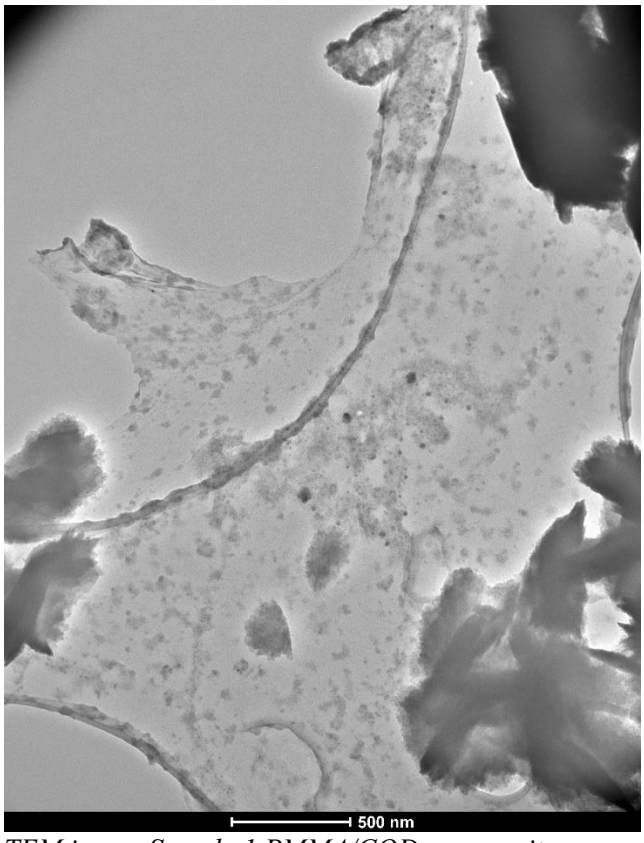

Figure 1A *TEM image Sample 1 PMMA/CQDs composites.*

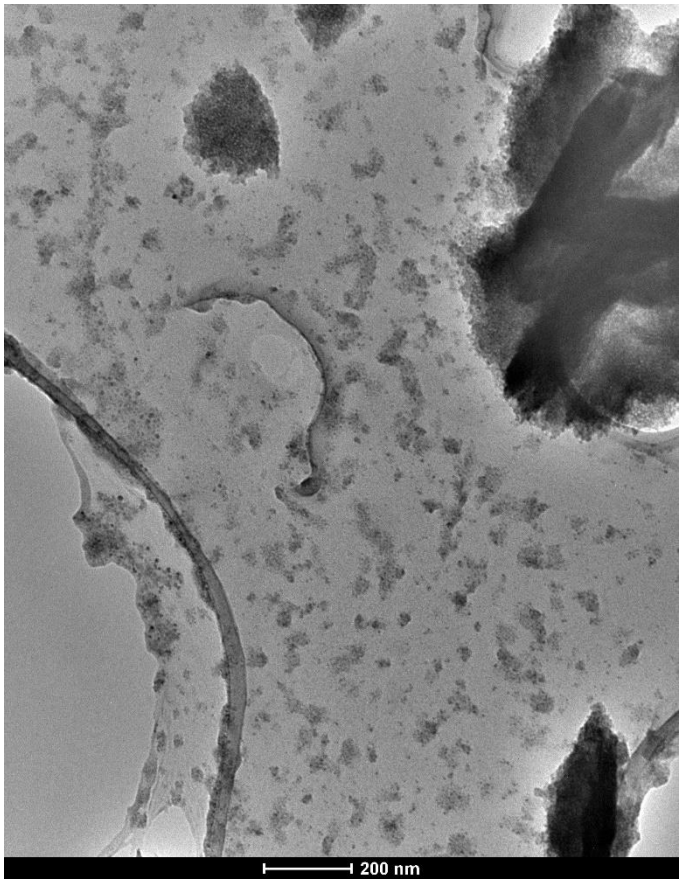

Figure *2* *A TEM image Sample 2 PMMA/CQDs composites.*

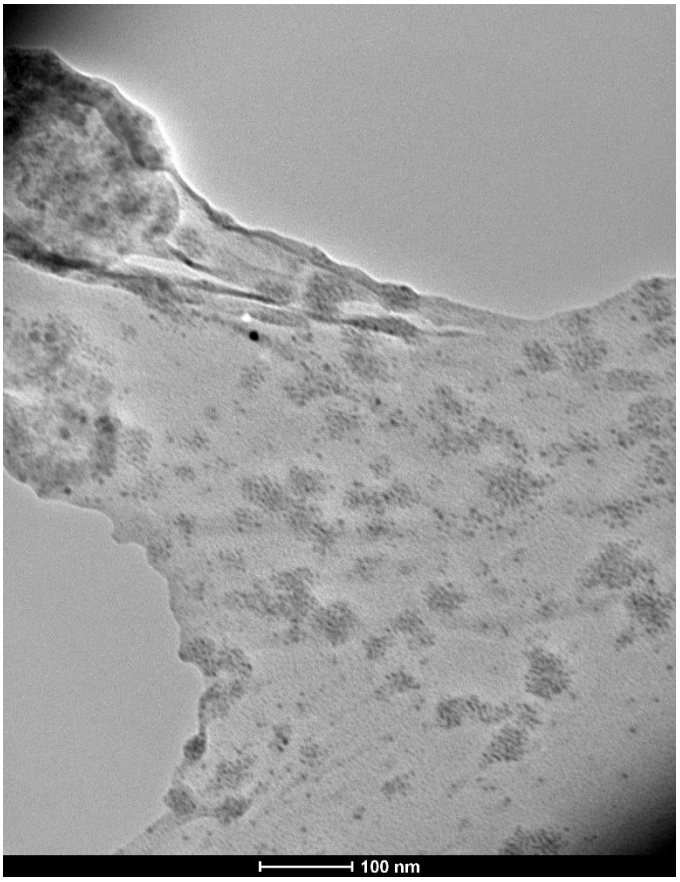

Figure 1A *TEM image Sample 3 PMMA/CQDs composites.*